THE OPEN UNIVERSITY
Science: a third level course
S342 Physical Chemistry: Principles of chemical change

BLOCK 6
PHYSICAL METHODS FOR CHARACTERISING SURFACES

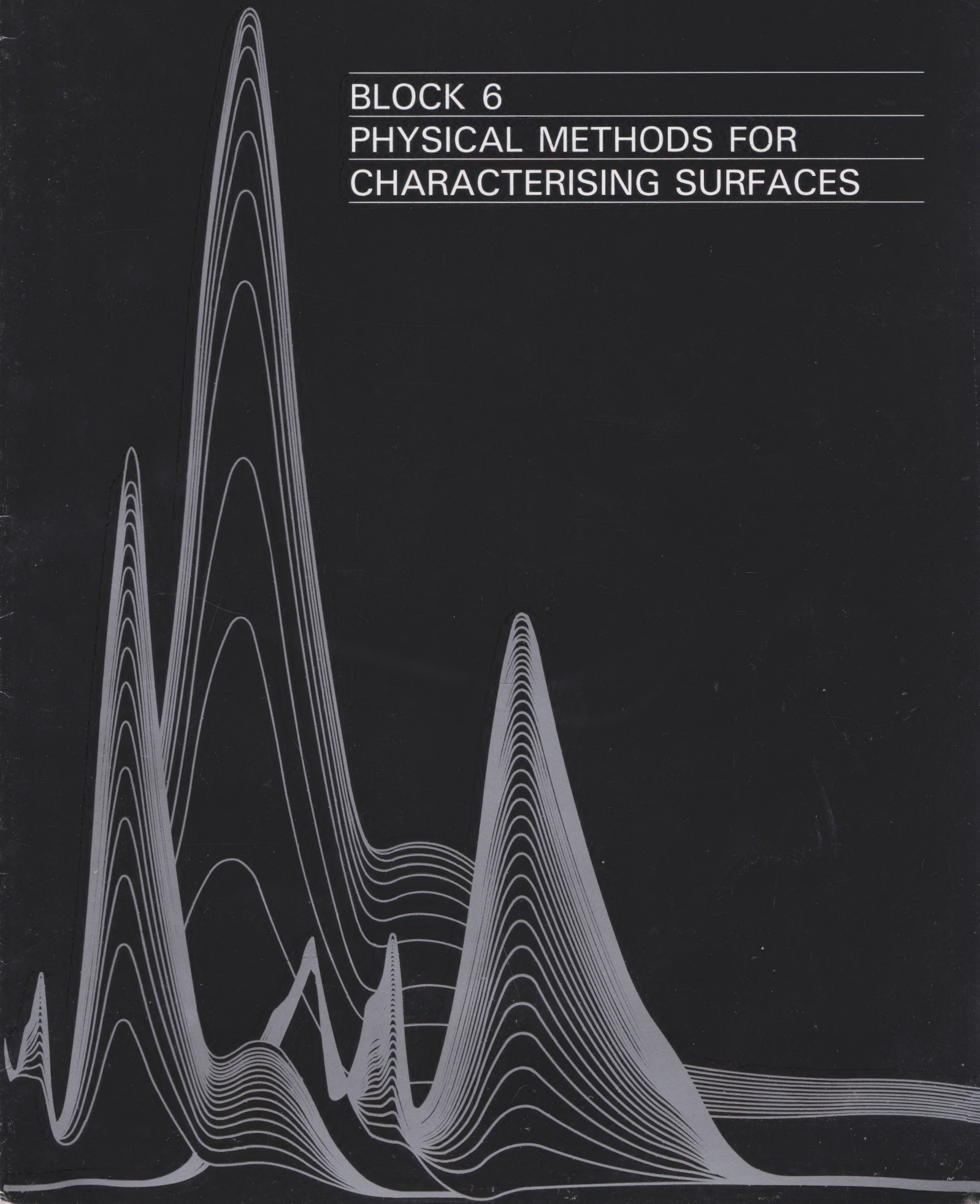

S342 Course Team

Course Team Chair and General Editor
Kiki Warr

Authors
Keith Bolton *(Block 8; Topic Study 3)*
David Johnson (*Block 6*)
Michael Mortimer (*Blocks 2 and 5*)
Lesley Smart (*Block 6*)
Peter Taylor *(Blocks 3 and 4; Topic Study 1)*
Keith Trigwell (*Topic Study 2*)
Kiki Warr *(Blocks 1, 7 and 8; Topic Study 2)*

Consultants
J. Dwyer *(University of Manchester Institute of Science and Technology; Topic Study 2)*
Dr P. C. Engel *(University of Sheffield; Topic Study 1)*
Dr J. M. West *(University of Sheffield; Topic Study 3)*

Course Support Staff
Peter Fearnley (*Course Coordinator from 1984*)
Keith Trigwell (*Course Manager to 1983)*

Editors
Ian Nuttall
Dick Sharp

BBC
Barrie Whatley

Graphic Designer
Jo Cotter

Graphic Artist
Janis Gilbert

Assistance was also received from the following people:
Professor P. G. Ashmore
Philip Butcher (*CALCHEM*)
George Loveday (*Staff Tutor*)

THE OPEN UNIVERSITY
Science: a third level course
S342 Physical Chemistry: principles of chemical change

BLOCK 6
PHYSICAL METHODS FOR CHARACTERISING SURFACES

Prepared by an Open University Course Team

CONTENTS

The Open University Press

The Open University Press
Walton Hall, Milton Keynes,

First published 1985.
Reprinted 1991.

Designed by the Graphic Design Group of the Open University.

Typeset by Composition House Ltd, Salisbury, Wilts and
printed in England by Staples Printers St Albans Limited at The Priory Press.

ISBN 0 335 16188 X

This text forms part of an Open University course. The complete list of Blocks in the Course is printed at the end of this text.

For general availability of supporting material referred to in this text please write to: Open University Educational Enterprises Limited, 12 Cofferidge Close, Stony Stratford, Milton Keynes, MK11 1BY, Great Britain.

Further information on Open University courses may be obtained from the Admissions Office, The Open University, P.O. Box 48, Walton Hall, Milton Keynes, MK7 6AB.

1.2

STUDY GUIDE FOR BLOCK 6

This Block is equivalent to 1.5 units, or $1\frac{1}{2}$ weeks work. It describes some of the newer techniques that have been used to study surfaces, notably low energy electron diffraction (LEED), and certain kinds of electron spectroscopy. The description is interwoven with an account of the contribution that the techniques have made to the elucidation of the mechanism of ammonia synthesis by the Haber–Bosch process. At first reading, no attempt should be made to unravel these two threads: it is best to read the Block through from start to finish.

After a short introduction, X-ray photoelectron spectroscopy (XPS) is dealt with in Section 3, and Auger electron spectroscopy (AES) in Section 4. Brief applications to the ammonia problem are mentioned here, and then, in Section 5, there follows a sustained account of how the mechanism of the Haber process has been clarified with the help of electron spectroscopy.

The next stage is the introduction of low energy electron diffraction in Section 8, but a necessary preliminary is the important notation of Miller indices, so this is presented first in Sections 6 and 7. LEED studies of nitrogen adsorbed on iron surfaces are described at the end of Section 8, and in Section 9 these are complemented by information obtained from electron energy loss spectroscopy (EELS). This helps us to formulate theories of promoter action in the industrial iron catalyst in Section 10, prior to the final summary of Section 11.

The TV programme (TV 6) provides supporting material for Sections 4.4, 5 and 8.4.2.

1 INTRODUCTION

In Block 5, you met some of the basic ideas and techniques that are used in the study of heterogeneous catalysis. They included adsorption isotherms, the description of adsorption in terms of potential energy diagrams, and the determination of the surface areas of catalysts by the BET method. Most of these ideas are more than 40 years old, but they have been, and continue to be, extremely productive. However, during the past 20 years new physical methods for characterising the solid–gas interface have been invented, and it is with some of these methods that this Block is concerned. We emphasise that the new techniques have not replaced the older ones; they merely complement them, and in many cases they have only confirmed what was previously thought to be highly probable. Nevertheless, their influence on the study of solid–gas reactions has been profound, and in this Block we shall illustrate that influence with a number of examples. We shall, however, concentrate especially on one particular process. In Block 1 you took a close look at the *thermodynamics* of the catalysed synthesis of ammonia. In this Block, we shall examine what is known about the *mechanism* of this reaction. Let us begin therefore by looking again at the conditions under which ammonia synthesis is carried out.

Ammonia is made by the reaction of nitrogen with hydrogen, usually at pressures of about 250 atm and temperatures of about 750 K, in the presence of a catalyst composed mainly of iron:

$$N_2(g) + 3H_2(g) = 2NH_3(g) \qquad (1)$$

As you know, the catalyst's essential role is to raise the speed of reaction or, more strictly, the speed at which equilibrium is reached. Even so, it is still necessary to run the reaction at 750 K to ensure an economically acceptable rate. As you saw in Block 1 (Section 7), the high temperature has an adverse effect upon the equilibrium yield of ammonia: at 1 atm and 750 K, this yield is less than 1 per cent, and it is only by expensively raising the pressure above 150 atm that economic yields of 20–30 per cent can be achieved. (The percentage of ammonia in the exit gas is usually less than this because, to increase the *rate of production*, the throughput of gas is made so fast that equilibrium is not reached in the converter.) Clearly then, the performance of the catalyst is far from ideal. Let us look more closely at its composition.

One very famous catalyst for ammonia synthesis was invented in 1910, three years before the German company, Badische Anilin und Soda Fabrik (BASF), brought the first high-pressure ammonia plant on stream. A research team working for this company found that the performance of the iron catalyst was substantially improved if small amounts of potassium and aluminium oxides were present. Similar catalysts are still widely used today, although small amounts of other oxides, such as calcium oxide, are usually added as well. Such catalysts are said to be *multiply promoted*. They can be prepared by fusing or sintering an iron oxide such as magnetite (Fe_3O_4) with much smaller amounts of potassium nitrate, calcium carbonate and alumina (Al_2O_3) at about 1 900 K. The solid produced on cooling contains oxygenated potassium, calcium and aluminium, there being about 2 per cent aluminium, 2 per cent calcium and 0.5 per cent potassium by mass. In this state, it is said to be in the *unreduced form*. To prepare it for industrial use, it must be converted into the *reduced form*. This can be done by slowly raising its temperature in the presence of nitrogen and hydrogen until the operating temperature of the plant is reached. The catalyst is then active and ready for use.

multiply promoted

The thermodynamics of ammonia synthesis were given a thorough airing in Block 1, but a major gap in your knowledge of the reaction is concerned with its mechanism. We list here some of the obvious questions that need answers:

1 What is the nature of the catalyst surface?

2 What is the mechanism of the reaction, and which step, if any, is rate-limiting?

3 What is the active site on the catalyst surface?

4 What role do the promoters play?

Even today, more than 80 years after Haber's work, we do not have full answers to these questions, and in this Block we do not have the space to give you a full account of existing knowledge. Nevertheless, we hope to show you how modern physical methods, in combination with the older techniques described in Block 5, have helped to supply partial answers to the four questions.

2 PREPARING CLEAN SURFACES FOR STUDY

Before a surface can be examined by the new physical methods, it must be thoroughly cleaned. This involves the removal of any adsorbed gases that contaminate the surface. These may have come from the surrounding atmosphere or even from within the bulk of the solid itself. The surfaces of metal samples are effectively cleaned by heating under vacuum. If this is not sufficient, then a more powerful method is to subject them alternately to argon-ion (Ar^+) bombardment and heating under vacuum. The heating gets rid of any argon adsorbed on the surface and also helps eliminate structural faults. Great care has to be exercised when bombarding surfaces as it is very easy to destroy the ordered surface completely, which somewhat defeats the object of the exercise!

Transition metal surfaces are often contaminated by carbon which diffuses to the surface from the bulk metal during vacuum heat treatment. In this case it is sometimes necessary to use controlled oxidation to eliminate the carbon, followed by treatment with hydrogen to get rid of the oxygen!

To prevent recontamination, surfaces have to be studied under very high vacuum conditions. Conventional high vacuum systems work at about 10^{-6} Torr, (1 Torr = 1 mmHg = 133.322 Pa; 760 Torr = 1 atm), but even at this pressure about ten molecules or atoms will collide with each atom on the surface every second. If only 10 per cent of the collisions result in a molecule sticking to the surface, the cleaned surface would be completely recontaminated in one second! A satisfactory pressure for performing surface experiments is about 10^{-9}–10^{-10} Torr; such an *ultra-high vacuum* (*UHV*) can be attained using sophisticated

ultra-high vacuum (UHV)

modern pumping techniques. These pressures reduce the collision rate of molecules with the surface to one every few hours—which gives enough time to perform an experiment.

Once a surface has been thoroughly cleaned and prepared, it is ready for examination by the techniques described in this Block. The experimental arrangements for some of these techniques will be shown in TV programme 6. First, we will look at one type of spectroscopy that you have met before—X-ray photoelectron spectroscopy.

3 X-RAY PHOTOELECTRON SPECTROSCOPY

3.1 Introduction

X-ray photoelectron spectroscopy (XPS)

X-ray photoelectron spectroscopy (*XPS or X-PES*) is just one branch of electron spectroscopy—the latter being defined as the study of electrons emitted when matter is irradiated with photons or bombarded with particles. You have already met some of the results of XPS studies in the Science Foundation Course and in the Second Level Course. There, we used photoelectron (PE) spectra of gaseous atoms and simple molecules to provide evidence for the presence of quantised energy levels. As an example, Figure 1 shows the diagrammatic PE spectra of some of the noble gases. Notice that the scale is given in increasing energy to the *right* of the diagram. In the krypton spectrum, we have given you two energy scales for comparison—in joules, the SI unit you are familiar with, and in electronvolts, eV*, the unit commonly used by researchers in this field. Note also that the scales are broken so that the peaks occur in groups separated by large energy gaps of the order of hundreds of electronvolts.

SFC 1
SLC 1

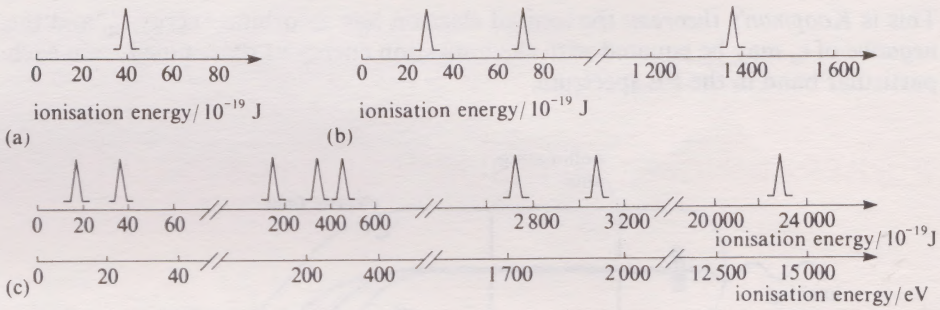

Figure 1 Schematic photoelectron spectra of (a) helium, (b) neon and (c) krypton.

☐ Do you recall how the peaks arise in these spectra?

■ In PE spectroscopy, light of a fixed energy is shone on the sample. This excites electrons which are ejected, or ionised. Each peak thus corresponds to removal of an electron from a particular atomic energy level.

☐ Now try labelling the peaks in Figure 1 according to which orbital the electron was ionised from.

■ The most tightly bound electrons (corresponding to the highest ionisation energies) will be in the 1s levels—these peaks thus lie farthest to the right in each diagram. Label them now. They are followed by (in order of *decreasing* ionisation energy) 2s and 2p for neon and 2s2p, 3s3p3d, and 4s4p for krypton.

* An electronvolt is the kinetic energy acquired by an electron that has been accelerated by a potential difference of 1 volt; 1 eV ≡ 1.602×10^{-19} J.

The origin of the large energy gaps now becomes clear—they lie between different shells. To ionise electrons in the deeper *core levels* requires high energy radiation, and X-rays are usually used (Figure 2a). The valence electrons, however, can usually be ionised using less energetic ultraviolet radiation (Figure 2b). You will see in a moment that the distinction between these two forms of PE spectroscopy is very important. In this Course we shall be concentrating chiefly on XPS; ultraviolet photoelectron spectroscopy (known as UPS or U-PES) is discussed in detail in another Third Level Course*.

core levels

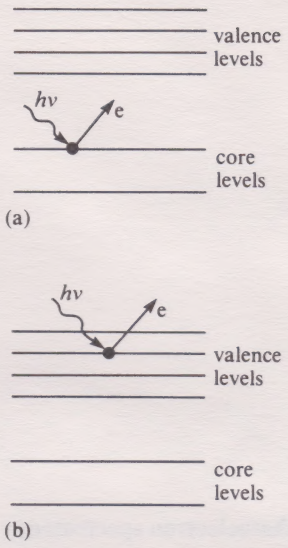

Figure 2 Photoelectron processes using (a) X-rays, (b) ultraviolet radiation.

Figure 2a shows X-rays exciting electrons from an inner shell into a vacuum so that ionisation takes place. The kinetic energies of the emitted electrons are measured to give information about the electronic energy levels. As you may recall from the Science Foundation Course, the kinetic energy of an electron emitted from an atom or molecule by radiation of energy $h\nu$ is given by the *Einstein equation*†:

$$E_k = h\nu - I \qquad (2)$$

where E_k is the kinetic energy of the emitted electron, I is the ionisation or binding energy of that electron, h is Planck's constant and ν is the frequency of the radiation (note that in the Foundation Course the symbol f was used). So if ν is known and E_k can be measured experimentally, the binding energy of the electron can be determined. A plot of the observed kinetic energies of the emitted electrons (or of their calculated binding energies) versus the intensity (or number of electrons emitted per second) gives the PE spectrum.

□ Which electronic levels will the electrons with the highest kinetic energy have come from—higher or lower?

■ Higher: the higher the level, the lower the binding energy, I, and the larger the value of E_k (cf. equation 2).

If we make the assumption that the photoionisation occurs without any adjustment in the energies of the other orbitals (the so-called *frozen-orbital approximation*), then for ionisation from orbital a:

frozen-orbital approximation

$$I_a = -\epsilon_a \qquad (3)$$

This is *Koopman's theorem*: the ionised electron has an orbital energy ϵ_a, and the *negative* of ϵ_a may be equated with the ionisation energy as determined from each particular band in the PE spectrum.

Koopman's theorem

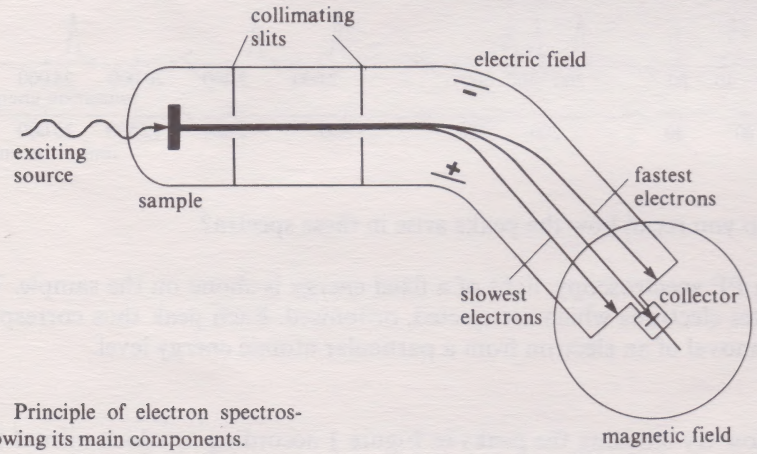

Figure 3 Principle of electron spectroscopy, showing its main components.

The general principles involved in obtaining electron spectra are the same whatever the exciting medium, be it X-rays or ultraviolet radiation (or, indeed, a beam of electrons, as we shall see later); the end result is that the kinetic energies of electrons have to be measured. One method of energy analysis is carried out in a double-focusing spectrometer using either electrostatic or magnetic fields—the basic principles being the same as in a mass spectrometer. The experimental arrangement is shown schematically in Figure 3. In XPS, the sample is excited by X-rays—normally aluminium K_α (1 487 eV) or magnesium K_α (1 254 eV)—and electrons are

SFC 3

* TLC 1 † SFC 2

emitted from a core level. These electrons then pass through a collecting system of slits into the energy analyser. This consists of charged plates, which spread the beam out according to the velocity (and therefore the kinetic energy†) of the electrons. Slower electrons follow a tighter curve than faster ones. To detect each of the velocities in turn, the strength of the magnetic field can be varied so that electrons of different velocity arrive successively at the collector. The result is a plot of electron current versus field strength—but this is effectively a plot of the number of electrons against the kinetic energy of the electrons.

The exciting X-rays penetrate hundreds of nanometres into the solid sample. However, the photoelectrons produced can escape from a depth of only about 2 nm or less—the escaping electrons have a high probability of being inelastically scattered through collisions with bound electrons. *Because of this, XPS samples only a thin surface layer of a solid material.* Although this makes it a slightly unreliable technique for studying bulk samples, *it makes XPS very sensitive as a surface technique* and of growing importance in the study of heterogeneous catalysis, where the reactions take place at the surface.

SLC 1

As you saw in the Second Level Course, these principles apply equally well to molecules: the only difference is that peaks in the PE spectrum now correspond to ionisation from *occupied molecular orbital* levels. For example, consider the complete PE spectrum of carbon monoxide, CO (Figure 4a): as with the PE spectra of atoms (Figure 1), the peaks clearly fall into two groups with a large gap of several hundred electronvolts between. The two strong peaks at high binding energy correspond to ionisation from C(1s) and O(1s) core levels; the other group is due to ionisation from the valence molecular orbitals. These are shown for comparison in the molecular orbital diagram in Figure 4b. Notice that the $2\pi^*$ and $6\sigma^*$ orbitals do not feature in the spectrum—there are, of course, no electrons occupying them.

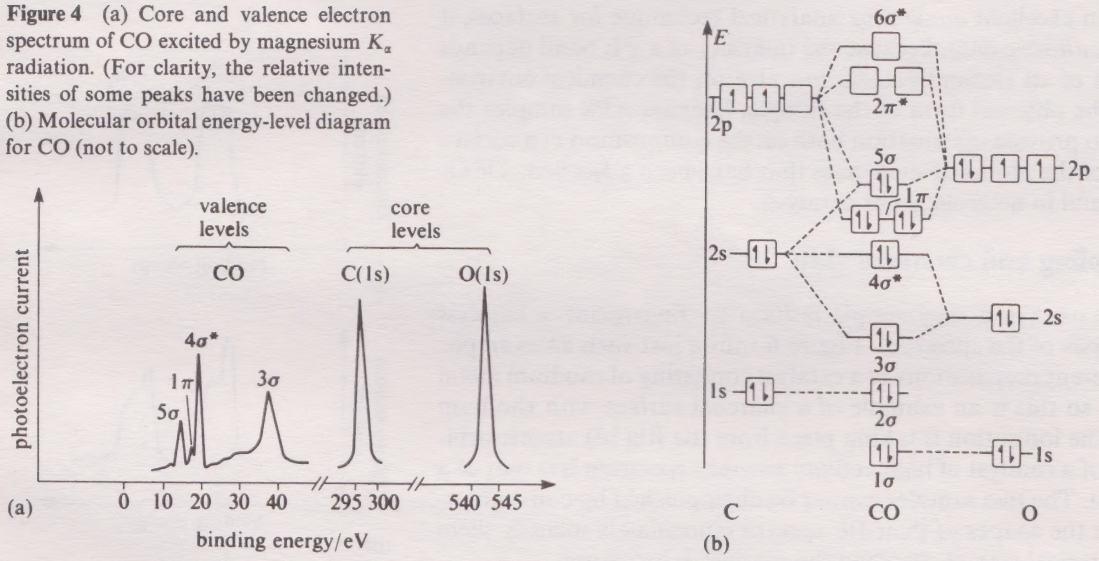

Figure 4 (a) Core and valence electron spectrum of CO excited by magnesium K_α radiation. (For clarity, the relative intensities of some peaks have been changed.) (b) Molecular orbital energy-level diagram for CO (not to scale).

SLC 2

Don't worry about the molecular orbital diagram and its labels: it is covered in detail in the Second Level Course, but you will not be expected to construct or use such diagrams in this Course. We shall deal almost exclusively with core levels, and as you can see in Figure 4a these are labelled as the atomic orbitals of the constituent atoms. A full PE spectrum for carbon dioxide, CO_2, would show a different pattern of peaks in the valence region because, of course, the bonding is completely different in this molecule. What is important, from our point of view, is that it *does* still show the two intense peaks due to ionisation from the C(1s) and O(1s) core levels, and that these occur in more or less the same positions as in the CO spectrum. (We shall see later that there are slight differences in the positions of the peaks and that this can provide useful information.)

† From $E_k = \frac{1}{2}mv^2$, where m and v are the mass and velocity of an electron.

3.2 XPS as an analytical technique

XPS spectra have been obtained for every element in the Periodic Table. Ionisation of the core electrons from each atomic orbital provides a list of ionisation energies for each element. These are sufficiently characteristic to be used for *qualitative analysis* (that is, the atoms of any element can be detected by their characteristic pattern of peaks).

SAQ 1 Steel, as you know, contains many elements other than iron. Figure 5 shows the XPS spectrum of a steel surface, produced using aluminium K_α X-radiation (1 487 eV). This spectrum plots the *kinetic energies* of the electrons and has peaks at 415, 479, 615, 955, 1 049, 1 137, 1 203, 1 258, 1 322, 1 375 and 1 424 eV. Use these peak positions and the binding energies in Table 1 to identify the elements present other than iron.

Figure 5 XPS spectrum of a steel surface.

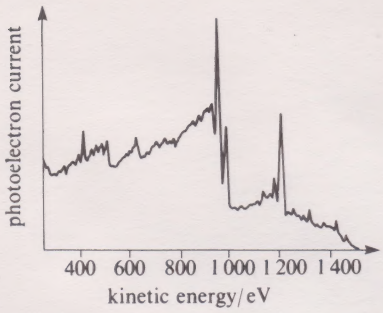

Table 1 Electronic binding energies (in eV) for some selected elements

Element	Core level*				
	$K(1s_{1/2})$	$L_1(2s_{1/2})$	$L_2(2p_{1/2})$	$L_3(2p_{3/2})$	$M_1(3s_{1/2})$
carbon	284				
oxygen	532	24			
sodium	1 072	63			
phosphorus	2 148	191	135	134	16
sulphur	2 472	229	165	164	16
calcium	4 036	438	350	347	44
nickel	8 333	1 008	872	855	112

* These labels are explained in Section 4.3. Don't worry about what they mean just now.

Although XPS makes an excellent *qualitative* analytical technique for surfaces, it provides only crude *quantitative* data, because the intensity of a PE band depends not only on the amount of an element present but also on the chemical environment of the atom and the physical form of the sample. Because XPS samples the surface layers, it is able to provide information both on the composition of a surface and also on the nature of the atoms or molecules that have been adsorbed. This is why it is particularly useful in heterogeneous catalysis.

3.3 Spin–orbit coupling and chemical shift

XPS can sometimes be used in a very simple fashion to 'fingerprint' a catalyst without a detailed analysis of the spectrum. Figure 6 shows just such an example. These are spectra of different preparations of a catalyst consisting of rhodium metal dispersed on charcoal—so this is an example of a charcoal surface with rhodium atoms adsorbed on it. The ionisation is taking place from the Rh(3d) atomic orbitals. Spectrum a is that of a catalyst of high activity whereas spectrum b is that of a spent or inactive catalyst. The two samples cannot be distinguished by conventional chemical analysis, yet the shapes of their PE spectra immediately identify them and so give a purely empirical way of checking the catalyst prior to use.

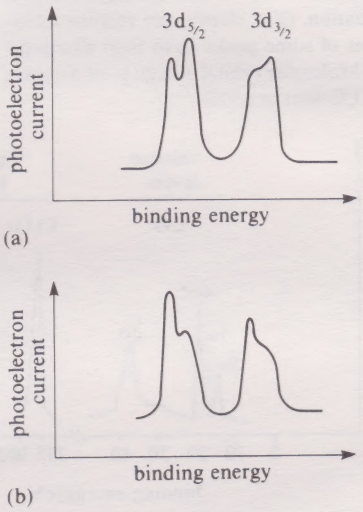

Figure 6 The rhodium 3d signals in the XPS spectrum of a rhodium–charcoal catalyst system: (a) high activity sample; (b) inactive sample.

The rhodium spectra in Figure 6 present two features that you have not encountered before: first, there are *two* 3d peaks (labelled $3d_{5/2}$ and $3d_{3/2}$) and second, each of these peaks is itself split into two. We shall consider each feature in turn.

3.3.1 Spin–orbit coupling

The appearance of two 3d peaks in each spectrum in Figure 6 is due to a phenomenon known as *spin–orbit coupling*. It arises from the interaction between the spin of an electron and its orbital motion, and is magnetic in character. A moving charged particle creates a magnetic field, so an electron possesses a magnetic moment because of its spin: any orbital motion also gives rise to a magnetic field. These two magnetic fields can interact with one another. When they are aligned parallel they reinforce one another, but when they are aligned antiparallel they partially cancel out. This gives two possible energy levels and hence two peaks (a doublet) in the PE spectrum. However, as you have seen from spectra such as the core levels in Figure 4a, not all lines are split in this way: this is because not all electrons possess orbital motion. Electrons in s orbitals have zero orbital motion (the l quantum number equals zero) and so *s-electrons do not show spin–orbit coupling.*

spin–orbit coupling

SFC 4
SLC 2

j, quantum number

What do the labels in Figure 6 represent? The subscripts are values of a quantum number, j, which is given by the so-called 'vector sum'* of the orbital quantum number, l, and the spin quantum number, s. For the case of a single electron, $s = \pm\frac{1}{2}$, and the practical result of the formal definition of j turns out to be:

$$j = l \pm \tfrac{1}{2} \qquad (4)$$

To take an example: for a single electron in a p orbital, $l = 1$, so the j values are given by $j = (1 + \frac{1}{2})$ and $j = (1 - \frac{1}{2})$, that is, $\frac{3}{2}$ and $\frac{1}{2}$.

□ Try the same for yourself for a single electron in a d orbital.

■ You should have got $\frac{5}{2}$ and $\frac{3}{2}$. For a d orbital, $l = 2$, so the j values are given by $(2 + \frac{1}{2})$ and $(2 - \frac{1}{2})$. These are the subscripts on the two different energy levels in the rhodium spectra in Figure 6.

On the other hand, the doubling or splitting of *each* of the signals in Figure 6 indicates the presence of rhodium in two *chemically different* forms on the surface —perhaps rhodium metal and an oxide, Rh_2O_3. This is due to the effect called chemical shift.

3.3.2 Chemical shift

During our earlier discussion of carbon monoxide and carbon dioxide (Section 3.1), we hinted that the binding energies of inner-shell electrons actually change very slightly with chemical environment. These changes can be detected in the kinetic energies of ejected electrons using modern high resolution instruments and are known as *chemical shifts*. The origin of this perturbation lies in the electrostatic interaction between the valence and core electrons. The magnitude and direction of a chemical shift give evidence as to the type of bonding of the atom concerned: a shift is measured as a deviation from the orbital energy value of the free element in its standard state. Here we shall use chemical shifts mainly to study surfaces or indeed atoms or molecules adsorbed on surfaces. Two kinds of example in particular call for our attention.

Non-equivalent atoms. Figure 7 shows an example from inorganic nitrogen chemistry: the spectrum is due to ionisation from N(1s) core levels in sodium azide, NaN_3: notice that *two* peaks are distinguishable. This is because the azide anion, N_3^-, has the structure $[\bar{N}{=}\overset{+}{N}{=}\bar{N}]$, where the two terminal nitrogen atoms are identical but in a different chemical environment from the middle nitrogen atom. This causes the binding energies of N(1s) electrons in the terminal and centre atoms to be different (*both* binding energies will be different again from the binding energy of an N(1s) electron in the free element)—thus we see two peaks. The *approximate* intensity ratio of the two peaks is 2:1, corresponding to two equivalent nitrogen atoms in one environment and one in another.

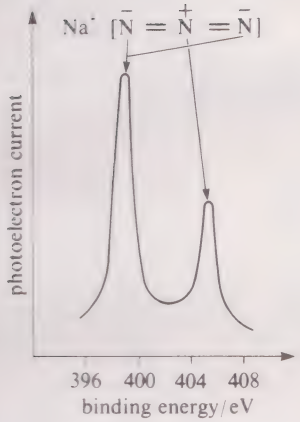

Figure 7 The N(1s) XPS spectrum of sodium azide, NaN_3. Peaks due to positively and negatively charged nitrogen are clearly distinguished.

SAQ 2 Figure 8 shows the N(1s) XPS spectrum of $Na_2N_2O_3$. Three possible structures, **1**–**3**, were originally suggested for the $N_2O_3^{2-}$ anion. Does the XPS spectrum distinguish between these possibilities? (Remember from the Second Level Course† that **1** is a resonance structure with $[\bar{O}{-}\bar{N}{-}O{-}N{=}O]^{2-}$ and consequently is a symmetrical molecule.)

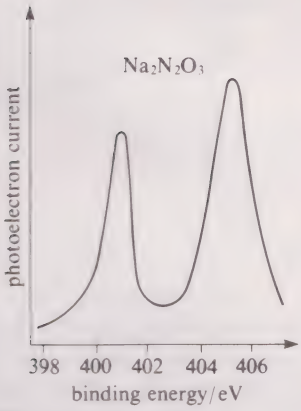

Figure 8 The N(1s) XPS spectrum of sodium oxyhyponitrite, $Na_2N_2O_3$.

$[O{=}N{-}O{-}\bar{N}{-}\bar{O}]^{2-}$ **1**

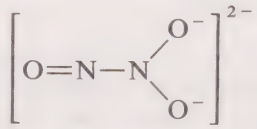

2

$[\bar{O}{-}N{=}N{-}O{-}\bar{O}]^{2-}$ **3**

Trends in bonding. Figure 9 shows the change in chemical shifts for the C(1s) levels of a range of simple gaseous carbon compounds. (The plot shown is actually for calculated chemical shifts versus experimental observations, and it takes the C(1s) level for carbon in methane, CH_4, as the zero reference point, whereas normally it

* Don't worry about this term—*vector* merely means that the quantity has both magnitude *and* direction.
† SLC 3

would be the element carbon.) The whole range of chemical shifts from CH_4 to CF_4 is only 11 eV. The direction the shifts are measured is with *increasing* ionisation energy to the *right* of the diagram.

□ Find CO and CO_2 in Figure 9. In which is the C(1s) electron more strongly held? Can you think of a reason why?

■ The C(1s) electron is more tightly bound in CO_2 than in CO as it lies further to the right of the diagram. Similarly, the C(1s) electron is more tightly bound in CF_4 than in CH_4. These differences in chemical shift can be explained in terms of *electronegativity*.†

The oxygen atom is more electronegative than the carbon atom, and so withdraws electron charge density from the latter. As a consequence the carbon atom becomes slightly positively charged, and it becomes more difficult to ionise the core electrons because their binding energy increases. Since CO_2 has two oxygen atoms, as against the one of CO, this effect is approximately doubled for carbon dioxide, and the binding energy of the C(1s) electrons in CO_2 is correspondingly greater. Figure 9 also shows the effect of the very electronegative fluorine atom on the range of simple fluorocarbons, (CH_4), CH_3F, CH_2F_2, CHF_3 and CF_4, where the increasing electron-withdrawing effect of additional fluorines increases the binding energy of the C(1s) electrons.

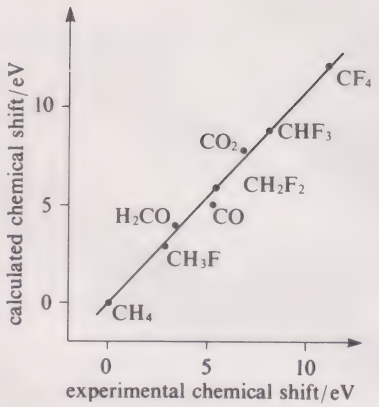

Figure 9 Correlation between calculated chemical shifts for the 1s level of carbon in some small gaseous molecules and the experimentally determined chemical shift.

SAQ 3 Figure 10 shows the C(1s) XPS spectrum of ethyl trifluoroethanoate, $CF_3COOC_2H_5$. Assign each peak to the appropriate carbon atom in the compound.

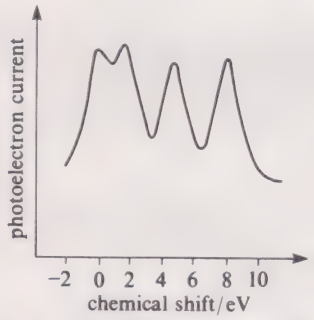

Figure 10 The C(1s) XPS spectrum of ethyl trifluoroethanoate.

The data shown in Figure 9 refer to gaseous molecular compounds. Unfortunately, when XPS chemical shifts are obtained from *solid* compounds, the correlation with the electronegativity of the surrounding atoms is much poorer. There are also other problems associated with the interpretation of XPS chemical shifts in solids. For instance, one example involves different *oxidation states** of a metal. One of the lead oxides, Pb_3O_4, is known from X-ray crystallography studies to contain a mixture of octahedrally co-ordinated Pb(IV) atoms and three-coordinate (pyramidal) Pb(II) atoms in the crystal, yet the Pb(4f) XPS spectrum has only *one* broad peak. The reason for this is obscure: it may be due to the molecular charge distribution; alternatively, it could be due to the fact that XPS is sampling only the *surface* layers and these may have a different composition from the rest of the crystal.

Despite this example, a change in chemical shift for an atom on a solid surface is usually an indication of a change in the chemical environment of that atom. We shall now see how this idea can help us in the study of the ammonia catalyst.

3.4 An XPS study of the ammonia catalyst

In its initial, unreduced form, the multiply-promoted catalyst that is used for ammonia synthesis contains oxygen, potassium, aluminium, calcium and iron. It is then activated by heating it in the presence of nitrogen and hydrogen. What chemical changes occur during activation?

Figure 11 shows the XPS spectrum of the Fe($2p_{3/2}$) core level, for a typical catalyst, at various stages of the activation process. Spectrum 1 was obtained from the starting material, and spectra 2–5 at successive intermediate stages until the final activated catalyst was reached (spectrum 6). The Fe($2p_{3/2}$) peak for metallic iron occurs at about 707 eV, whereas for oxygenated iron compounds, such as Fe_2O_3 and Fe_3O_4, the peak occurs at about 711 eV.

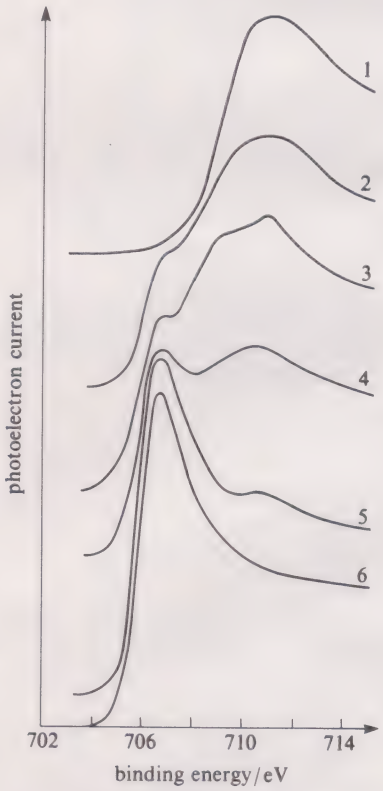

Figure 11 The Fe($2p_{3/2}$) peak in the XPS spectrum of a multiply-promoted ammonia synthesis catalyst at different stages of the activating process: the degree of reduction increases in the sequence 1 ⟶ 6.

□ What happens to the iron in the catalyst during activation?

■ The initial and final Fe($2p_{3/2}$) peaks correspond closely to those of oxygenated and metallic iron, respectively. It seems that oxygenated iron is reduced to metallic iron by the hydrogen.

* SLC 5 † SLC 4

SLC 6

By contrast, XPS studies also show that core binding energies for potassium, aluminium and calcium in the catalyst are unchanged by activation. From the Second Level Course, you know that compounds of these elements are, in general, much harder to reduce to the metallic state than those of iron. This result is therefore not unexpected; potassium, calcium and aluminium presumably remain in an oxygenated form.

In Section 3.2, we noted that XPS can provide us with crude *analytical* information about the surface region. Such data are a weighted average across a probing depth of 1–2 nm and are only semi-quantitative. Nevertheless, they allow us to make interesting comparisons between the composition of the surface region and the composition of the bulk catalyst, which can be determined by orthodox analytical procedures. Table 2 shows information of this kind for an unreduced catalyst.

Table 2 Major surface and bulk compositions (in mole per cent) of an unreduced industrial ammonia synthesis catalyst.

element	Al	K	Fe	O	Ca
surface concentration (per cent)	10	22	4	60	2
bulk concentration (per cent)	2.0	0.35	40.5	53.2	1.7

□ What is striking about these results?

■ The promoting elements, potassium and aluminium, are many times more prominent at the surface than in the bulk. Conversely the principal catalytic element, iron, has a far lower concentration at the surface.

Table 3 shows that, for the most part, these characteristics remain true when we turn to the active, reduced catalyst. However, activation does result in a substantial increase in the surface concentration of iron, although this is still far below the bulk concentration. Note that our conclusion that activation is associated with reduction of oxygenated iron is consistent with the lowering of the concentration of surface oxygen, although on some occasions other changes at the surface nullify this lowering. Clearly XPS is a valuable means of studying surfaces, especially when combined with its sister technique, Auger spectroscopy (pronounced 'Oh-Jhay' in the French manner), which is discussed in Section 4.

Table 3 Major surface compositions (mole per cent) of the catalyst of Table 2 in the reduced and unreduced forms

element	Al	K	Fe	O	Ca
unreduced (per cent)	10	22	4	60	2
reduced (per cent)	13	20	10	50	5

3.5 Summary of Section 3

1 When a substance is irradiated with X-rays, electrons may be ejected from the inner or core levels. If the kinetic energy of the ejected electrons is measured, the orbital energy may be calculated using Koopman's theorem.

2 XPS samples only the top layers of a solid and so is particularly useful for surface studies.

3 Spin-orbit coupling arises from the magnetic interaction of the spin of an electron and its orbital motion. It results in two possible energy levels and hence two peaks in the PE spectrum (except for s electrons.)

4 A peak in the PE spectrum of a compound or an adsorbed molecule may be in a slightly different position from that in the spectrum of the free element, because the binding energy of a particular electron is affected by its chemical environment. These differences, called chemical shifts, can provide information on chemical structure and environment.

5 XPS studies on the ammonia catalyst show that activation involves the *reduction* of iron but not of the promoting elements. In both the reduced and the unreduced catalyst, potassium and aluminium are much more, and iron much less prominent at the surface than in the bulk.

4 AUGER ELECTRON SPECTROSCOPY (AES)

Auger spectroscopy (AES)

Back in 1923, Auger was investigating the trajectories of electrons emitted from argon when it was bombarded by X-rays; he used a Wilson cloud chamber to follow the path of the electrons and he noticed that the emission of an electron was often accompanied by the emission of a *second electron which travelled more slowly.*

Figure 12 shows the electron events that lead to the ejection of such a *secondary* or *Auger electron.* Incident X-rays ionise a core electron (step 1) leaving a *vacancy* or *hole.* An electron from a higher energy level quickly fills this hole (step 2) and in so doing releases a quantum of energy. This released energy can be emitted as radiation which is called X-ray fluorescence, a subject we shall not be pursuing in this Course. However, the released energy can also be reabsorbed by the atom (*now an ion*) and cause a second electron to be ejected (step 3). These secondary or Auger electrons can have a range of kinetic energies which when determined and plotted against intensity give an Auger spectrum. Auger electrons can also be produced when the exciting source is a beam of energetic electrons rather than X-rays. In this situation the exciting electrons are known as the *primary electrons.*

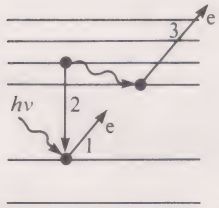

Figure 12 A diagrammatic representation of electron events leading to the ejection of an Auger electron.

primary electrons

4.1 Experimental

As we indicated in the previous Section, Auger electrons can be produced using either X-rays or accelerated electrons as the exciting source; an experimental set-up such as the double-focusing spectrometer shown earlier in Figure 3 can be used to determine their kinetic energies. A *retarding-grid analyser* can also be used to plot their energy distribution: a variable voltage, V, is applied to a grid in the path of the electrons; the potential is increased until the electron flow just stops—the more energetic the electron the higher the voltage needed to stop it—and the spectrum is obtained by plotting V against the measured electron current, I.* This method is also used in the apparatus designed for another physical technique that is discussed later (Section 8.2)—low energy electron diffraction (LEED). Because of this, some research groups find it convenient to combine the Auger and LEED equipment so that both studies can be carried out on the same crystal surface by changing the electron optics. In these circumstances, for Auger spectroscopy an electron gun is employed at 'grazing' incidence (not at normal (90°) incidence as in LEED) to provide energies in the range 2–3 keV; this geometry gives better sensitivity as the low energy Auger electrons are then more likely to escape from the crystal.

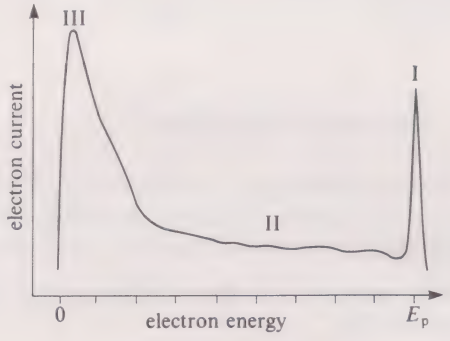

Figure 13 Energy distribution of electrons back-reflected from a surface bombarded by primary electrons of energy E_p.

When a surface is bombarded with a primary electron beam, three distinct regions may be observed in the spectrum (Figure 13). Some of the electrons are *elastically scattered* (that is, the electrons do not lose any energy on scattering): of these, those that are scattered in phase produce the diffraction pattern observed in LEED —seen as the sharp peak, I, in Figure 13. Region II is associated with primary electrons that have undergone energy losses and is known as the *characteristic loss region.* This gives a high background spectrum, which is due to the primary electrons being scattered time and again in their progress through the solid sample and

elastic scattering

characteristic loss region

* Note that the same symbol, I, is conventionally used to represent current and binding energy. Try not to confuse the two uses.

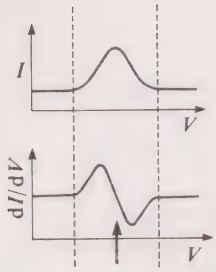

Figure 14 Idealised shapes of detected Auger signals. The peak centre is indicated by an arrow.

losing energy in the process. Region III is concerned with the secondary electrons, where Auger transitions occur. Separation of the Auger peaks from the high background is performed by plotting the first derivative of the collector current, dI/dV, against V†, when they become easily distinguishable—having the characteristic shape shown in Figure 14.

AES has no selection rules—there are no forbidden transitions. Auger electrons rarely have energies greater than 500 eV and so can escape from the sample only if they come from atoms that are close to the surface (about 2 nm or less). Like XPS therefore, the technique is of great value in the study of surfaces. In addition, *each element has a characteristic Auger spectrum* by which it can be identified (this is amplified in the next Section).

For the lighter elements (C, O, N, S) the technique is very sensitive; indeed, in studies where these elements are adsorbed on a surface, the limit of detection is about 10^{13} atom cm^{-2}, less than one hundredth of a monolayer. The intensity of an Auger peak is *approximately* proportional to the surface coverage, and if careful calibrations are made it is sometimes possible to make quantitative measurements. So, like its companion technique XPS, Auger spectroscopy can be used to study surfaces that have atoms or molecules adsorbed on them.

The technique can also detect heavier elements; the main snag here is that the spectra become increasingly complicated as the atomic number increases, as there are more and more energy levels from which transitions can occur. Another, more general drawback of AES is that when an energetic electron beam is used as the exciting source, the surface under study can easily be destroyed: this rarely happens when using X-rays as the exciting source.

4.2 Nomenclature in AES

The notation usually adopted for AES is that commonly used in atomic spectroscopy: the K, L, M . . . shells refer to those with principal quantum number $n = 1, 2, 3 \ldots$ and so on. Numerical subscripts (1, 2, etc.) are attached to these labels in order to indicate the number of *electron states* within the shell, this number being determined by finding the possible values of j—(cf. Section 3.3.1). The simplest example involves one electron in the valence shell, so we shall look at sodium.

The ground-state electronic configuration of sodium is $1s^2 2s^2 2p^6 3s^1$, which gives the electron energy levels:

$$K(1s_{1/2}),\ L_1(2s_{1/2}),\ L_2(2p_{1/2}),\ L_3(2p_{3/2}) \text{ and } M_1(3s_{1/2})$$

The K shell is unsplit because there is no spin–orbit coupling for s electrons. The L shell, however has *three* states: again, the s orbital is unsplit as there is no coupling—this gives the L_1 level. For the electrons in the p orbitals, $l = 1$ so $j = \frac{3}{2}, \frac{1}{2}$ (arising from $j = l \pm s$) giving two states L_2 and L_3. The three L states are numbered sequentially, with the orbitals from which they arise given in brackets afterwards. (For sodium, the L_2 and L_3 states are very close in energy, and are commonly shown as one level, labelled $L_{2,3}$.)

The value of this notation is that it allows us to give a precise description of the processes involved in producing a given Auger electron. Take the process outlined in Figure 15, for example. In step 1, the primary beam causes ionisation from a core level, K, producing a sodium ion, Na^+. In step 2, a 2p electron falls from the $L_{2,3}$ level into the hole created by the initial ionisation, and this releases sufficient energy to knock out a further electron from the $L_{2,3}$ level (step 3) leaving a doubly charged Na^{2+} ion. The Auger electron is then denoted by three letters, placed in order according to its history: (a) the hole produced by the initial ionisation; (b) the source of the electron filling the hole; (c) the source of the Auger electron.

□ Write down the label for the Auger electron emitted in Figure 15.

■ The label is $KL_{2,3}L_{2,3}$.

† In some spectra the conversion from I to N (the number of electrons emitted), and from V to E (the electron binding energy), is made. Such spectra are plotted as dN/dE against E.

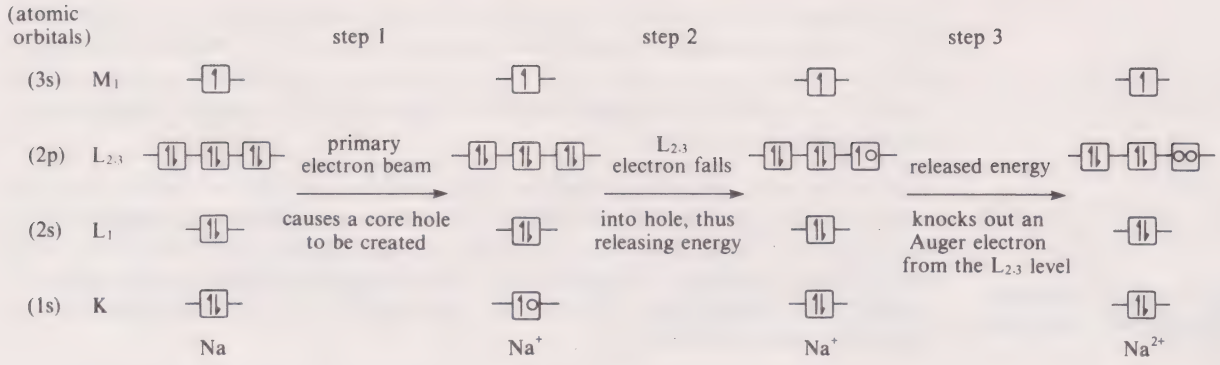

Figure 15 The formation of an Auger electron from sodium.

Many Auger transitions involve the valence shell electrons. Labelling the electron for an *unbonded atom* is no problem—thus in the example in Figure 15 the electron from the valence shell of sodium would be labelled M_1. However, things become rather more complicated in the case of compounds, where the atomic orbitals have now interacted to form bands or molecular orbitals. To get around this complication, electrons from valence orbitals in molecules are simply denoted by the capital letter, V, in the notation.

According to Koopman's theorem, the energy at which the Auger electron is observed is given, to a first approximation, by the difference between the binding energies of the electrons that participate in the process.

□ Try to work out the kinetic energy of the Auger electron, E_{Auger}, for the process $KL_1L_{2,3}$ in sodium. (It helps to write out the sequence of events as in Figure 15, seeing where energy is put in and where it is given out.)

■ For the $KL_1L_{2,3}$ process:

$$E_{\text{Auger}} = \epsilon_K - \epsilon_{L_1} - \epsilon_{L_{2,3}} \qquad \textbf{(5)*}$$

The process is shown in Figure 16: energy $(\epsilon_K - \epsilon_{L_1})$ is released when the L_1 electron falls into the hole in level K; $\epsilon_{L_{2,3}}$ of this energy is then used up in ionising a $L_{2,3}$ electron—this leaves $(\epsilon_K - \epsilon_{L_1} - \epsilon_{L_{2,3}})$, which is imparted to the Auger electron as kinetic energy.

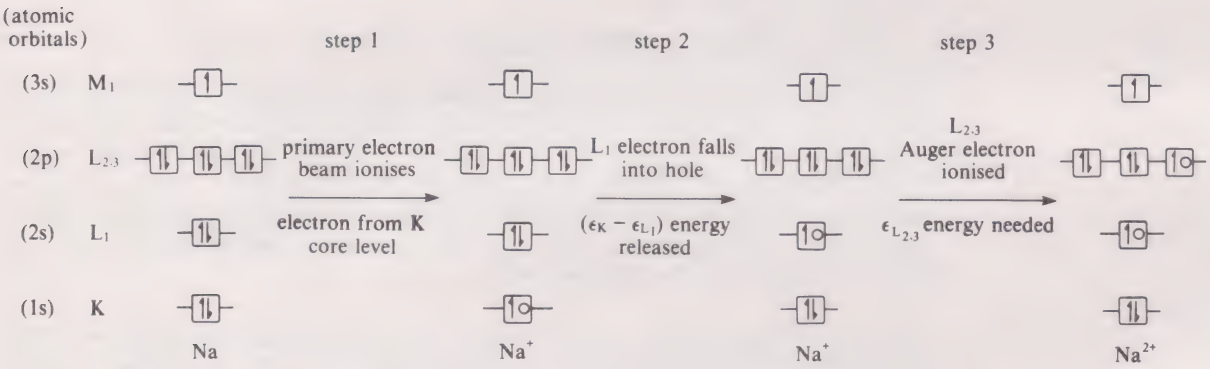

Figure 16 Energy changes in the formation of a $KL_1L_{2,3}$ Auger electron from sodium.

Notice that equation 5 highlights a very important fact, that *Auger electron energies are independent of the energy of the incident radiation.* This enables Auger peaks to be distinguished when they appear in PE spectra, because when the energy of the exciting radiation is changed, the kinetic energies of the photoelectrons change but those of the Auger electrons stay the same. (If electrons are used as the exciting source then this involves accelerating them to a different velocity. If X-rays are used, then in order to change the incident frequency, the X-ray target has to be changed—for instance from aluminium X-radiation (1 487 eV) to magnesium X-radiation (1 254 eV).)

* The binding energies ϵ_K, ϵ_{L_1} and $\epsilon_{L_{2,3}}$ are ionisation energies of the sodium *atom.* In the last step of the Auger process, the electron is lost from a *singly charged ion*, for which the energy levels are different: this introduces an error into equation 5 (which can be corrected for). However, the error is not large enough to prevent the equation being useful for the identification of observed Auger transitions.

As in XPS, each element has a characteristic AES spectrum which can be used for the qualitative analysis of surfaces, including the detection of contamination. For example, Figure 17 shows an Auger spectrum of a titanium sample with peaks due to contamination by phosphorus, sulphur, carbon, oxygen and fluorine. (These elements are probably present in the sample due to the method of preparation, and occur throughout the sample not just on the surface.)

Figure 17 The Auger spectrum of a titanium sample.

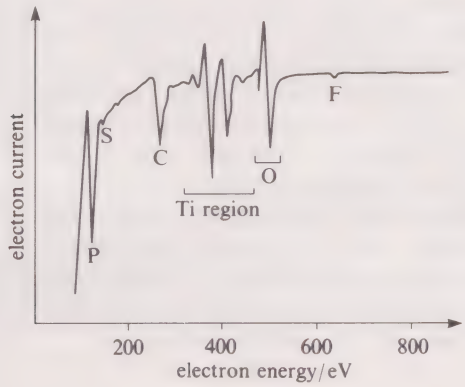

The preparation of atomically clean surfaces by the methods we described in Section 2 has largely been put on a quantitative basis with the availability of AES. In this case, the aim is to see if the pure surface has been recontaminated after cleaning.

SAQ 4 Figure 18 shows the Auger spectrum of a nickel surface. Use the data in Table 4 to determine the impurities present in the sample.

Figure 18 The Auger spectrum of a nickel sample.

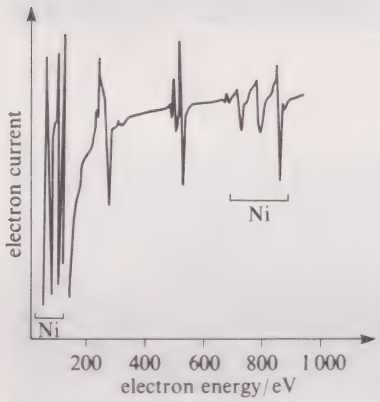

Table 4 Auger electron energies for selected elements

Element	Major peak/eV
carbon	271
nitrogen	379
oxygen	503
fluorine	647
phosphorus	120
sulphur	152
chlorine	181

4.3 Scanning Auger electron spectroscopy

scanning Auger electron spectroscopy

Unlike the X-ray beam used in XPS, an electron beam can be focused by means of electric and magnetic fields. The degree of focusing can be varied to sample different areas of a surface, but at present, the smallest area from which spectra can be collected is about $10^{-14}\,m^2$. In *scanning Auger electron spectroscopy* (*SAES*), a surface area of, say, $10^{-8}\,m^2$ is systematically scanned with the finely focused beam. The electron analyser can be tuned to the energy of a particular Auger transition for a particular chemical element. As the primary beam moves across the surface, the variation in intensity of the emitted Auger electrons is a direct reflection of the distribution of the chemical element within the area which is scanned. As in a television set, the intensity variation can be made visible on a fluorescent screen. This information can therefore provide a map of the distribution of a particular element within a given area of the sample.

sputter-ion etching

SAES instruments can also include a facility for *sputter-ion etching* where the surface is progressively eroded by bombardment with an argon-ion beam. This enables features *below* the surface to be investigated, and also allows the determination of composition as a function of depth into a material—known as

'*depth profiling*'. Effectively, therefore, SAES can provide three-dimensional materials analysis. In the next Section we will see how this has been used in investigating the properties of the ammonia catalyst, but first we will look at an example where such techniques have been used in corrosion investigations.

depth profiling

A copper pipe was found to be badly pitted; an AES study was made on part of a black region of the pipe. The spectrum in Figure 19a shows the *average* composition over the corroded area, and reveals the large amounts of carbon and oxygen (as well as copper, of course), together with many other impurities. Now look at how the spectrum changed after 7.5 nm were ion-sputtered away (Figure 19b). The carbon peak has decreased, but the oxygen and chlorine peaks have increased significantly. Evidently, the carbon was present only in an overlayer (in fact, it came from adjacent pipes carrying fuel oil). The SAES images in Figures 19c—f show how localised the distribution of carbon, oxygen and chlorine is. (The whiter the area, the higher the concentration of the element under study.) Notice particularly, from Figures 19c and 19e, that chlorine occurs in regions where copper is also found, a coincidence probably due to the presence of copper(I) chloride (CuCl). So, the elements responsible for corrosion proved to be oxygen and chlorine. A search for the source of these elements then showed how to protect the pipe.

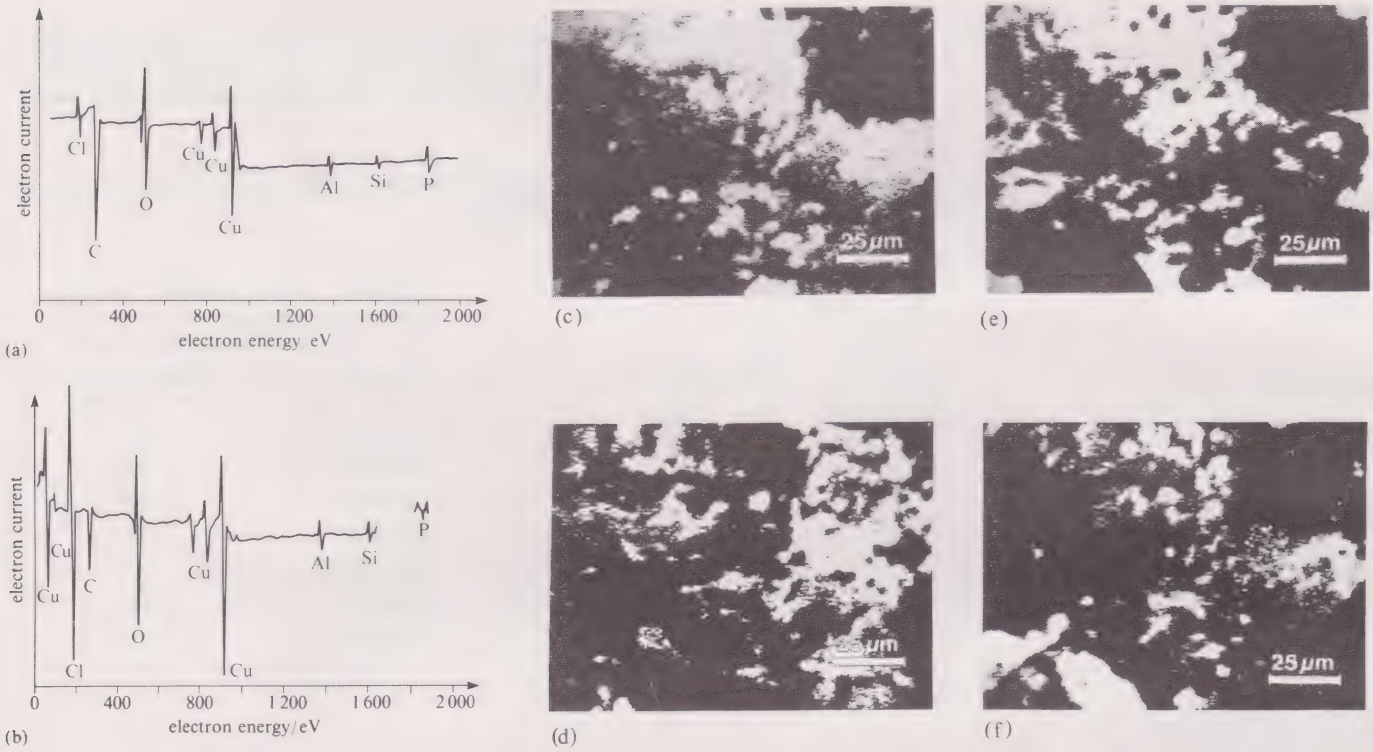

Figure 19 An AES investigation of a corroded copper pipe. (a) The Auger spectrum of the pipe as received; (b) the spectrum after 7.5 nm had been sputter-etched away. (c)–(f) SAES images of an area of the copper pipe for (c) copper, (d) carbon, (e) chlorine, (f) oxygen.

SAQ 5 Figure 20 shows the depth–composition profile for a silicon-based nickel–chromium resistor. The plots are obtained in the following way: an Auger spectrum of the resistor is obtained and analysed to determine the elements present. The peak heights of each element are then plotted against time as the surface is gradually sputtered away, so you can see the change in concentration below the surface (Figure 20a). A suitable calculation translates these peak heights into percentage atomic composition (Figure 20b). The sputter-ion rate was 20 nm per min. Describe the composition at depths of 10, 100 and 200 nm.

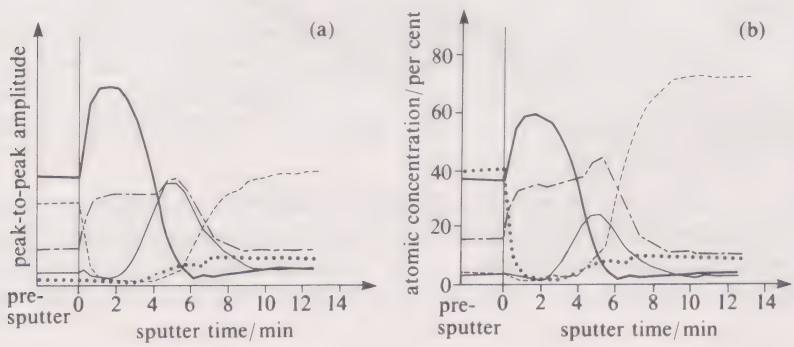

Figure 20 Computer-generated depth–composition profiles of a nickel–chromium resistor plotted as a function of (a) peak-to-peak height and (b) atomic concentration.

oxygen
nickel
silicon
carbon
chromium

4.4 An SAES study of the ammonia catalyst

Figure 21 shows Auger maps for the elements aluminium, calcium, iron and potassium within an area of $10^{-8}\,m^2$ on the surface of the multiply-promoted catalyst used in ammonia synthesis. The following conclusions can be drawn:

1 There are marked lateral variations in the concentrations of all four elements.

2 Calcium and aluminium segregate in areas of their own; in particular, they tend to concentrate in areas where iron is absent. In this respect however, the behaviour of aluminium is not quite so extreme as that of calcium, because a little aluminium is also scattered throughout the iron regions.

3 Potassium mainly occurs where the iron is.

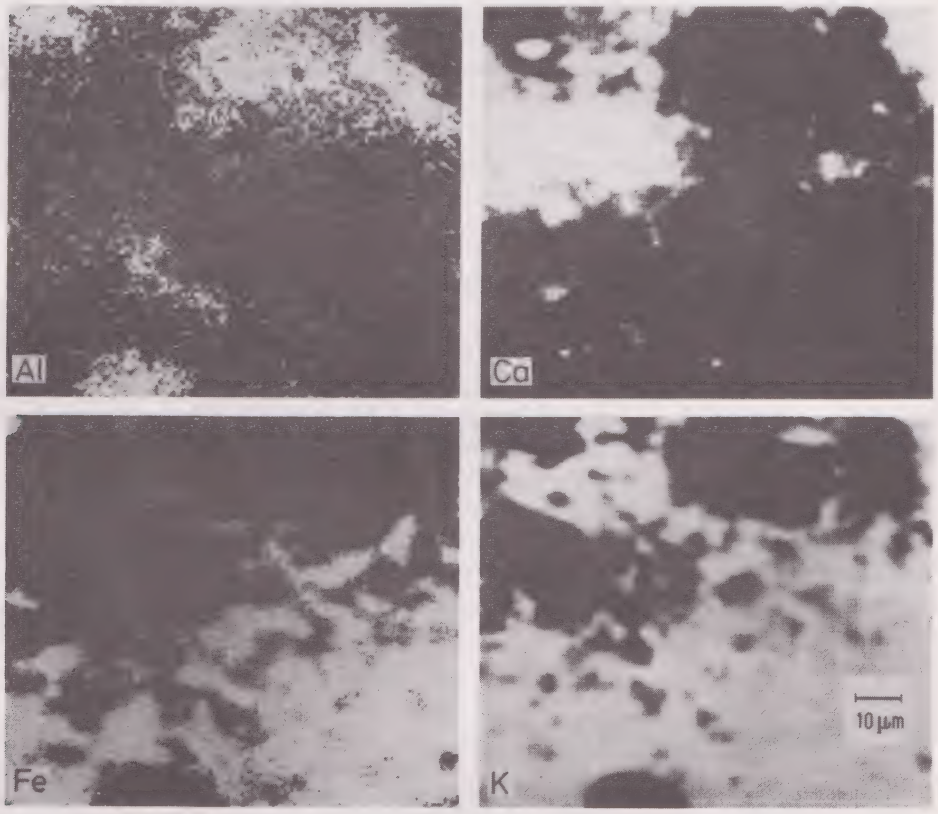

Figure 21 Maps obtained by SAES which show the distribution of aluminium, calcium, iron and potassium within a particular area of $10^{-8}\,m^2$ on the surface of an ammonia synthesis catalyst.

The occurrence of calcium and aluminium at the boundaries of iron regions implies that these elements fill a particular type of promoting role.

What role is that?

It implies that they act as *structural promoters* in the sense described in Block 5: they prevent sintering between iron crystallites during and after the reduction process. Figure 21 suggests that calcium does this in a gross sense by separating relatively large iron regions. To some extent this is also true of aluminium, but its additional fine scattering across the major areas of iron implies a further and more delicate role: oxygenated aluminium helps to break up the major iron concentrates into tiny micro-crystallites. Such conclusions agree with long-standing measurements of the total iron surface area of the reduced catalyst which were made from studies of the chemisorption of carbon monoxide. Figure 22 shows how both the free iron surface area and the ammonia yield vary as the percentage of oxygenated aluminium by weight increases under particular flow conditions.

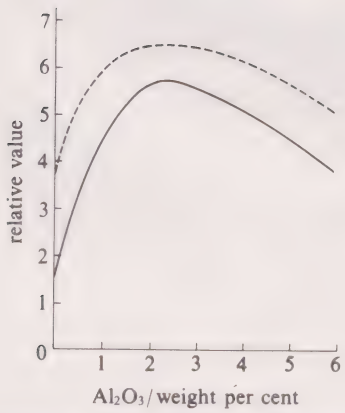

Figure 22 The variation in percentage ammonia yield (dashed curve), and in the free iron surface area (continuous curve) of an Fe–Al_2O_3 catalyst, with Al_2O_3 content.

How is this consistent with the idea that aluminium is a structural promoter?

Both the iron surface area and the ammonia yield reach a maximum in the region of 2.5 per cent Al_2O_3. We presume that at this point, oxygenated aluminium deposits itself in thin layers between small iron crystallites. This prevents sintering,

and leads to a 3–4-fold increase in surface area. Beyond the 2.5 per cent level, oxygenated aluminium presumably begins to cover the iron surface and to prevent chemisorption.

Figure 22 also provides other valuable information. Although several chemical elements are prominent at the surface of the catalyst, it suggests that only one is a strong candidate for the site of the ammonia synthesis reaction.

> Which one is it?

The parallel between the ammonia yield and the free iron surface area suggests that it is iron, which, as you saw in Section 3.4, is present in the metallic state. Iron therefore is the main catalytic element, and aluminium and calcium are structural promoters. This leaves potassium. Its role must be very different from that of aluminium because its presence in an $Fe–Al_2O_3$ catalyst is known to *decrease* the free iron surface area, even though the ammonia yield is increased. This suggests that potassium is a *chemical or electronic promoter* in the sense used in Block 5 (Section 4), and such a view is strengthened by the intimate association of potassium with the main catalytic element, iron, in the Auger maps in Figure 21. More information about this association can be deduced from the observation that quite mild argon ion sputtering causes a drastic reduction in the surface concentration of potassium, but not in that of iron.

> What does this suggest about the spatial distribution of iron and potassium at the surface?

Figure 21 shows that the two elements occur in similar areas of the surface. The sputtering experiment suggests that the potassium (with its bound oxygen) is uppermost, and is therefore preferentially removed. The potassium layer must be very thin, perhaps only a single atom thick, because otherwise, the measured 'surface concentration' of the underlying iron would not approach the 10–20 per cent values determined by AES and XPS. Further discussion of the role of potassium will be deferred until we have learnt more about the mechanism of the reaction.

4.5 Summary of Section 4

1 After an inner electron is lost by an ionisation process a vacancy is created which one of the remaining electrons may fill. The consequent release of energy may cause the ejection of a further electron, known as an Auger electron.

2 The Auger spectrum for each element is well documented, making AES a valuable analytical technique.

3 There are no selection rules in Auger spectroscopy.

4 An Auger peak is labelled according to the three-step process that created it.

5 Because the electron beam in an Auger spectrometer can be focused on small areas, analysis of the Auger electrons can provide a two-dimensional map of the distribution of each element on a sample surface.

6 Ion-sputtering techniques can be used to determine the variation of the concentration of each element with depth.

7 In the active catalyst, iron in the metallic state is the main catalytic element; calcium and aluminium are structural promoters concentrated at the boundaries of the iron surface regions; oxygenated potassium is a chemical or electronic promoter which forms a thin layer over the metallic iron.

SAQ 6 Figure 23a shows points marked 1, 2 and 3 within the area scanned in Figure 21. The Auger electron spectra obtained by focusing on each of these points are shown in Figure 23b–d. Assign each of the three spectra to the point from which it was obtained.

SAQ 7 What would an oxygen Auger map for the area scanned in Figure 21 look like?

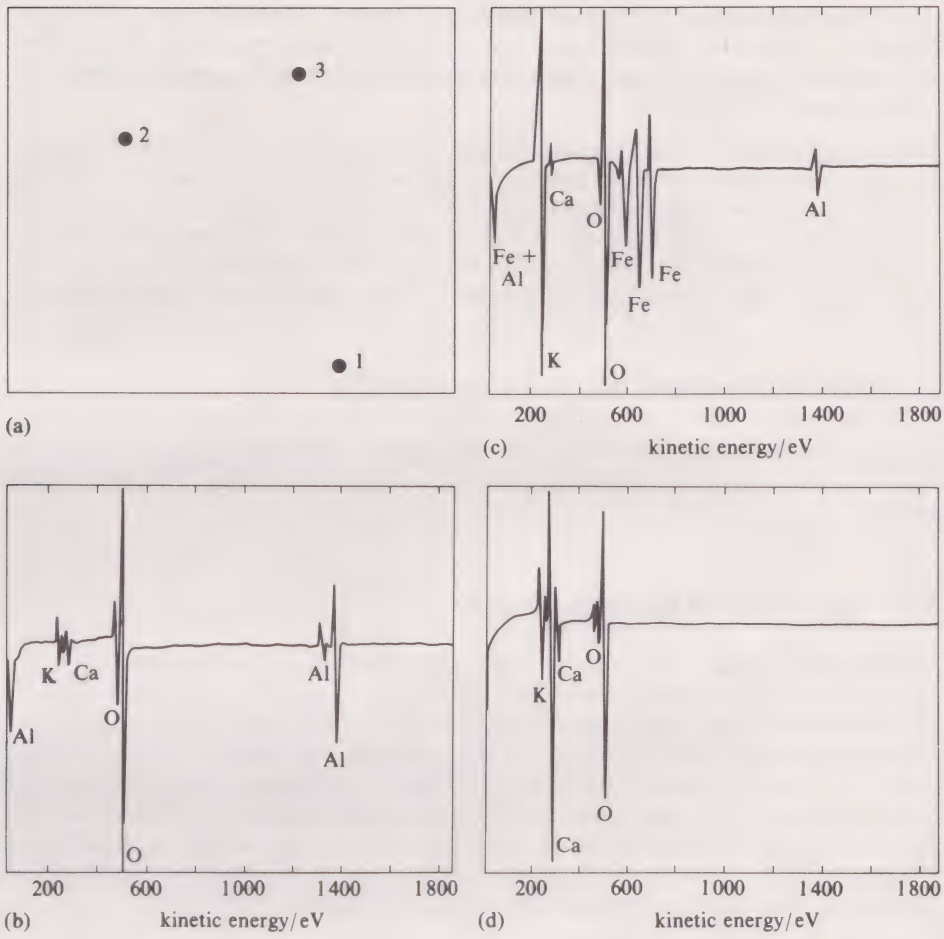

Figure 23 (a) Three points labelled 1, 2 and 3 from within the area scanned in Figure 21; (b), (c) and (d): three spectra, one obtained from each of these three points.

5 ELECTRON SPECTROSCOPY AND THE MECHANISM OF AMMONIA SYNTHESIS

In Sections 3.4 and 4.4, we described how electron spectroscopy is used to examine the catalyst surface. Now we shall see what light it throws on the mechanism of ammonia synthesis by investigating the species that the catalyst surface adsorbs. However, the approach that we shall use has certain weaknesses, and before continuing, it is only proper to mention these.

First, there is some danger that the radiation used during electron spectroscopy might damage surface layers. This danger is greater with AES whenever the exciting radiation is an electron beam, so this is a strong argument for supplementing AES experiments of this kind with XPS whenever this is possible. Second, there is a problem that the new techniques share with traditional kinetic measurements: only the most stable surface intermediates are detected. Yet less stable intermediates, with very short lifetimes and tiny concentrations, may play a vital role in the mechanism.

However, the most serious weakness of the approach followed in the rest of this Block is that it is remote from the world of the real industrial process. This remoteness is of two kinds. First, we have seen that the surface of the industrial catalyst shows complicated lateral variations in composition and crystalline form. It is hard to draw mechanistic conclusions about such a surface, and it is often necessary to simplify the system. For this reason, many of the experiments that we shall describe have been performed on pure metallic iron, or even on a particular surface of a crystal of the metal. Second, we are interested in the mechanism of a process that is performed at pressures of about 200 atm, but the operating pressure of our modern surface techniques cannot exceed 10^{-6} atm, and is often very much less. How then do we know that the information provided by the techniques is relevant at indus-

trial operating pressures? This difficulty is, of course, a general one which is not peculiar to ammonia synthesis, and it is known as the 'pressure gap'. As we shall see, however, there is evidence that in the particular case of ammonia synthesis, the pressure gap is bridgeable.

Because the process involves the reaction of *two* gases to form a product on a metal surface, there are several experiments that are worth doing. We could for instance investigate an iron surface after exposure to N_2, to H_2, to N_2/H_2 mixtures, or to NH_3. However, over 50 years ago it was established that, at the same temperature and nitrogen pressure, the initial rate of adsorption of nitrogen alone on the catalyst is similar to the initial rate of ammonia synthesis when some hydrogen is present.

What important conclusion does this suggest?

It suggests that adsorption of nitrogen includes the rate-limiting step in ammonia synthesis. We therefore look first at the adsorption of nitrogen on a clean iron surface.

5.1 Adsorption of nitrogen on iron

Suppose that a clean iron surface at 100 K is briefly exposed to flowing nitrogen at 10^{-7} atm, and the XPS spectrum of the surface is recorded. The immediate result is the appearance of a single peak at 399.0 eV in the N(1s) region of the spectrum. Interesting changes occur, however, if the surface is now treated in two different ways. First, the exposure at 100 K and 10^{-7} atm is prolonged, and the pressure is then reduced to 10^{-12} atm. The only N(1s) peak now appears at 397.0 eV. Second, after the initial exposure at 100 K, the temperature of the surface is steadily increased to 300 K. Most of the adsorbed nitrogen desorbs at about 160 K, but a little is retained, and at 300 K, there is only a single N(1s) peak at 397.0 eV.

Can you suggest a molecular interpretation of these results?

In Block 5 (Section 8.3), you saw that the physical adsorption of dinitrogen, at temperatures close to 80 K, is often used in the BET method for the determination of surface area. So the low temperature of 100 K used here suggests that the rapidly appearing adsorbed species that gives rise to the signal at 399.0 eV is N_2(ad). As expected, this is weakly held, because neither the desorption at 160 K nor the evacuation to 10^{-12} atm at 100 K leaves any trace of it on the surface. However, during a prolonged exposure at 100 K, or during heating, some N_2(ad) seems to be converted, relatively slowly, into a different species. This species is strongly held by the surface and gives an N(1s) XPS signal at 397.0 eV. An obvious proposal to test is that this signal is due to adsorbed monatomic nitrogen: does N_2(ad) dissociate on the iron surface at 100 K to give adsorbed atoms?

More definite evidence of the origin of the 397.0 eV signal is provided by a study of iron nitride, Fe_4N. Under normal conditions, the reaction

$$4Fe(s) + \tfrac{1}{2}N_2(g) = Fe_4N(s) \qquad (6)$$

is thermodynamically unfavourable, but the compound can be made by heating iron with ammonia:

$$4Fe(s) + NH_3(s) = Fe_4N(s) + \tfrac{3}{2}H_2(g) \qquad (7)$$

Thus when a hot iron surface is exposed to pure ammonia, layers of Fe_4N are deposited on the surface. The XPS spectrum of these surface layers contains a single N(1s) peak at 397.0 eV. The *unit cell* of Fe_4N is shown in Figure 24.

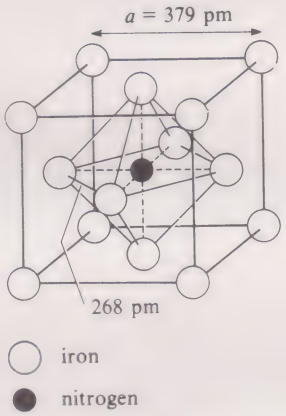

Figure 24 The unit cell of Fe_4N; the nitrogen coordination is picked out with dashed lines.

SLC 7

□ To what species can the 397.0 eV peak be assigned?

■ Since it occurs in the XPS spectrum of Fe_4N, and since Fe_4N contains monatomic nitrogen (Figure 24), we assign the N(1s) peak at 397.0 eV to monatomic nitrogen bound to iron.

It is clear that the adsorbed monatomic nitrogen is very strongly held on the iron surface. The 397.0 eV signal appears, for example, when the iron surface is exposed to gaseous nitrogen at temperatures as high as 700 K.

5.2 Adsorption of hydrogen on iron

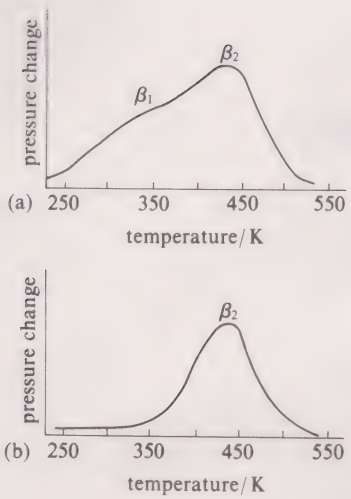

Figure 25 Thermal desorption spectra for hydrogen on Fe(110): (a) after saturation of the iron surface at 140 K; (b) after 3 minutes exposure to 10^{-10} atm of hydrogen at a surface temperature of 345 K.

Measurements at fixed temperatures in the 130–600 K range show that the rate of adsorption of hydrogen on iron is many times greater than that of nitrogen. Here we shall be concerned only with the state of the hydrogen on the surface. To this end, Figure 25a shows a thermal desorption spectrum, of the kind discussed in Block 5 (Section 6.3.3), for a particular iron surface saturated with adsorbed hydrogen. The surface is labelled Fe(110): this notation is explained in Section 6.2. The peak at about 430 K, and the shoulder in the 340 K region indicate two adsorption states labelled β_2 and β_1, respectively, containing similar amounts of hydrogen.

□ When the clean iron surface is exposed to hydrogen, which state will tend to be filled first?

■ The state most stable to desorption is the one most strongly held, that is the one with the highest desorption temperature. This is β_2 and it will tend to be filled first.

In fact, a controlled exposure of 3 minutes to H_2 at about 10^{-10} atm and 345 K saturates the β_2 state, but keeps β_1 empty. This is evident from the desorption spectrum of the surface after such an exposure (Figure 25b).

If the sample with β_2 full is then cooled to 140 K, and exposed to D_2 (deuterium) at 10^{-10} atm for 45 minutes, the β_1 state is now filled. The thermal desorption spectrum then looks like Figure 25a. During desorption, adsorbed gas is first obtained mainly from β_1, and then mainly from β_2. However, the gas compositions at these two different stages are identical: in both cases, the desorbed gas consists of H_2, HD and D_2 in the molar ratio 1:2:1.

What does this suggest about the condition of the adsorbed hydrogen?

Before the desorption temperatures are reached, the hydrogen and deuterium have distributed themselves evenly throughout the β_1 and β_2 states. This suggests a complete mobility of adsorbed gas on the surface. The two-fold proportion of HD is discussed in more detail in the answer to SAQ 8; here we merely note that the high value shows that by the time of detectable desorption, at temperatures around 250 K, the H—H and D—D bonds of the original gas molecules have been broken. This indicates that, at the temperature of ammonia synthesis, any hydrogen adsorption is dissociative, the hydrogen being bound on the surface in a monatomic state. The same conclusion is drawn from studies of hydrogen adsorption on iron surfaces other than Fe(110). We shall return to the nature of the β_1 and β_2 states in Section 8.4.4.

5.3 Adsorption of ammonia on iron

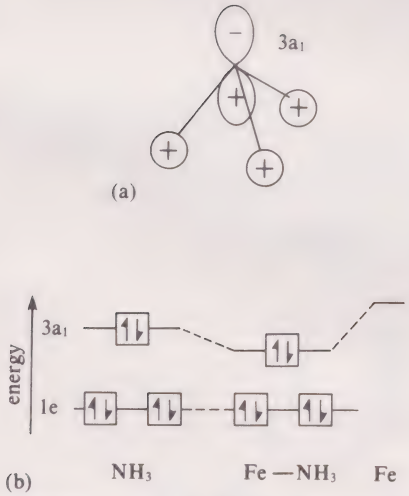

Figure 26 (a) The moderately bonding $3a_1$ molecular orbital in ammonia; (b) orbital energy level diagram for bond formation between an ammonia molecule and an iron surface.

If ammonia synthesis follows a particular reaction pathway, then under the same conditions, the backward reaction, the decomposition of ammonia into nitrogen and hydrogen, must retrace this pathway. (This is a simple consequence of the Principle of Microscopic Reversibility, which is not covered in this Course.) We can therefore get useful information about the mechanism of ammonia synthesis by studying the adsorption and decomposition of ammonia on iron. Some especially useful results have been obtained from UPS which, as you know from Section 3.1, provides information about the energies of valence molecular orbitals.

The UPS spectrum of gaseous ammonia contains two broad bands centred approximately on 11 and 17 eV. The first band is assigned to an ionisation from the highest occupied molecular orbital which is formed by combining the nitrogen $2p_z$ and hydrogen 1s orbitals (Figure 26a). This molecular orbital is bonding, though only moderately so, and is labelled $3a_1$†. As you can see, it generates considerable electron density along the three-fold axis of the molecule on the side remote from the hydrogen atoms. Not surprisingly, therefore, its electrons are the nearest molecular orbital equivalent to the nitrogen lone pair in the simple Lewis structure of ammonia. The second band, at 17 eV, is assigned to an ionisation from a more strongly bonding, degenerate pair of orbitals labelled 1e. They are formed by combining the nitrogen $2p_x$ and $2p_y$ orbitals with the hydrogen 1s orbitals. The $3a_1$ and 1e energy levels are shown on the left of Figure 26b.

SLC 8

† This notation was introduced at Second Level, but do not worry if you have forgotten its precise meaning. Here it is used merely to label orbital energy levels.

What sort of bond might be formed when ammonia is chemisorbed on a transition metal surface?

One possibility is that ammonia might form a σ-bond by donating the nitrogen lone pair to a vacant orbital on the metal surface. As shown in the Second Level Course, this type of bonding is found in compounds like $H_3\overset{+}{N}—\overset{-}{B}F_3$, for example. Now, the separation of the two bands in the UPS spectrum of ammonia is about 6 eV.

SLC 9

□ Would you expect this separation to increase or decrease on chemisorption?

■ In the molecular orbital version of our picture of chemisorption, donation of the nitrogen lone pair must be represented by formation of a bonding orbital from the $3a_1$ orbital of ammonia and a vacant orbital on the metal surface. Since the 1e orbitals are not involved in this process, the band separation should be reduced (see Figure 26b).

In Figure 27, spectrum 1 is the UPS spectrum of a clean Fe(110) surface. Spectrum 2, which was obtained after ammonia adsorption at 175 K, contains two bands centred on 6.6 and 11.2 eV; these are attributed to non-dissociatively adsorbed ammonia. The absolute energies of these bands are quite different from those obtained for the gaseous molecule because the two energy scales have different zeros: in Figure 27 the energy zero is an energy level of metallic iron labelled E_F. However, the energy *separations* of the bands can still be usefully compared, and as we predicted, it is less for the adsorbed ammonia.

If after ammonia adsorption at 175 K, the temperature is then raised above 400 K, spectrum 4 results. The single peak at about 4.8 eV is also observed after nitrogen adsorption on iron at room temperature and above.

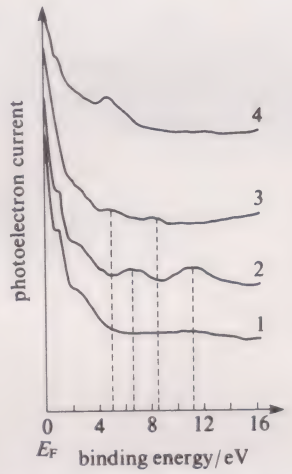

Figure 27 UPS spectrum of ammonia adsorbed on Fe(110): (1) clean surface; (2) after ammonia adsorption at 175 K; (3) after exposure to ammonia at 350 K; (4) after ammonia adsorption at 175 K followed by warming to 450 K.

□ To what do you attribute this peak?

■ At higher temperatures, nitrogen is adsorbed dissociatively on iron, so the 4.8 eV peak is due to N(ad). On warming, adsorbed ammonia must decompose to give adsorbed monatomic nitrogen.

Spectrum 3 is obtained after exposure of the surface to ammonia at intermediate temperatures of about 350 K. The peaks at 5.0 and 8.5 eV differ from those observed for either N(ad) or NH_3(ad).

What might they be due to?

They are presumably intermediates in the decomposition of NH_3(ad) to give N(ad). Obvious possibilities are NH_2(ad) and NH(ad). The identification problem has been tackled by mass spectrometry, which you met in the Science Foundation Course. The iron surface was exposed to ammonia at room temperature, and then periodically bombarded with argon ions as the temperature was slowly increased through the 350 K region. Some of the adsorbed species were detached and ionised by the ion bombardment, so they could then be detected in a mass spectrometer. Figure 28 shows the variation, with temperature, of the signals for the ions NH^+ and $NH_3{}^+$: the signal for $NH_2{}^+$ was negligible. These signals are a measure of the relative surface concentrations of the neutral adsorbed species.

SFC 3

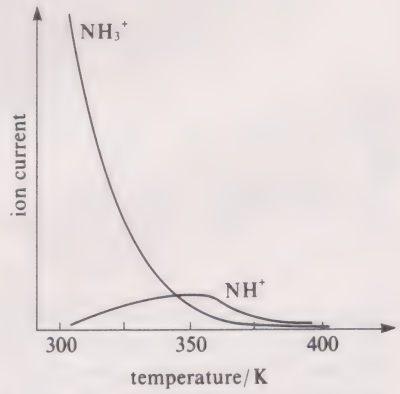

Figure 28 The variation with temperature of the mass spectrometric signals for NH_3^+ and NH^+, obtained by argon-ion bombardment of an Fe(110) surface that had been exposed to ammonia at 300 K.

Clearly, ammonia is non-dissociatively adsorbed at room temperature but complete desorption occurs at less than 390 K. At 350 K its surface concentration is small, and the only other detectable adsorbed nitrogen species is NH(ad). The latter must therefore be responsible for the bands at 5.0 and 8.5 eV in the UPS spectrum at 350 K. Above 350 K, NH begins to decompose to monatomic nitrogen which, as you have just seen, can also be detected by UPS.

At this point therefore, we have examined the individual adsorption, on iron, of the three major gaseous constituents of the ammonia synthesis equilibrium. We now turn to studies of the synthesis reaction itself.

5.4 Ammonia synthesis on an industrial catalyst

The experiments described in Sections 5.1–5.3 were performed at very low pressures on pure iron surfaces. We shall now try to get closer to genuine synthetic conditions by describing experiments in which a 1:3 molar mixture of nitrogen and hydrogen at about 1 atm pressure is allowed to equilibrate over a multiply-promoted activated iron catalyst at 630 K.

In the first experiment, the gaseous mixture formed at equilibrium is pumped off while the catalyst remains at 630 K. Figure 29a shows the XPS spectrum in the N(1s) region.

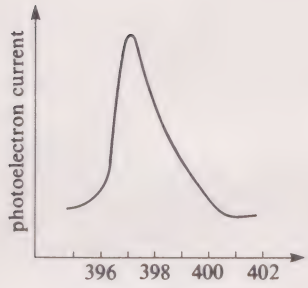

(a)

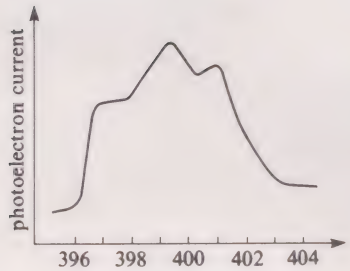

(b)

Figure 29 XPS spectra of an industrial catalyst used for ammonia synthesis following equilibration with a 1:3 molar mixture of N_2 and H_2: (a) after evacuation at the reaction temperature of 630 K; (b) after cooling to room temperature followed by evacuation.

☐ What species is present?

■ From Section 5.1, the peak at 397 eV is characteristic of monatomic nitrogen bound to iron.

It seems then, that after evacuation at 630 K, this is the only nitrogen species left on the iron surface. It is obviously very strongly held: in fact, it disappears only on evacuation at temperatures above 700 K.

Suppose now that after equilibration at 630 K, evacuation is performed not at 630 K, but after cooling to room temperature. The XPS spectrum of the surface is then as shown in Figure 29b. The 397 eV peak is now present as a shoulder, and there are two additional N(1s) peaks at 399 and 401 eV. The latter is virtually identical with the peak energy of an iron surface exposed to ammonia at 126 K, so we assign it to NH_3(ad). The remaining peak at 399 eV has been attributed to either NH or NH_2, but when the surface is slowly reheated, the 401 eV peak disappears at about 370 K, followed by the 399 eV peak at 470 K. The spectrum then looks like Figure 29a—only monatomic nitrogen remains.

Thus at synthesis temperatures of about 630 K on a real industrial catalyst, monatomic nitrogen is the only surface species stable to evacuation. The evidence in this Section shows that other nitrogen species are desorbed below 500 K, and Section 5.2 suggests that this is also true of adsorbed hydrogen.

This resistance of monatomic nitrogen to desorption leads us to an important result. If we carry out ammonia synthesis at something like working industrial pressures and temperatures, evacuate while the catalyst remains hot, and then determine the surface concentration of adsorbed gas, this should resemble the surface concentration of adsorbed atomic nitrogen under the *original reaction conditions.*

Careful experiments of this kind have been performed on pure iron catalysts using AES for the analysis. A KVV Auger transition for nitrogen occurs at about 380 eV, and a prominent LMM peak for iron is observed at 650 eV. The intensity ratio of these two peaks is a measure of the N:Fe mole ratio within the escape depth of the Auger electrons. Let us label it ρ. A calibration discussed later in SAQ 20 shows that a value of $\rho = 0.9$ corresponds to N:Fe = 1:2. Now, when a 1:3 N_2:H_2 mixture at 1 atm and 580 K reacts for 30 minutes over the Fe(111) face of an iron crystal, steady-state conditions for ammonia synthesis are reached on the catalyst. After evacuation at 580 K, ρ is typically about 0.1.

What does this tell you about the nitrogen coverage at the steady state?

When $\rho = 0.9$, N:Fe = 1:2, so when $\rho = 0.1$, the N:Fe ratio is about 1:18; the coverage is small, and very far from saturation. In addition, crude XPS analyses have been used to determine N:Fe ratios on a real industrial catalyst after the equilibrations at 1 atm and 630 K described earlier in this Section. Again, the values are only about 1:15. We shall see the importance of this point in the next Section; here we simply note that we can establish it because of a fortunate combination of desorption temperatures in which monatomic nitrogen *alone* is retained under evacuation. Thus, in these particular studies of ammonia synthesis, the 'pressure gap' can be bridged.

5.5 A possible mechanism

We have shown that nitrogen undergoes dissociative adsorption on iron, and that as the temperature is lowered there is evidence of an adsorbed molecular precursor for the monatomic state. In Section 5.2, hydrogen was shown to adsorb dissociatively, and in Section 5.3 we described how N(ad), NH(ad) and NH_3(ad) can be detected during ammonia decomposition on iron. Most of this evidence was obtained at temperatures well below 550 K, so during industrial ammonia synthesis, the surface concentrations of N_2(ad), H(ad) and NH_3(ad) will probably be small. However, as noted in Section 5, important intermediates may well be present in very low concentrations, so this does not prevent us from including them in a mechanism. The evidence therefore favours the following mechanistic scheme:

$$H_2(g) \longrightarrow 2H(ad) \quad (8)$$

$$N_2(g) \longrightarrow N_2(ad) \quad (9)$$

$$N_2(ad) \longrightarrow 2N(ad) \quad (10)$$

$$N(ad) + H(ad) \longrightarrow NH(ad) \quad (11)$$

$$NH(ad) + H(ad) \longrightarrow NH_2(ad) \quad (12)$$

$$NH_2(ad) + H(ad) \longrightarrow NH_3(ad) \quad (13)$$

$$NH_3(ad) \longrightarrow NH_3(g) \quad (14)$$

Of the species in these equations, there is only one for which we have not found evidence: this is NH_2(ad), which is discussed in SAQ 10.

In Sections 5, 5.1 and 5.3, we have given reasons for believing that step 10 is rate-limiting. This can now be reinforced. Suppose that step 10 was not rate-limiting, but was faster than the subsequent hydrogenation in steps 11–13.

> Would the surface concentration of N(ad) during ammonia synthesis be large or small?

It would steadily build up to a value close to saturation because removal of N(ad) by steps 11–14 would be slower than its formation by step 10. On the other hand, if step 10 is rate-limiting, and therefore slower than the subsequent hydrogenations, the surface concentration of N(ad) will be small. As we have seen, this is the case.

Again, for many years, some chemists supported an alternative mechanism in which the rate-limiting step was the *associative* adsorption of nitrogen. This was then followed by fast hydrogenation of N_2(ad).

> What would happen to the surface concentration of N(ad) if this mechanism was correct?

Electron spectroscopy tells us that step 10 occurs. If the associative mechanism were correct, there would be some steady conversion of N_2(ad) into N(ad) and the latter's concentration would build up towards a saturation value. As this does not happen, the associative mechanism is ruled out.

Finally, the kinetics of ammonia synthesis is a complicated problem which we shall not discuss. All we will do is to note that our proposed mechanism is, in fact, quite consistent with those rate laws that have been worked out.

5.6 Summary of Section 5

1 Gaseous nitrogen undergoes dissociative adsorption on iron at temperatures of 100 K and above. The adsorption proceeds through a rapidly formed, adsorbed molecular precursor, which subsequently dissociates relatively slowly.

2 Above about 150 K, hydrogen undergoes very rapid dissociative adsorption on iron. The gas is thermally desorbed below 500 K *in vacuo*.

3 During the adsorption and subsequent decomposition of ammonia on iron, NH_3(ad), NH(ad) and N(ad) can be detected on the surface of the catalyst by UPS and mass spectrometry.

4 The species N(ad) is very strongly held on an iron surface. Its very high desorption temperature enables us to bridge the pressure gap and determine its concentration on the catalyst surface under conditions approaching those used in industrial ammonia synthesis. This concentration is well below the saturation value.

5 Our proposed mechanism of ammonia synthesis is the one embodied in steps 8–14. Step 10 is rate-limiting.

SAQ 8 The molecules $^{28}N_2$ and $^{30}N_2$ are composed of ^{14}N and ^{15}N atoms, respectively. A 1:1 molar mixture of $^{28}N_2$ and $^{30}N_2$ is adsorbed on an iron surface at 125 K. Thermal desorption then occurs at about 160 K, and the evolved gas is a 1:1 mixture of $^{28}N_2$ and $^{30}N_2$. However, if the initial adsorption is performed at 300 K, thermal desorption requires a temperature of 800 K, and the evolved gas is a 1:2:1 mixture of $^{28}N_2$, $^{29}N_2$ and $^{30}N_2$. Explain.

SAQ 9 In Section 5.4, an industrial catalyst, cooled to room temperature after equilibration with N_2 and H_2 at 630 K, gave an N(1s) signal at 399 eV. Why can this signal not be assigned to N_2(ad) which, as we saw in Section 5.1, has an N(1s) peak at 399.0 eV?

SAQ 10 The Fe(110) surface studied in Section 5.3, when exposed to ammonia at 130 K, gives an N(1s) peak at 401 eV. However, exposure at 350 K gives a peak at 397.3 eV which, when the surface is heated to 500 K, narrows and shifts to 397.0 eV. Try to assign these peaks to surface species proposed in Section 5.3, and then, by a process of elimination, suggest an assignment for the 399 eV signal mentioned in SAQ 9.

6 THE STUDY OF SINGLE CRYSTALS

We now turn to the detailed structural changes that take place during adsorption on the catalyst surface. We shall be especially interested in whether the relative positions of the surface iron atoms are altered during adsorption, and in how the nitrogen atoms are arranged at the solid–gas interface. Thus we need to know the initial arrangement of the surface iron atoms *before* adsorption begins. This knowledge will be denied to us if we study a normal catalyst because the iron on which the reaction occurs is *polycrystalline*. The numerous crystals will expose many kinds of crystal face or plane at their surfaces, and on each different plane there will be a different arrangement of iron atoms.

The solution to this problem is to study *single* crystals of iron, which under normal conditions are body-centred cubic. If we prepare such crystals, we shall then be able to select a particular crystal plane on which the atomic arrangement is known, and investigate adsorption and reaction on it. To discuss the results of these investigations, however, we must first revise your knowledge of crystal structures and then introduce a very elegant notation which is used to specify and distinguish the individual crystal planes.

6.1 Crystal structures of metals

As you may recall from the Second Level Course, the crystalline structure of a solid consists of a periodically repeating array of atoms, molecules or ions. The metal structures in which we are particularly interested are restricted to three types: *body-centred cubic* (b.c.c.), *cubic close-packed* (c.c.p.)—otherwise known as *face-centred cubic* (f.c.c.)—and *hexagonal close-packed* (h.c.p.).

SLC 10

SAQ 11 (*revision*) Try to describe briefly (using diagrams if necessary) each of the three structures mentioned above, that is: (a) body-centred cubic; (b) cubic close-packed; and (c) hexagonal close-packed. What is the *coordination number* of an atom in the bulk (interior) of each of these structures? If the top face of the unit cell forms the metal surface in each case, how does the coordination number vary from the bulk to the surface?

SLC 11

6.2 Miller indices

When crystals are split, they often cleave so that the crystal faces are either parallel to the sides of the unit cell or parallel to planes in the crystal that contain a high density of atoms or ions. Similarly, crystals tend to grow with faces parallel to the unit cell or to high density planes.

Miller indices

SLC 12
SLC 13

It is convenient to be able to refer to the crystal surfaces in some way—to give them a label. This is normally done by using *Miller indices* to define the orientation of crystal faces (planes) with respect to the chosen unit cell. We'll see how this notation is developed by considering a *two-dimensional lattice* for simplicity. For example, Figure 30 shows a *square net*, where each lattice point represents an identical environment in the crystal, and *so could represent one atom, ion, molecule or part of a molecule in a section through a crystal.*

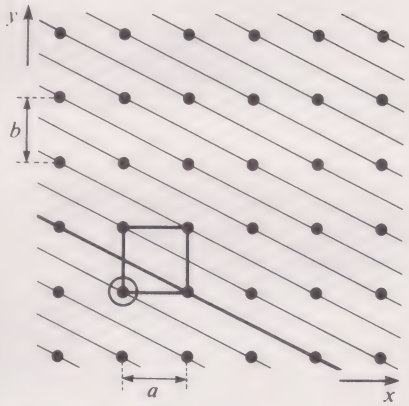

Figure 30 A square net showing a unit cell of side a and a set of lines.

A two-dimensional net is defined by the directions of the axes x and y, the angle between them γ and the repeat distances a and b (a is the repeat distance in the x direction and b in the y). In Figure 30, $a = b$ and $\gamma = 90°$—so this is called a square net. A unit cell is marked on the diagram with an (arbitrary) origin marked by a circle. The *set* of parallel lines shown can be defined by two indices, given the symbols h and k, where h and k are the number of parts into which a and b, the unit cell edges, are divided by the lines. More formally, we define the indices (hk) of a line so that the line intercepts a at a/h and b at b/k. For example, if the line cuts a in half, the intercept is $a/2$ and therefore the h index equals 2. The best method to adopt for determining the indices is as follows (refer to Figure 30):

1 Locate the line passing through the origin of the unit cell;

2 Find the line *next to this one* and see how it divides each cell edge adjacent to the origin;

3 Decide whether the position of the intercepted cell edge is positive or negative with respect to the origin and the direction of x or y.

□ In Figure 30, how are a and b divided by the heavy line? What are the indices of the set of lines?

■ The heavy line leaves a undivided but divides b into two: both cell edges lie on the positive side of the origin. The indices (hk) of the set of lines are therefore (12), spoken of as the 'one-two' set of lines.

If a line is parallel to a unit cell edge, there is no intercept at all in that direction and the index becomes zero. If the intercepted cell edge lies on the negative side of the origin then the index has a bar on top (like a negative sign, only on top instead of at the side); for example $(1\bar{2})$, called the 'one-bar-two' lines.

SAQ 12 Figure 31 shows four different sets of lines drawn on a *rectangular* net ($b \neq a$, $\gamma = 90°$). What are the indices of these lines?

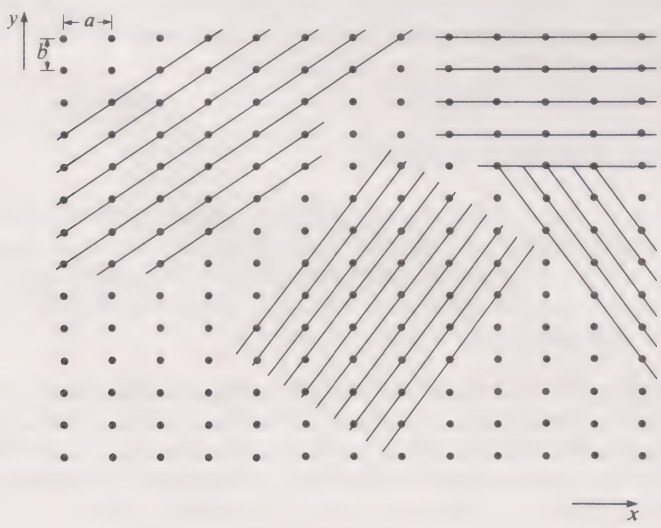

Figure 31 A rectangular net showing four sets of lines.

☐ Look again at Figure 60, in the answer to SAQ 12. What relationship do you see between the density of lattice points on the lines, the spacing of the lines, and the values of the indices?

■ The lines with the highest density of points are wider spaced and have lower number indices. Lines with high indices are more closely spaced and have a lower population of points.

The rules for Miller indices in three dimensions (*hkl*)—where *l* is the index referring to the *z* direction—are a simple extension of those above, so let's try an example. Figure 32 shows various sets of planes marked on two adjoining unit cells of a face-centred cubic lattice of cell length *a*. The positive directions of the *x*, *y* and *z* axes are shown and these conform to the conventional *right-hand rule* (Figure 33) for defining the direction of axes with respect to one another. Look at Figure 32a.

☐ How do the shaded planes intersect the unit cell edges? Write down the Miller indices of these planes.

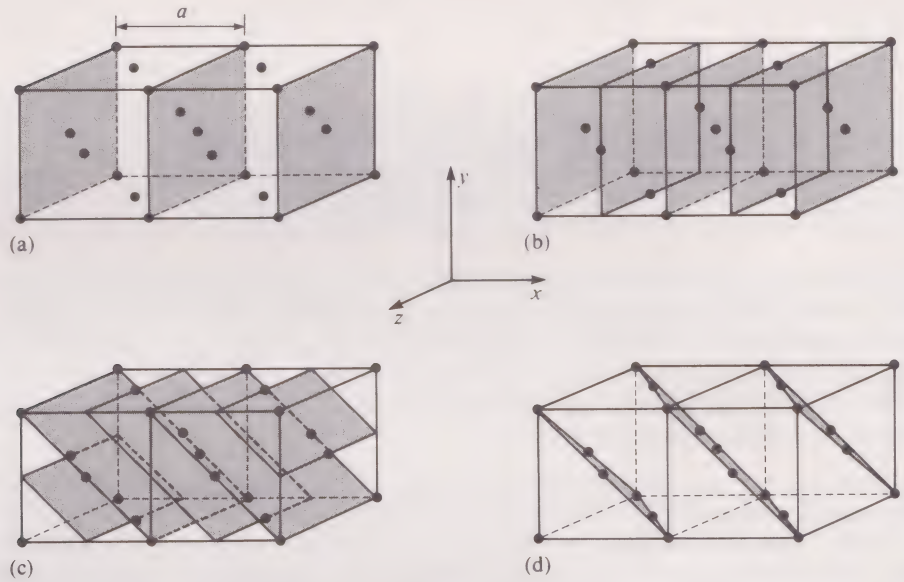

Figure 32 Planes in the face-centred cubic lattice (two unit cells are shown).

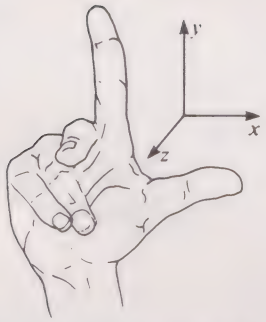

Figure 33 The right-hand rule for naming axes.

■ The shaded planes lie parallel to both the *y* and *z* directions and leave *a*, the cell edge in the *x* direction, undivided. The Miller indices are thus (100), and the planes are spoken of as the 'one-oh-oh' planes.

SAQ 13 What are the indices of the shaded planes in Figures 32b–d?

SAQ 14 Figure 34 shows planes in a body-centred cubic lattice; what are their Miller indices?

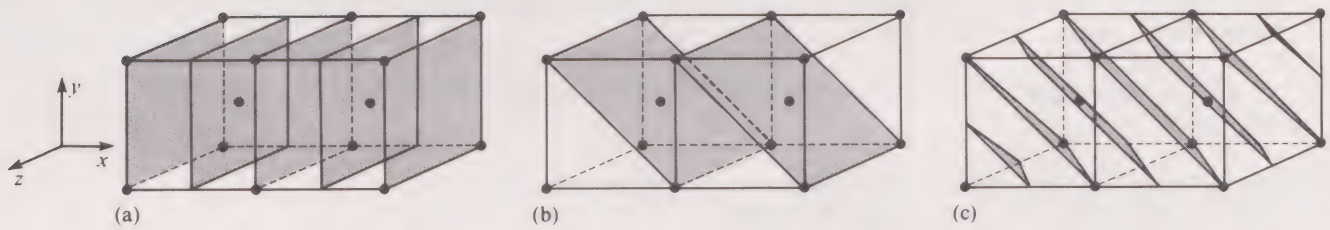

Figure 34 Planes in the body-centred cubic lattice (two unit cells are shown).

Knowledge of the structures of metals, iron in particular, and of iron nitride, Fe_4N (Figure 24), is going to be extremely useful as we use LEED to continue our investigation of surfaces, and in particular as we look more closely at the mechanism of ammonia synthesis. Consequently we need to know the positions of the atoms on some important planes in these structures. The following SAQ gives you the chance to work this out for yourself. Try it now.

SAQ 15 The two structures we'll be most concerned with are face-centred cubic, f.c.c. (remember that this is the unit cell for cubic close-packing), and body-centred cubic, b.c.c., which is the structure adopted by metallic iron. Draw the pattern of atomic positions you would expect to find on the following surfaces: (a) Fe(100); (b) Fe(110); (c) Fe(111)—this is very difficult to see, so don't spend too much time on it; (d) f.c.c. (100); (e) f.c.c. (110); (f) f.c.c. (111)—again, this is difficult to see, but it may help to remember that planes *perpendicular* to the body diagonal in a face-centred cubic unit cell contain the *close-packed layers*. In each case, indicate what you take to be the most appropriate two-dimensional unit cell.

SLC 14

As we shall use these arrangements time and time again, Figure 61 (which forms part of the answer to SAQ 15) is printed on a loose-leaf sheet for easy reference. Notice that this sheet also shows two important planes in Fe_4N. In the case of $Fe_4N(002)$, the planes shown alternate with others containing just iron atoms. (You may like to check that the internuclear distance given is correct, by referring back to the unit cell in Figure 24 and working out the relevant crystal plane.) As with the examples in SAQ 15, the arrangement on the $Fe_4N(111)$ plane is difficult to see from the unit cell diagram, so we ask you to accept that this is correct.

7 REACTION KINETICS ON DIFFERENT CRYSTAL PLANES IN METALLIC IRON

Figure 61 shows that there are marked differences in the relative positions of atoms on the three prominent, low-index planes of metallic iron. Obviously these differences might lead to differences in rates of reaction at such surfaces, so we shall next compare the kinetics of nitrogen adsorption and ammonia synthesis on the (100), (110) and (111) planes. After that we shall begin looking for answers to the detailed structural questions posed in Section 6.

In Section 5.4, we saw that nitrogen and iron gave Auger signals at 380 and 650 eV, respectively, when nitrogen is adsorbed on an iron surface. We can use the peak intensity ratio, ρ, as a measure of the surface concentration of monatomic nitrogen, and follow the rate of adsorption of nitrogen. Thus, Figure 35 shows, for the Fe(100) and Fe(111) planes, how ρ varies with nitrogen exposure at a series of temperatures. By exposure, we mean the nitrogen pressure multiplied by the exposure time, the unit being the Langmuir, L, which is equal to 10^{-6} Torr s. The nitrogen pressure was 4×10^{-4} Torr in all the experiments, so the units along the x axis are proportional to the exposure time.

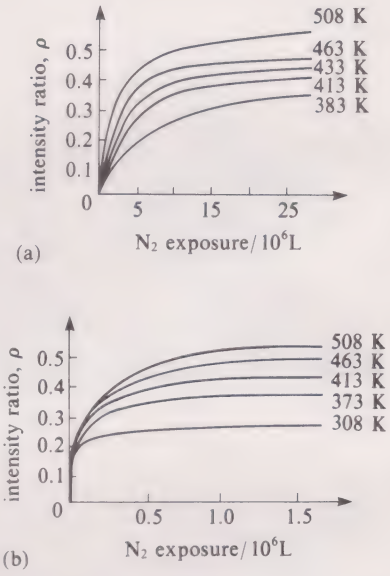

Figure 35 Rates of nitrogen adsorption on iron followed by plotting the N(380 eV):Fe(650 eV) Auger signal intensity ratio, ρ, against nitrogen exposure: (a) on Fe(100); (b) on Fe(111).

□ At comparable temperatures, which set of planes adsorbs nitrogen more quickly?

■ At comparable temperatures, a particular ρ value is reached at a much smaller exposure on the Fe(111) plane. Nitrogen uptake on this plane is much more rapid.

At very low coverages, which plane has the larger activation energy for adsorption?

The plots in Figure 35b converge to a single curve as they approach the origin: the initial rate of adsorption does not change perceptibly with temperature, so the activation energy for initial adsorption on the Fe(111) plane is virtually zero. By contrast, on the Fe(100) plane (Figure 35a), the initial rate increases with temperature and the activation energy for initial adsorption is positive (actually about 15 kJ mol^{-1}).

On the Fe(110) plane, the rate of nitrogen uptake is even lower, and the activation energy even higher than on Fe(100). The differing rates of adsorption on the three planes are well illustrated by Figure 36. Although the three curves were obtained at

different temperatures, it is obvious that the rates of adsorption vary in the order (111) > (100) > (110). If a comparison is made at a typical ammonia synthesis temperature of 683 K, the ratio of initial rates is 60:3:1.*

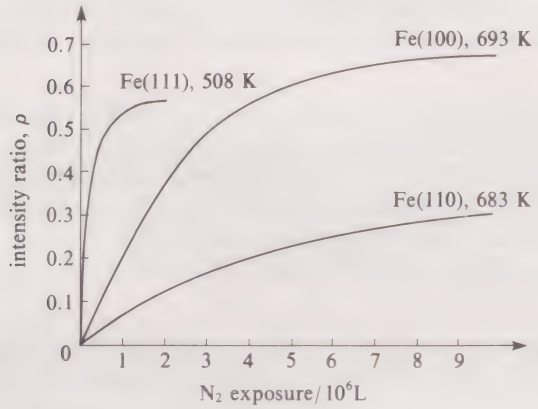

Figure 36 Rates of nitrogen adsorption on iron followed by plotting the N(380 eV):Fe(650 eV) Auger signal intensity ratio, ρ, against nitrogen exposure on Fe(100), Fe(110) and Fe(111).

The pressures under which this comparison was made, about 10^{-7} atm, are very far from those of industrial ammonia synthesis. Nevertheless, because we believe that the dissociative adsorption of nitrogen is the rate-limiting step, it would be encouraging if the relative activities of the three planes towards ammonia synthesis and nitrogen adsorption were similar. This seems to be the case. For instance, the rate of synthesis of ammonia from a 3:1 stoichiometric mixture of hydrogen and nitrogen at 20 atm and 798 K has been studied on each plane. The ratio of initial rates for the (111), (100) and (110) planes is 418:25:1. This order is the one that we would expect. The very different activities of the three crystal planes suggest that different things happen at the three surfaces during nitrogen adsorption and ammonia synthesis.

8 LOW ENERGY ELECTRON DIFFRACTION (LEED)

SFC 5

Low energy electrons have a wavelength of the same order of magnitude as the interatomic spacings within crystals and so can be *diffracted* by crystals. The penetration of these electrons into the crystal is limited to the first few atomic layers of the crystal because of interelectronic repulsions which scatter the electrons: on average, penetration is small. The technique is thus particularly suitable for surface studies. (This is unlike X-rays which have very high penetration and thus the diffraction of X-rays is used to study the three-dimensional structure of crystals.) The diffraction patterns obtained from low energy electrons can be used to determine accurate atomic positions on crystal surfaces. The technique can also be extended to look at the rearrangement of surface atoms that may take place as a function of temperature or exposure to gases, by taking diffraction patterns both before and after the reaction has taken place.

8.1 Notation of simple surface structures

SLC 15

Figure 61 shows clearly that the surface of a simple crystalline solid, such as a metal, consists of a regular two-dimensional array of atoms. Just as, in the Second Level Course, we chose unit cells to represent regular three-dimensional structures, so we can choose a unit cell to describe the repeating two-dimensional pattern of a surface. It is always possible to choose a *primitive* unit cell (one with lattice points at the corners only), but sometimes a *centred* cell (with a lattice point within the cell as well as four at the corners) shows the symmetry of the structure more clearly (for example, Fe(110) in Figure 61).

* Potassium, as we have seen, is a chemical promoter in the catalyst for industrial ammonia synthesis. It is interesting that if the Fe(100) and Fe(111) planes are pre-dosed with potassium atoms, the rates of adsorption of nitrogen on both planes *increase*. But they increase by different amounts in such a way that they become nearly identical. We return to this subject in Section 10.

The structure of a surface is often different from that of the underlying substrate —even for pure metal crystals. It is useful to have a shorthand notation with which to describe the unit cell of the surface with respect to the unit cell of the layer of atoms immediately below the surface (that is, of the bulk crystal). (Remember that we are now talking about two-dimensional unit cells in *both* cases—of the surface layer of atoms, *and* of the layer of atoms immediately below the surface representing the bulk of the crystal.)

substrate structure

If the arrangement of atoms on the surface of a pure crystal is identical with that in the bulk, then the surface is said to have the *substrate structure* and is designated (1×1). For example, the structure of the (111) face of the metal platinum is written Pt(111) – (1×1). Without, for the moment, considering what this particular unit cell looks like, we know immediately from this notation that the Pt(111) face of the crystal has exactly the same structure as the (111) plane of Pt atoms lying immediately below the surface.

If a gas is adsorbed on the surface of a crystal, it may or may not form a surface structure with the same unit cell as the substrate. (In this situation, the substrate is now the *surface* of the crystal.) If the unit cells are identical, then it is denoted in the same way as above but with the addition of its chemical symbol. So for instance, when oxygen atoms adsorb on the (111) face of a silicon crystal they have the same structure (and therefore unit cell) as the substrate and this is written: Si(111) – (1×1)O.

Frequently, however, the atoms forming the surface layer, or the adsorbed atoms, are *not* arranged in the same way as the substrate—but the relationship may be very simple. For instance, when hydrogen adsorbs on the (211) face of tungsten, the hydrogen atoms arrange themselves in such a way that the edges of the hydrogen unit cell are both double the length of the underlying tungsten substrate unit cell. A surface unit cell that has both sides double the length of the substrate unit cell and is still primitive is designated (2×2). Thus the above example would be written W(211) – (2×2)H. If only one cell side is double in length the notation becomes (2×1) where the length doubles in the x direction, and (1×2) where it doubles in the y direction. If the cell is centred rather than primitive, then a letter c is added, for example $c(2 \times 2)$.

A surface structure not only varies in size with respect to the substrate, but can also have a different orientation. A surface unit cell that is rotated with respect to the substrate is described by the letter R followed by the number of degrees of rotation. A very common example of this is shown in Figure 37: the small dots represent a substrate square net (unit cell marked in heavy lines) and the atoms adsorbing on this surface are shown by the larger circles. The obvious unit cell to choose for the *adsorbed layer* is the centred one shown on the left.

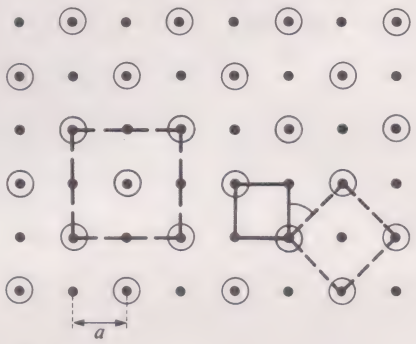

Figure 37 A substrate is shown (square net of side a, substrate atoms as dots) with adsorbed atoms as open circles. The unit cell of the substrate is drawn in solid lines, and two possible unit cells for the adsorbed layer in dashed lines.

☐ What is the notation for the larger unit cell on the left?

■ The larger unit cell has sides double the length of the underlying substrate; it is also centred—it is thus a $c(2 \times 2)$ cell.

However, there is also a primitive unit cell for the adsorbed layer which is rotated with respect to the substrate unit cell; it is depicted on the right-hand side:

☐ What is the unit cell dimension of the primitive cell, and through how many degrees has it been rotated (the angle marked in Figure 37)?

■ The side of the primitive cell is a *diagonal* of the underlying square net of side a—it therefore has cell sides of $\sqrt{2}a$. The angle of rotation is 45°.

The notation for the primitive rotated cell is thus $(\sqrt{2} \times \sqrt{2})$R45°, showing clearly its relationship in both *size* and *orientation* to the substrate. Neither the centred nor the primitive rotated cell is more 'correct' than the other, because both describe the structure completely, but it is sometimes more convenient to choose one rather than the other.

Figure 38 Some common surface structures, with adsorbed atoms shown as circles. A convenient unit cell is shown for each structure.

SAQ 16 Figure 38 shows some simple substrate structures (dots) with adsorbed species (circles) forming an overlying net. Give the shorthand notation that describes each of the adsorbed layers.

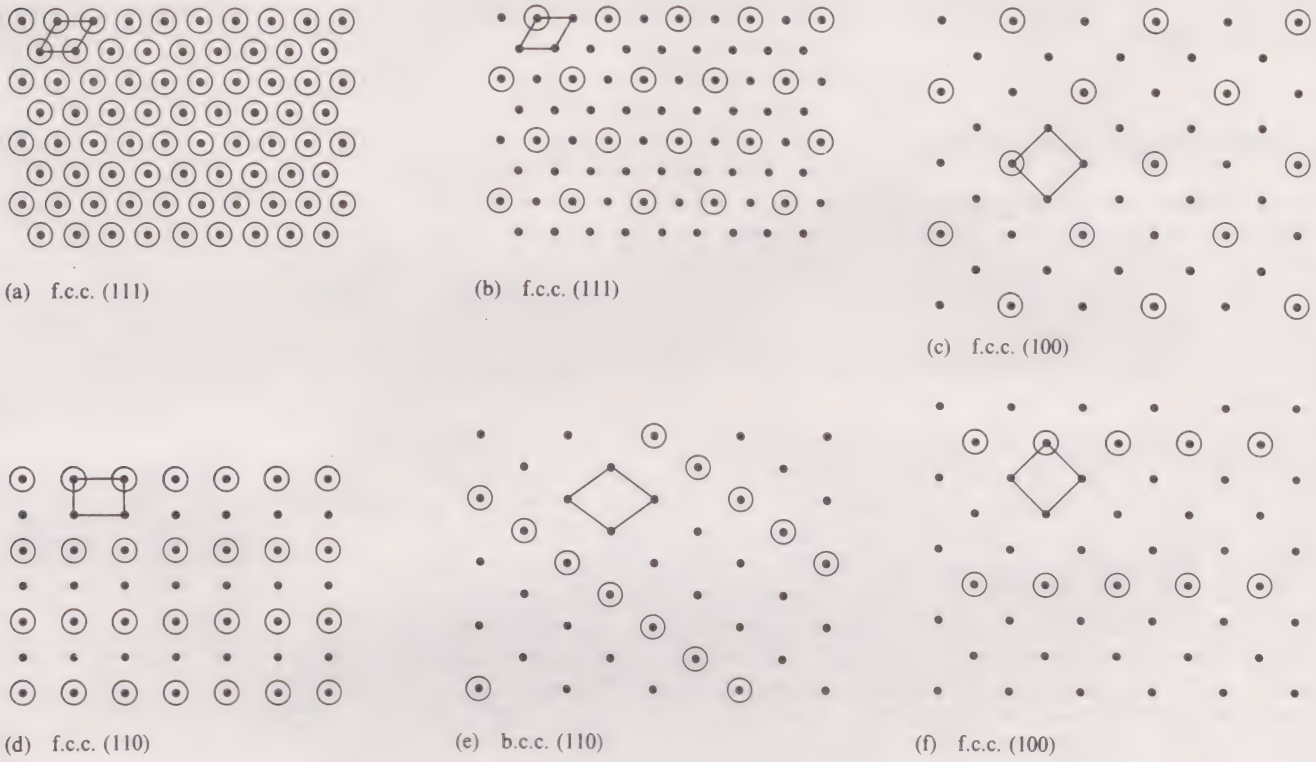

8.2 The LEED experiment

Figure 39 shows the arrangement for a LEED experiment. Low energy electrons are emitted by a heated metal or oxide filament (cathode); these are drawn to an anode (not shown) by an accelerating potential and focused at right angles (normal incidence) to the surface of the single crystal sample, using electrostatic lenses.

Figure 39 LEED apparatus.

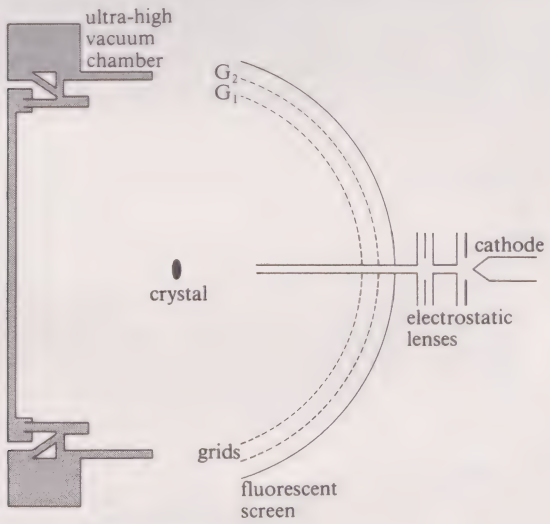

Those electrons that are elastically scattered (that is they do not lose energy in the scattering process) contain the diffraction information. The back-scattered electrons impinge on the fluorescent screen which displays the diffraction pattern. The *majority* of the electrons (about 95 per cent at 5 kV) are *inelastically scattered*, that is, they lose energy during the scattering process, and these have to be separated off from the elastically scattered portion. An arrangement of charged grids repels all electrons that have lost energy, allowing only the elastically scattered electrons

through. The latter are then accelerated towards the fluorescent screen, which is raised to a large positive potential of between 3 and 5 kV. The diffraction pattern can then be observed visually or reproduced photographically.

Ultra-high vacuum has to be maintained in the LEED chamber to ensure that the crystal surface remains clean and that the electrons are not scattered by any molecules of gas present.

8.3 Interpreting LEED pictures

8.3.1 Diffraction by a one-dimensional lattice

We'll start by considering the simplest situation—diffraction by a row of identical atoms (a one-dimensional lattice). This is basically the same situation as the 'two slit problem', described in some detail in the Science Foundation Course. If a beam of electrons impinges on a row of atoms then diffraction can occur if the distance between the atoms, d, is of the same order of magnitude as the wavelength, λ, of the electrons.

SFC 6

The scattered rays (electrons) *constructively interfere* when they are exactly *in phase* with one another and the diffracted intensity maximises. Put another way, the diffracted rays *destructively interfere* unless the difference in pathlength is zero or an integral number of whole wavelengths. This is illustrated in Figure 40 for normal incidence (at right angles that is, as in the LEED experiment). It follows that the condition for constructive interference is that the difference in distance travelled by each diffracted ray must be an integral number of wavelengths—this difference is usually called the path difference, Δ. From Figure 40b we can see that ray A follows the path A → B → C →, and ray D is diffracted from point E. The difference in the distance travelled by these two rays is BC, so we can say that: path difference Δ = BC. From the geometry of a right-angled triangle we can see that:

$$\sin\theta = \mathrm{BC/BE} = \Delta/d \qquad (15)$$

If the condition for constructive interference holds then $\Delta = n\lambda$, where n is an integer, giving:

$$\sin\theta = n\lambda/d \qquad (16)$$

At first sight, Figure 40 makes it look as though the intensity maxima radiate along lines in space. From equation 16 you can see that angle θ is a constant for particular values of n and λ, but, of course, the wave can be scattered in all possible directions still keeping θ constant—thus the line you see in Figure 40 sweeps out a cone and *the diffracted maxima lie on the surfaces of cones* (Figure 41 should make this clear) with each cone corresponding to a particular value of n. As n increases the cones get successively narrower, starting from a flat circle where $n = 0$.

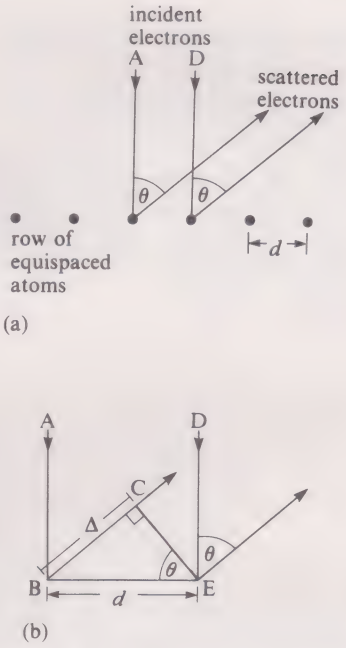

Figure 40 (a) Diffraction by a one-dimensional row of point scatterers (atoms), for normal incidence; (b) detail.

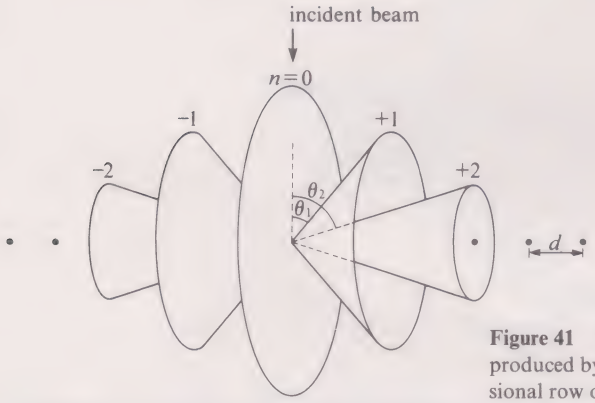

Figure 41 Cones of scattered radiation produced by diffraction from a one-dimensional row of point scatterers.

Suppose a diffracting row of atoms is placed at the centre of curvature of a fluorescent screen which forms part of spherical surface. The row of atoms is, of course, tiny compared with the radius of the sphere. Then the diffraction pattern produced would be a set of *parallel lines* where the cones intersect the screen (Figure 42). The lines lie at right angles to the row of atoms and appear with equal spacings. The

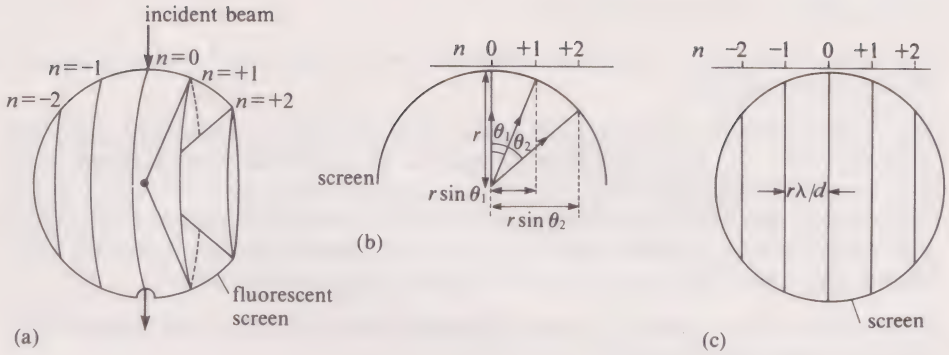

Figure 42 (a) and (b) The relationship between cones of scattered radiation and a LEED screen (only the $n = +1$ and $+2$ cones are shown, for clarity). (c) Diffraction pattern produced by a one-dimensional array of point scatterers.

positions of the spacings are given by $r \sin \theta_n$ (see triangles drawn in Figure 42b) where r is the radius of the screen. Substituting for $\sin \theta$, using equation 16, gives the positions of the spacings as $nr\lambda/d$. With different values of n this gives lines of equal spacings:

$$\text{diffraction spacing} = r\lambda/d \qquad \textbf{(17)}$$

It is important to note that this spacing is inversely proportional to the lattice spacing, d.

8.3.2 Diffraction by a two-dimensional lattice

We have seen that diffraction from a one-dimensional array of atoms results in a family of cones of diffracted rays—so what would we expect to see when electrons are diffracted from a two-dimensional net of atoms? Figure 43 shows a simple model which can be used to interpret the result. This is quite a complicated diagram, but we can break it down into several simple steps. It shows a simple rectangular net of atoms with unit cell dimensions a and b. We can simplify the problem by treating it as two one-dimensional arrays at right angles to one another. Consider the diffraction from a row of atoms in the x direction (lattice spacing a): they will produce a family of cones that comply with equation 16, so that $n\lambda = a \sin \theta$ (where n is an integer). In Figure 43, this is the set of cones similar to part of the set in Figure 41. Again, a row of atoms in the y direction (lattice spacing b) will also produce a family of cones—at right angles to the first set—given by $n\lambda = b \sin \theta$. These are the cones coming 'out of the page' in Figure 43. (For clarity, these cones are shown in the $-y$ direction.)

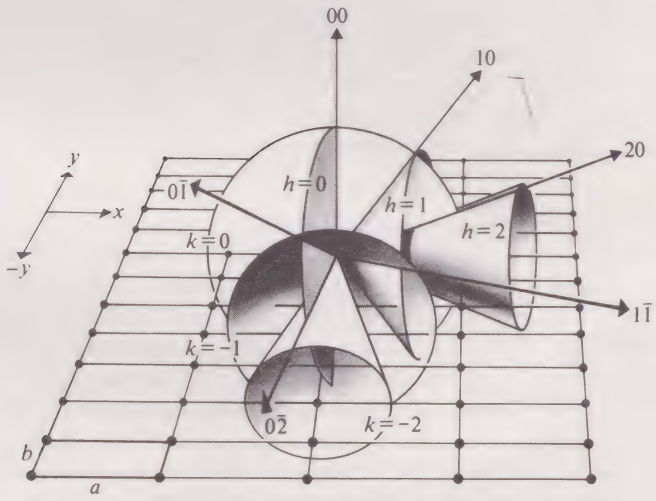

Figure 43 Cones of radiation produced by a two-dimensional net of point scatterers. Diffraction maxima occur in directions defined by the lines along which the cones intersect.

Because the two families of cones are at right angles to one another, they intersect. The cones all radiate from the same position in space (the net of atoms) and *where two cones intersect a straight line is formed.* These lines of intersection are shown as heavy arrows in Figure 43.

You may not find it easy to visualise that two cones intersect to form a straight line and so we have devised a simple model-building experiment to illustrate this point. Stop and try it now if you can.

Model-building exercise: diffraction cones

You need: stiffish paper or thin card; compasses (*or* a circular object such as a plate); a pencil; scissors; sellotape.

Figure 44 illustrates the three stages of making the model. Draw a circle on the paper and mark the centre. We found a circle of diameter 16–20 cm (6–8 inches) convenient. Make three cuts in it as illustrated in Figure 44a. The next stage is tricky! Twist the circle as shown in Figure 44b, until you can slide the *small inner* cut (2) down through the small *outer* cut (1). This forms one cone. Now sellotape together the two straight edges, and a second cone is formed, Figure 44c, which clearly intersects the first cone in a straight line.

(This model is a special case of two cones intersecting because here they only intersect at the one line—where they just touch.)

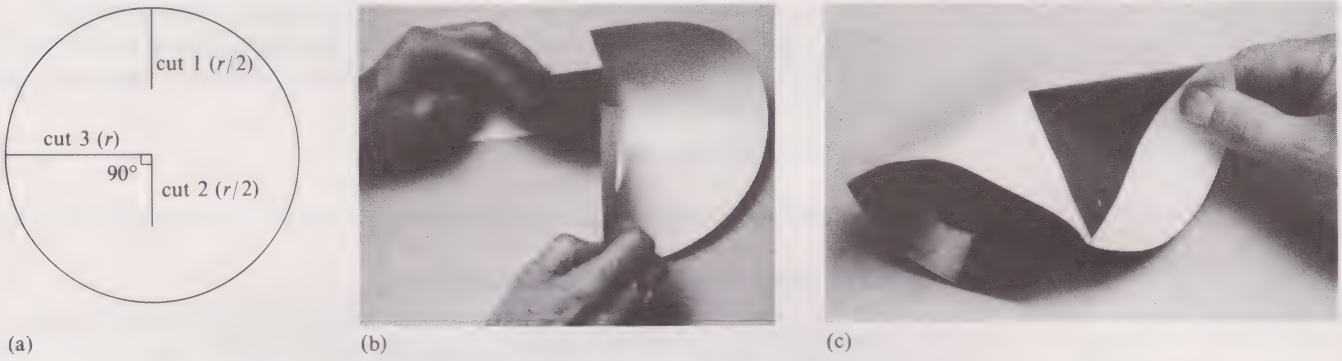

Figure 44 (a) A circle of radius r for the cone model; (b) making the model; (c) the finished model, showing the line of intersection.

Clearly, we need to be able to define the cones diffracted by the atoms of spacing a separately from those diffracted by atoms of spacing b, so n is replaced by a new symbol for each case—h for the a spacing and k for the b spacing. We can now write, for the row of atoms of spacing a:

$$h\lambda = a \sin \theta_h \qquad \textbf{(18)}$$

and for the row of spacing b:

$$k\lambda = b \sin \theta_k \qquad \textbf{(19)}$$

where h and k are both integers. The condition for diffraction to occur from the two-dimensional net is that *both* equations must be satisfied. This is true only along the lines of intersection.

We are now in a position to label the lines produced by the intersection of the cones. Look again at Figure 43. When the cone labelled $h = 0$ (the central flat circle at right angles to the plane of the paper) intersects the cone labelled $k = -1$, the resulting line is labelled $0\bar{1}$. Similarly when the $h = 2$ cone intersects the $k = 0$ cone (the flat circle in the plane of the paper) the line labelled 20 is produced. We can generalize this to say: when a cone h intersects a cone k the resulting line is given the label hk.

All that remains is to consider what the actual LEED picture will look like. Try to imagine the spherical fluorescent screen placed with the diffracting net in Figure 43 at its centre. Clearly, where each *line* strikes the screen it will produce a *spot*. We can also see from Figure 45 how these spots are produced: Figure 45a shows the lines produced by diffraction from the row of atoms of spacing a with $h = 0, \pm 1, \pm 2$, and Figure 45b shows the pattern for a row of atoms of spacing b at right angles to a with $k = 0, \pm 1$; Figure 45c shows the combination of these two, and clearly the diffraction condition holds only at the *intersection* of the lines, yielding the pattern of spots shown in Figure 45d. This, then, is what we expect a LEED photo to look like. Each spot is labelled in the same way as the line that produced it—this is known as *indexing* the spots.

SAQ 17 Index the spots in the hypothetical LEED pattern shown in Figure 45d; use Figures 45a–c to find the origin of each spot.

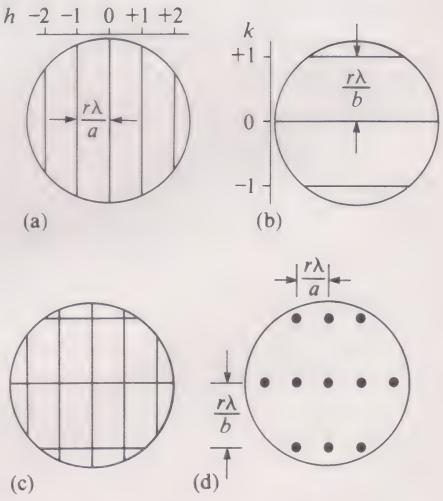

Figure 45 The diffraction patterns produced by one-dimensional rows of atoms in (a) the x (spacing a) direction, and (b) the y (spacing b) direction. (c) The combination of (a) and (b). (d) The diffraction pattern produced by a two-dimensional rectangular net of atoms with unit cell dimensions a and b.

8.3.3 Information from LEED pictures

LEED is particularly useful as a surface technique because *the positions of all the spots in a LEED pattern are determined only by the top surface layer of atoms of the crystal.* Thus, a LEED pattern provides a great deal of information on the shape, size and symmetry of the two-dimensional unit cell describing the surface structure. Figure 61 (on the loose-leaf sheet) shows several of the surface structures that are commonly found for metals. Three of these typical atomic arrangements (square, rectangular and hexagonal) are illustrated in Figure 46, together with the diffraction patterns they would produce in a LEED experiment. Notice that a square unit cell produces a square diffraction pattern; similarly with a hexagonal unit cell. The rectangular unit cell produces a rectangular pattern, but the reciprocal relationship between unit cell dimension and diffraction spacing inverts the cell shape.

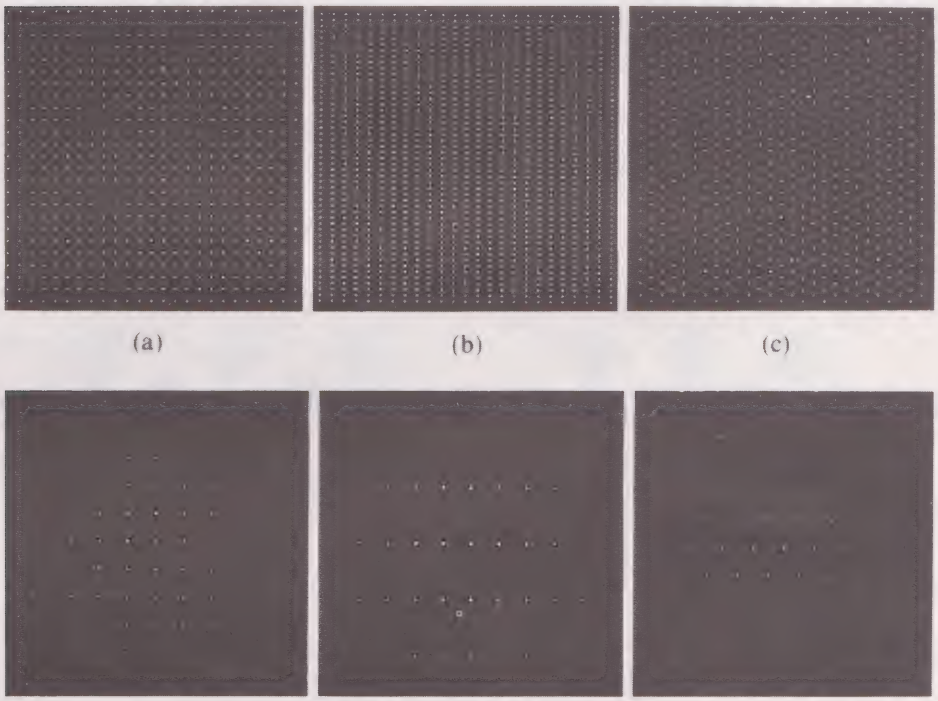

Figure 46 Three different atomic arrangements (top) with their corresponding diffraction patterns (bottom): (a) square; (b) rectangular; (c) hexagonal.

SAQ 18 Select from Figure 46 the diffraction patterns you would expect to find for the (100), (110) and (111) planes of platinum (platinum metal has a cubic close-packed structure), and for the (200) plane of iron (metallic iron has a body-centred cubic structure). Indicate for each the size of the two-dimensional unit cell in terms of the bulk three-dimensional unit cell length, a, and the equivalent spacing on the diffraction pattern. (You may find Figures 38 and 61 useful.)

In the simple metal structures that we have been considering, the relative positions of the spots in the LEED pattern tell us the size and shape of the unit cell, and so we can usually infer the unique positions of the atoms. Things are not this easy for more complex surface structures: to determine the exact position of atoms in the unit cell, the *intensities of the spots* also have to be analysed. This is a difficult and complicated task, but in favourable cases the problems can be overcome and precise results obtained.

8.4 Results obtained from LEED

8.4.1 Introduction

A lot of work has been carried out on low-index crystal faces of metals. These surfaces always have ordered structures, either with unit cells identical with the substrate or with unit cells that are integral multiples of the substrate unit cell. For instance, the different crystal faces of tungsten [(110), (100), (211)] and aluminium [(111), (100)] all give diffraction patterns characteristic of a (1×1) surface structure.

However, for our purposes, the main interest in investigating metal surfaces lies not in the structure of the clean surfaces themselves but in changes brought about by processes such as adsorption. The structure of the adsorbed layer and its method of bonding to the metal are of primary interest in the study of catalysis. When a gas adsorbs on a metal surface the spacing and symmetry of the LEED pattern is due to the adsorbed molecules or atoms since *they* now constitute the surface layer. The underlying metal atoms affect only the intensity of the pattern and not its size and shape. As an example, Figure 47 shows atoms adsorbed on interstitial sites on the (100), (110), and (111) surfaces of a c.c.p. metal. (Notice that not every possible adsorption site is occupied.)

□ What is the coordination number of each adsorbed atom? Are the adsorbed atoms occupying sites of maximum coordination?

■ In each case the adsorbed atom is occupying a site of maximum coordination—four-fold on the (100) and (110) faces and three-fold for the (111) face.

SAQ 19 For each example in Figure 47 write down the notation of the adsorbate surface structure as illustrated. Suppose all the interstitial sites on the (100) face are filled. Would the LEED pattern change, and what would be the notation of the adsorbate unit cell?

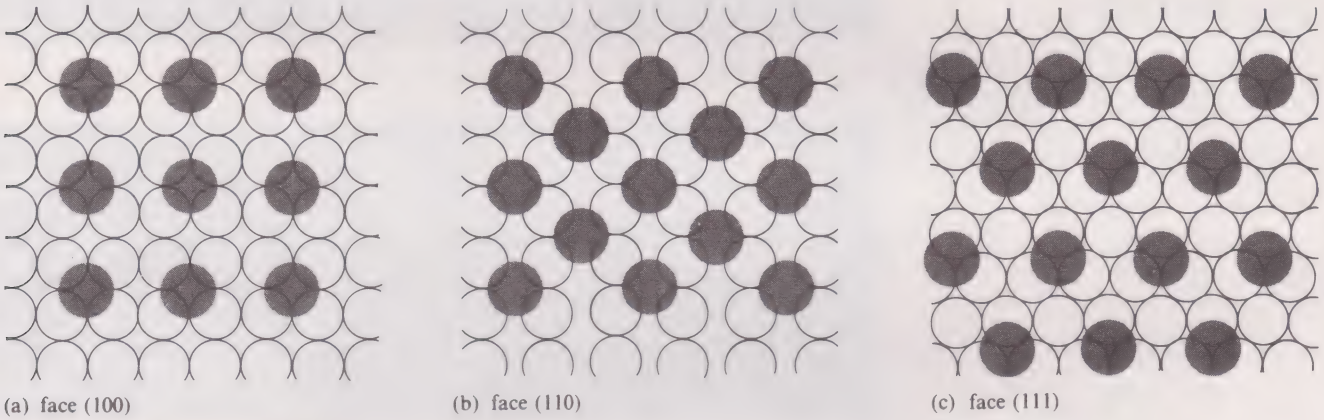

Figure 47 Possible adsorption patterns on low-index faces of a face-centred cubic metal.

One of the first analyses to be carried out that successfully interpreted the diffraction symmetry, spacing and intensity was that of sodium atoms adsorbed on the Ni(100) face (nickel has a c.c.p. structure). The results showed that the sodium atoms occupy sites with four-fold coordination. Oxygen, sulphur, selenium and tellurium atoms have also been shown to occupy four-coordinate bonding sites on Ni(100). In a different (but related) system, iodine has been shown to occupy the three-fold coordination sites on the Ag(111) face, similar to those shown in Figure 47c. In these simple systems, the chemisorbed atoms appear to seek sites that give them maximum coordination.

However, things are not always this simple. Oxygen atoms adsorbed on Ni(110) have been shown to lie on a two-fold bridging site, and the bond lengths and angles are close to those expected in compounds of the type M_2O, where M is the metal atom (Figure 48). Nevertheless, it seems to be true that adsorbed atoms on a surface often show a preference for sites of maximum coordination. We shall see further examples of this in the remaining sections.

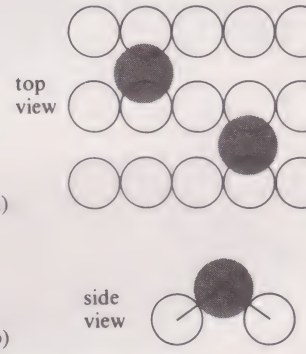

Figure 48 Adsorption in a two-fold bridging position: (a) top view; (b) side view.

8.4.2 LEED investigation of nitrogen adsorption on the Fe(100) plane

The (100) plane of metallic iron is shown in Figure 61 (loose-leaf sheet). The primitive unit cell is a square of side 286 pm. Nitrogen adsorption to saturation causes the appearance of additional spots in the LEED pattern, which then corresponds to a $c(2 \times 2)$ structure. An adsorption model compatible with this structure has been proposed, and it is shown in Figure 49. The sides of one unit cell for the adsorbed layer have been picked out.

□ Do the nitrogen atoms occupy high coordination sites on the iron surface?

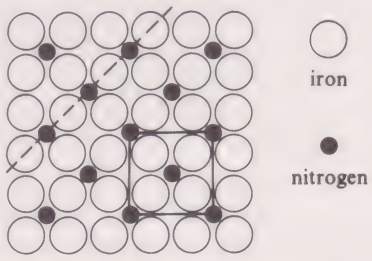

Figure 49 The proposed Fe(100) – $c(2 \times 2)$N structure produced by nitrogen adsorption on Fe(100). A unit cell is picked out at bottom right, and the Fe(110) plane is marked by a dashed line.

■ Yes. Their coordination number is 4, and this is the maximum possible on an Fe(100) surface.

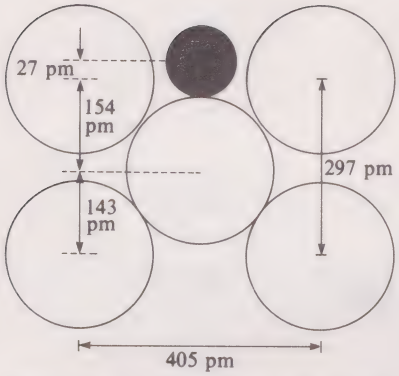

Figure 50 A cross-section on the dashed Fe(110) plane of Figure 49 at the surface.

A careful analysis of the LEED data has revealed the position of the nitrogen atoms in relation to the surface plane. Figure 50 is part of a cross-section on the (110) plane, which is marked by the dashed line in Figure 49. The normal separation of Fe(100) planes is 286 pm, but as Figure 50 shows, the separation between the surface plane of iron atoms and the one immediately beneath, is about 11 pm greater than this. Now look at the nitrogen atom. Because it has been drawn as a small sphere, it seems to be within the surface plane; notice, however, that its centre is slightly above the centres of the surrounding iron atoms (by about 27 pm).

Now compare Figure 49 with Figure 61. Does any plane in Figure 61 resemble Figure 49?

The geometry of the nitrogen-saturated Fe(100) plane is very similar to that of the (002) plane of Fe_4N shown in Figure 61g. The main difference is that the Fe—Fe distance within the plane is shorter by about 18 pm (268 pm instead of 286 pm). Such similarities have attracted a lot of attention. Let us consider why this should be so. Under normal conditions, iron nitrides are just thermodynamically unstable with respect to iron and dinitrogen, but they can be made, for example, by the reaction between iron and ammonia (equation 7 in Section 5.1). When compounds of iron and nitrogen are formed by such methods, the stoichiometry of Fe_4N with the structure in Figure 24 is often formed at the expense of other possible nitrides. Since the Fe_4N structure is strongly favoured, we might expect analogies between the new surfaces and prominent crystal planes in Fe_4N when *surface* structures are formed between metallic iron and nitrogen atoms.

There is one final point to make about Figures 49 and 50. They show that when nitrogen is adsorbed on the (100) face of iron, it hardly has any effect on the relative positions and internuclear distances of the iron atoms. These remain very much what they were before adsorption took place. This is why the relation of the new unit cell to the old is very simple. However, as we shall see, this is not a universal occurrence.

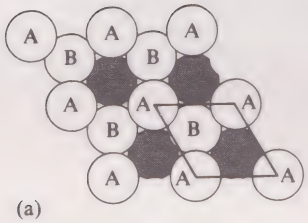

(a)

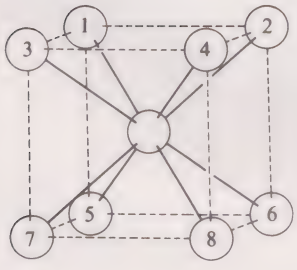

(b)

Figure 51 The body-centred cubic structure of metallic iron: (a) a view perpendicular to the Fe(111) plane showing a possible active site for ammonia synthesis; (b) the unit cell.

8.4.3 LEED investigation of nitrogen adsorption on the Fe(111) plane

As Section 7 showed, the Fe(111) plane is much more catalytically active than the Fe(100) and Fe(110) planes, so its geometry is worth a close look. The arrangement of the topmost atoms in the plane is shown in Figure 61c; the two-dimensional unit cell has hexagonal symmetry. Especially noteworthy is the fact that the structure is rather open: the distance between the iron atoms is 405 pm compared with 286 pm on Fe(100) (Figure 61a). This means that the two layers of iron atoms immediately beneath the (111) surface are very exposed. This is shown in Figure 51a, where atoms of the topmost layer are marked A. The layers beneath are visible within the large triangular spaces of layer A. One set of alternate spaces exposes the atoms of the first layer beneath, marked B: the other alternate set exposes the atoms of the layer beneath that, which are shaded.

Any bulk atom in the body-centred cubic structure has eight nearest neighbours lying at the corners of a cube, as in Figure 51b. However, the coordination number of the topmost atoms in Figure 51a (layer A) is 4, because four other neighbours are sliced away when the surface is formed. The four remaining neighbours are the three adjacent atoms of layer B beneath, and a fourth which is wholly obscured in Figure 51a because it lies vertically beneath the atom in layer A. The coordination numbers of the atoms in layer B and of the shaded atoms are both 7, because surface formation slices away only one atom from their respective coordination spheres. (To relate these coordination numbers to Figure 51b, stand the cube with the 1–8 diagonal vertical, and atom 1 uppermost. The view down the diagonal is now the viewpoint of Figure 51a. To obtain the four-coordination of an atom in layer A, remove atoms 1, 2, 3 and 5 of the cube. To obtain the seven-coordination of the atoms in layer B and the shaded atoms, simply remove atom 1.)

Some chemists claim that these very distinctive, exposed, seven-coordinate atoms are the active sites in ammonia synthesis. They believe that recesses of the sort bounded by the unit cell in Figure 51a are places where dinitrogen molecules are

conveniently drawn into the surface structure and broken down into adsorbed atoms. As we shall see, however, it is not easy to relate the LEED observations to such a view.

LEED shows that, above 510 K, the adsorption of nitrogen on Fe(111) produces a succession of five ordered structures as the coverage increases. These are (3×3), $(\sqrt{19} \times \sqrt{19})$R23.4°, $(\sqrt{21} \times \sqrt{21})$R10.9°, $(\sqrt{27} \times \sqrt{27})$R30° and (2×2). Clearly, in the second, third and fourth cases, the relationship of these new hexagonal unit cells to the old is rather complicated. Nevertheless, it can be worked out.

Figure 52 shows a triangle containing an angle of 120°, and a side of length c opposite to it. The geometry is such that the length c is related to the lengths of the other two sides by the equation:

$$c^2 = a^2 + b^2 + ab \qquad \textbf{(20)}$$

The angle β (opposite the side of length b) can be calculated from the relation:

$$\cos \beta = (2a + b)/2c \qquad \textbf{(21)}$$

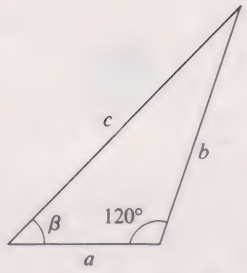

Figure 52 A triangle with an angle of 120°.

These expressions enable us to relate the unit cells of the five new ordered structures to that of the Fe(111) face. For example, Figure 53 shows unit cells for the first three structures, the primitive hexagonal cell for Fe(111) being shown in the top left-hand corners. In cases (b) and (c), dashed 120° triangles are also drawn on one side of the new unit cells. Look first at Figure 53c. (The unit cell in Figure 53b is the subject of SAQ 21.) Let the side of the primitive Fe(111) unit cell be x.

Figure 53 The arrangement of iron atoms on Fe(111) showing unit cells for the new surface structures generated by nitrogen adsorption. The original primitive hexagonal unit cell is shown top left in each case, and nitrogen coverage increases in the sequence a → b → c.

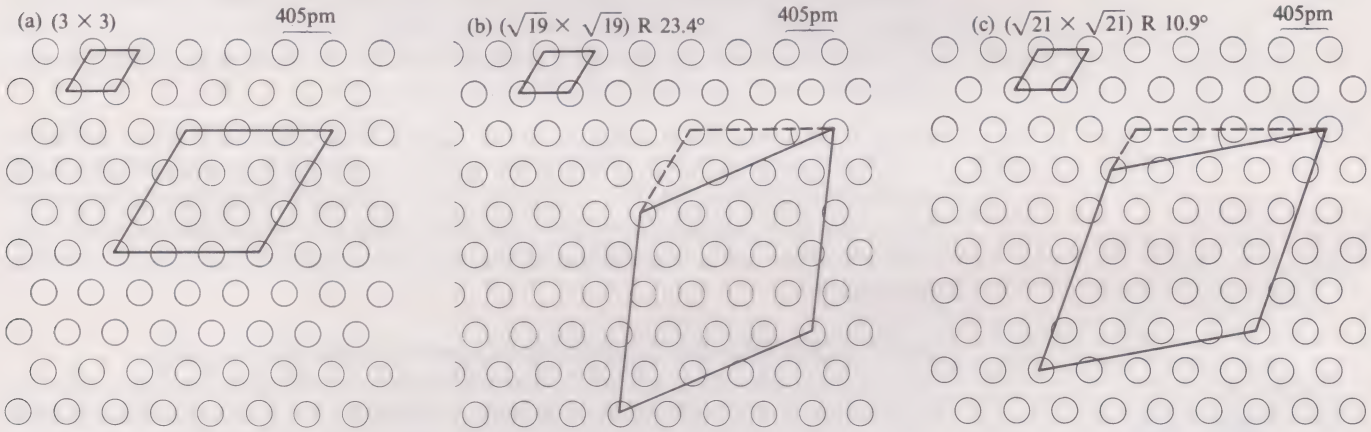

☐ What is the side of the new unit cell?

■ Use the dashed triangle and apply equation 20 with $a = 4x$ and $b = x$. Then c, the new unit cell side, is $\sqrt{21}x$.

☐ In the dashed triangle of Figure 53c, the angle of rotation of the new unit cell with respect to the old is also marked. What is the cosine of this angle?

■ Apply equation 21: $\cos \beta = 9/(2\sqrt{21})$ which gives $\beta = 10.9°$. Thus our proposed unit cell in Figure 53c is compatible with the LEED data.

But how are we to interpret the successive appearance of these new unit cells as nitrogen is adsorbed? Such complicated changes are not explicable in terms of an ordered adsorption of nitrogen on fixed iron sites, as on Fe(100). Instead it is believed that adsorption *alters* the relative positions of the iron atoms so that the iron surface is reconstructed. For example, one way of looking at this change is to say that in Figures 53b and 53c, only those adsorption sites on iron atoms at the corners of unit cells retain the marked relative positions. The other atoms are shifted about, although hexagonal symmetry must still be retained.

What is this new hexagonal arrangement of iron atoms like? One recent interpretation relies on an analogy with the planes in Fe_4N. As Figure 61h shows, on the (111) plane in iron nitride, there are only iron atoms arranged in hexagonal symmetry with an internuclear distance of 268 pm. The arrangement is shown again in Figure 54. Here we have drawn a unit cell which, as equations 20 and 21 show, is rotated with respect to the simple unit cell by 30°, and has a side $\sqrt{48}$ times the simple unit cell side. Now compare this large unit cell with that in Figure 53c.

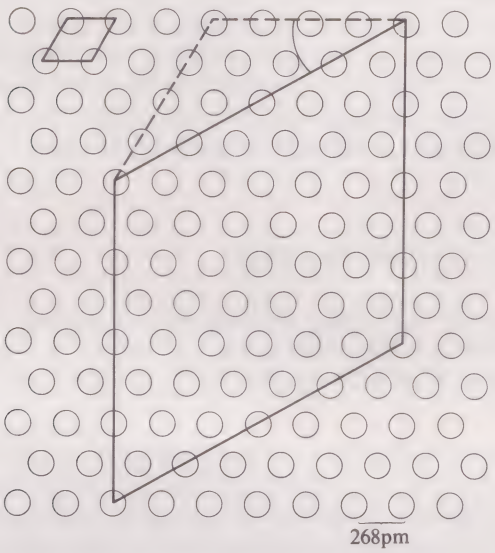

Figure 54 A unit cell on $Fe_4N(111)$ identical in size with that in Figure 53c.

Work out the sides of these two cells in picometres and compare them.

The unit cells seem to be a different size only because the scales are different. In Figure 53c, the internuclear distance is 405 pm, so the unit cell side is $405\sqrt{21}$ pm; in Figure 54, the internuclear distance is 268 pm, so the unit cell side is $268\sqrt{48}$ pm. These two values are effectively identical at 1 856 pm. It follows that if we rotate the layer in Figure 54 clockwise by $(30 - 10.9)°$, that is, 19.1°, we can lay it on top of Figure 53c such that the atoms at the corners of the two unit cells are exactly superposed. However, superposition occurs only for the corner atoms: because of the shorter internuclear distance in Figure 54, the atoms on this plane are much more densely packed.

This then is one possible interpretation of the curious unit cells in Figure 53. Adsorption of nitrogen on Fe(111) pulls the iron atoms closer together, and twists the surface plane with respect to parallel untouched planes beneath. The result is an arrangement of iron atoms very similar to that on the (111) plane in Fe_4N. This reconstruction of the Fe(111) surface, which is believed to occur not just on the topmost layer, but also on one or perhaps two layers beneath, makes it impossible to locate the nitrogen atom positions with confidence. They are assumed, however, to occupy high-coordinate sites (three-fold in this case: Figure 55) which, as we have seen, is a frequent preference for adsorbed atoms. Figure 24 (Section 5.1) shows that this is just the situation of the nitrogen atoms in Fe_4N with respect to the iron atoms on the adjacent $Fe_4N(111)$ plane. If this is the correct position of N(ad), it means that the unit cells of Figures 53 and 54 would be more conventional if they were slightly shifted, so that the corners lay over coordination sites, rather than over iron atoms.

Figure 55 The three-fold maximum coordination site for a nitrogen atom on Fe(111).

We conclude by pointing out a weakness in our understanding: the proposed importance of seven-coordinate sites to the catalytic activity of Fe(111), and the complicated reconstruction suggested by LEED, have not been reconciled.

8.4.4 LEED investigation of hydrogen adsorption on the Fe(110) plane

In Section 5.2 we looked into *hydrogen* adsorption on Fe(110); let us see how LEED studies can complement what we learnt. As hydrogen is adsorbed on the plane at 140 K, LEED studies reveal a sequence of new ordered structures: first a

(2×1) structure; then, as the fractional surface coverage, θ, increases, (3×1), and finally, at saturation, a (1×1) structure. The thermal desorption spectra of the three structures show that the amounts of adsorbed gas are in the ratio 3:4:6. Thus if $\theta = 1$ at saturation, then for the (2×1) structure $\theta = \frac{1}{2}$, and for the (3×1) structure, $\theta = \frac{2}{3}$.

A possible interpretation of these changes is shown in Figure 56. The large circles show the arrangement of iron atoms on the Fe(110) plane; a simple unit cell of this *substrate*, a parallelogram, is marked at the top of Figure 56a. The adsorbed hydrogen atoms are assumed to occupy chains of positions parallel to, say, the (001) or z direction. In Figure 56a alternate chains of hydrogen positions are occupied; in Figure 56b, adjacent pairs of occupied chains are separated by single chains of vacant sites; in Figure 56c, all hydrogen sites are occupied and we have saturation. The unit cells are drawn in each case, and as required, they are of the types (2×1), (3×1) and (1×1), respectively.

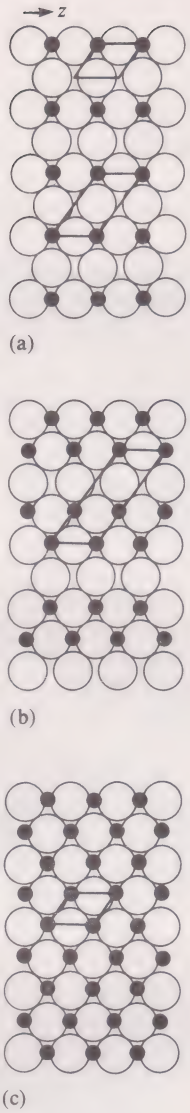

Figure 56 Possible structural models for the arrangement of adsorbed hydrogen atoms (black) in the ordered overlayers on Fe(110): (a) at $\theta = \frac{1}{2}$, a structure with a (2×1) unit cell; (b) at $\theta = \frac{2}{3}$, a structure with a (3×1) unit cell; (c) at $\theta = 1$, a structure with a (1×1) unit cell.

□ What are the H:Fe ratios in these three unit cells?

■ The numbers of hydrogens are 1, 2 and 1 respectively, the corresponding numbers of irons are 2, 3 and 1, so the ratios are 1:2, 2:3 and 1:1. Thus the proposed structures have the correct relative amounts of adsorbed gas.

This interpretation also accounts for the thermal desorption spectra of Figure 25. These showed the existence of two hydrogen states, β_1 and β_2, on the Fe(110) surface, each with a capacity of half saturation. The β_2 state is the more strongly held. We can assume that there are significant repulsions between adjacent chains of hydrogen atoms, and that this is the reason why, to begin with, only sites in alternate chains are occupied. These sites are the more tightly bound ones labelled β_2. At $\theta = \frac{1}{2}$ in Figure 56a, the β_2 state is full. From then on, a second type of occupied site appears in which hydrogen atoms experience repulsion from others in neighbouring chains. These are the less tightly bound sites which produce the peak labelled β_1 in Figure 25a.

8.4.5 Summary of Section 8.4

1 Adsorbed atoms often occupy high-coordinate sites on a metal surface. This happens during the dissociative adsorption of nitrogen on Fe(100) when a $c(2 \times 2)$ structure is formed without reconstruction of the metal surface.

2 Dissociative adsorption of nitrogen on Fe(111) does cause reconstruction, but there is still a resemblance to the Fe(100) case in that the new arrangement has some analogies with crystal planes in Fe_4N.

3 Dissociative adsorption of hydrogen on Fe(110) results successively in (2×1), (3×1) and (1×1) structures. Adsorption of hydrogen occurs on chains of high-coordinate sites, interchain repulsion generating two types of adsorption state with different binding energies.

SAQ 20 A clean Fe(100) surface was saturated with nitrogen by exposing it at 650 K until the ratio of the Auger peak intensities, N(380):Fe(650), labelled ρ, no longer increased. At this point, $\rho = 0.9$, and the LEED pattern gave evidence only of a $c(2 \times 2)$ structure. A 3:1 mixture of hydrogen and nitrogen at 580 K and 1 atm was then allowed to react over an iron surface. After 30 minutes reaction, followed by evacuation at 580 K and cooling, $\rho = 0.12$. What was the approximate N:Fe ratio at the catalyst surface during the reaction?

SAQ 21 Show that the unit cell in Figure 53b is compatible with the $(\sqrt{19} \times \sqrt{19})$R23.4° structure observed during nitrogen adsorption on Fe(111).

SAQ 22 At one stage during nitrogen adsorption on Fe(111), a $(\sqrt{27} \times \sqrt{27})$R30° structure appears. Can you draw a unit cell of the type shown in Figure 53 for this structure?

9 DETECTION OF SURFACE VIBRATIONS USING ELECTRON ENERGY LOSS SPECTROSCOPY (EELS)

SLC 16 In the Second Level Course, we described how information about bonding in molecules can be obtained by using infrared radiation to excite the energies of *molecular* vibrations. In the final stage of our study of ammonia synthesis, we shall show how information about the bonding of adsorbed molecules on iron surfaces can be obtained by exciting the energies of *surface* vibrations.

In Section 4.1, we noted that when a surface is bombarded with a primary electron beam, the electrons that then issue from the surface are of three types (cf. Figure 13). Some have been elastically scattered, some are secondary electrons produced by Auger transitions, and some are primary electrons that have suffered energy loss. It is the third type that concerns us here. Processes that are responsible for the losses include certain *electronic* transitions induced on the bombarded surface. However, we shall not discuss these. Our concern will be with energy losses caused by the excitation of *vibrations* of adsorbed species.

SLC 17 In some respects, the EELS technique resembles Raman spectroscopy, which was studied in the Second Level Course. In EELS, the source is a beam of monochromatic electrons, and in Raman spectroscopy it is monochromatic radiation, which is usually supplied by a laser. The loss peaks are equivalent to the Stokes lines in Raman spectra, where energy has been taken from the incident beam to excite the vibrational mode. One special advantage of EELS is that if conditions are right, excitations that are forbidden by selection rules in optical spectroscopy can be observed in EELS.

The major problems with the technique are caused by the small size of the energy losses and the poor resolution. The losses are usually quoted in millielectronvolts. Here we shall use wavenumbers (1 meV = 8.066 cm^{-1}), the units you are familiar with from infrared spectroscopy. Thus the excitation of a vibration at 1 000 cm^{-1} produces a relatively small energy loss of about 125 meV. In the spectrum, there is a so-called primary peak, which is produced by electrons that are elastically scattered. Recent improvements in instrumentation have made it possible to detect loss peaks within 50 meV of this primary peak. This is equivalent to about 400 cm^{-1}, a region where many important surface vibrations occur.

9.1 The adsorption of nitrogen on iron

Figure 57a shows the high resolution EELS spectrum of an Fe(111) surface after exposure to $^{30}N_2$ at 110 K. The spectrum in Figure 57b was obtained after the same exposed surface had been warmed to 170 K.

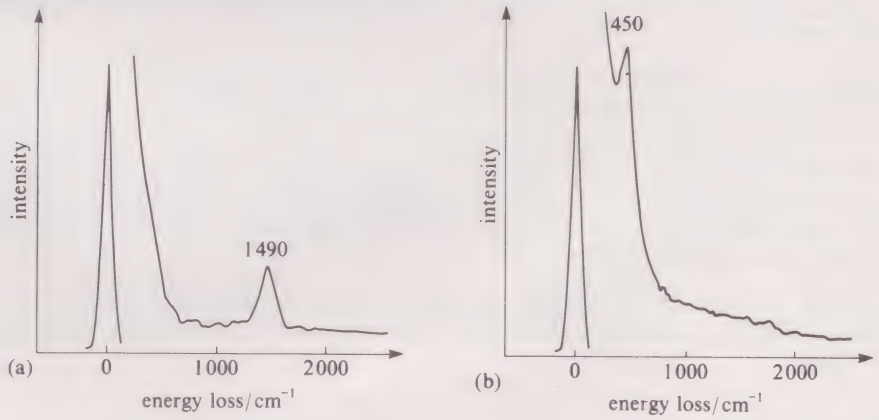

Figure 57 EELS spectra for $^{30}N_2$ adsorbed on Fe(111): (a) at 110 K; (b) at 170 K. The primary peak, which is much more intense than the energy loss peaks, is here shown separately as a spectrum of greatly reduced magnification.

To what adsorbed species would you assign the single peaks in each of these two spectra?

In Section 5.1, we saw evidence that nitrogen adsorbs on iron in the molecular form at about 100 K, but dissociates at higher temperatures. We therefore assign the 1 490 cm^{-1} peak to adsorbed $^{30}N_2$, and the 450 cm^{-1} peak to a vibration of monatomic nitrogen bound at the iron surface. (Substitution of $^{28}N_2$ for $^{30}N_2$ should increase the frequencies, but only by about 30 cm^{-1}.)

How are the two adsorbed species bound? In the case of dinitrogen, one possibility is the 'end-on' position of Figure 58a. This is how dinitrogen is bound on Ni(110) and in the dinitrogen transition metal complex, $[Ru(NH_3)_5N_2]Cl_2$. However, gas-phase Raman spectroscopy shows that in $N_2(g)$, the N—N stretching frequency is $2\,331\,cm^{-1}$, and infrared spectroscopy reveals that on Ni(110), and in $[Ru(NH_3)_5N_2]Cl_2$, it is lowered only to $2\,194\,cm^{-1}$ and $2\,130\,cm^{-1}$, respectively. If the band at $1\,490\,cm^{-1}$ is due to an N—N stretch, the low value rules out the end-on configuration.

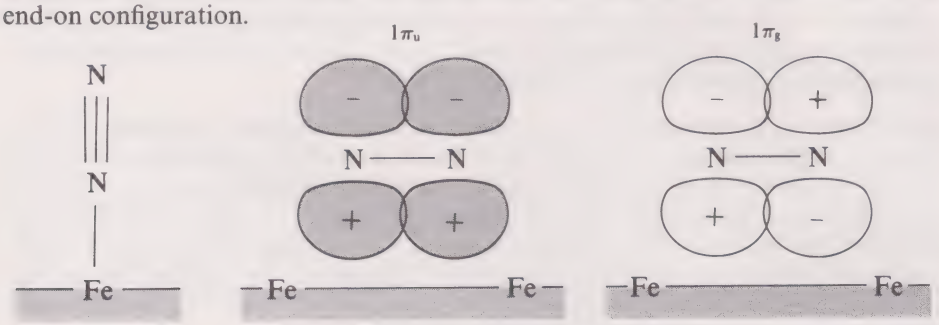

Figure 58 Possible N_2 configurations on an iron surface: (a) 'end-on'; (b) 'side-on', showing the filled $1\pi_u$ bonding orbital; (c) the vacant $1\pi_g$ antibonding orbital of N_2.

An alternative is a side-on π-complex of the kind shown in Figures 58b and 58c, in which π-orbitals on dinitrogen overlap with orbitals of more than one metal atom. An arrangement resembling this is found in certain titanium complexes, where titanium atoms are bound both to dinitrogen and to complicated ligands containing rings of carbon atoms. Each dinitrogen molecule is bound to three titanium atoms, and the stretching frequency is about $1\,300\,cm^{-1}$. Both this value, and the $1\,490\,cm^{-1}$ value on Fe(111), imply a bond order of two or less, because the stretching frequency in the di-imine molecule, HN=NH, is $1\,530\,cm^{-1}$. In the Second Level Course you saw that, according to molecular orbital theory, N_2 has the electronic structure $(1\sigma_g)^2(1\sigma_u)^2(2\sigma_g)^2(2\sigma_u)^2(3\sigma_g)^2(1\pi_u)^4$. The filled bonding π-orbital, $1\pi_u$, which is shown in Figure 58b, can donate electrons to vacant orbitals on the metal surface. The next orbital in energy above $1\pi_u$ is the vacant antibonding $1\pi_g$ (Figure 58c), and this can receive electrons from filled orbitals on the metal surface. It has been suggested that this second process in particular accounts for the lowering of the N—N bond order and stretching frequency that occurs when dinitrogen is adsorbed on Fe(111).

SLC 18

What contribution could such a lowering make to the rate of ammonia synthesis?

We have seen that the rate-limiting step in ammonia synthesis on iron is

$$N_2(ad) \longrightarrow 2N(ad) \qquad \textbf{(10)}$$

The lowering of the N—N bond order in $N_2(ad)$ should lower the activation energy and enhance the rate of this step; this in turn will increase the rate of ammonia synthesis.

As you can probably detect, our evidence that $N_2(ad)$ occupies a side-on position on Fe(111) is by no means definitive. Nor does it imply that the N_2 axis is parallel to the surface plane. As we saw in Section 8.4.3, the Fe(111) plane is very open with recesses into which a tilted N_2 molecule might be drawn and bound. The important point perhaps is that within the recesses, bonding of the N_2 molecule to more than one iron atom is possible, and our π-bonding mechanism for reducing the N—N bond order can become operative.

Finally we turn to the binding of N(ad) (Figure 57b). In the osmium complex $[O_3Os{\equiv}N]^-$, infrared spectroscopy gives an Os—N stretching frequency of $1\,020\,cm^{-1}$.

□ What does this suggest about the binding of N(ad) on Fe(111)?

■ The peak at $450\,cm^{-1}$ has far too low a frequency to be assigned to the stretching vibration of nitrogen bound to a *single* metal atom.

As expected then, it seems likely that monatomic nitrogen is bound on high-coordinate sites, the most obvious candidate being a capping position on the triangles of iron atoms as in Figure 55.

10 THE ROLE OF THE POTASSIUM PROMOTER IN AMMONIA SYNTHESIS

In Sections 3.4 and 4.4, we concluded that potassium is a *chemical* promoter of ammonia synthesis, and that a very thin layer of oxygenated potassium covers the metallic iron surface. Then, in Section 7, we pointed out that pre-adsorbed potassium atoms cause a differential increase in the rates of dissociative nitrogen adsorption on Fe(100) and Fe(111), thereby eliminating the sensitivity of the kinetics to the structure of the surface plane. One further piece of experimental information must now be added: thermal desorption measurements on iron at low temperature show that, for the process

$$N_2(g) \longrightarrow N_2(ad) \qquad \textbf{(9)}$$

the enthalpy of adsorption is about $-30\,kJ\,mol^{-1}$. However, if pre-adsorbed potassium atoms are present, the value is about $-50\,kJ\,mol^{-1}$.

> Can you relate this to the fact that potassium accelerates the process $N_2(g) \longrightarrow 2N(ad)$ on iron?

The argument can be expressed in terms of a Lennard-Jones potential energy diagram for dissociative adsorption. To find it, turn back to Block 5 (SAQ 9, Figure 11). If the value of ΔH for process 9 becomes more negative, then the N_2 curve is lowered, and the activation energy for the step

$$N_2(ad) \longrightarrow 2N(ad) \qquad \textbf{(10)}$$

falls—to about zero in this particular case. The lower value of ΔH for process 9 also generates a higher surface concentration of $N_2(ad)$. As noted in Block 5, both these effects tend to enhance the rate of process 10.

The secret of the effect of potassium seems therefore to lie in its ability to strengthen the binding between $N_2(ad)$ and the iron surface. In Section 9.1 we argued that this binding is associated with electron donation from filled surface metal orbitals to the vacant $1\pi_g$ antibonding orbital in N_2.

> Why might potassium encourage this process?

Potassium may be thought of as an electron-rich element: the atoms tend to become positively charged by donating electrons to any species that they become bound to. Electron density is thus accumulated by iron atoms in the vicinity of potassium, which enhances subsequent donation to the $1\pi_g$ orbital of dinitrogen, and strengthens the surface—N_2 binding. This is the current interpretation of the promoting influence of potassium. To apply it to the real industrial catalyst, we must attend to one final problem, and this is done in SAQ 24.

In Block 5 (Section 6.2), we noted the long-standing distinction that chemists have made between physical and chemical adsorption. The concept of physical adsorption involves van der Waals binding forces, and retention of the chemical identity of the molecule after adsorption has occurred. In the particular case of process 9, the value of ΔH of about $-30\,kJ\,mol^{-1}$ would normally be accepted as a sign that physical adsorption is occurring; yet in this Section, the adsorption process has been interpreted in terms of molecular orbitals—the basis of a theory of *chemical* bonding. This is an example of a conceptual change that might be encouraged by the new surface techniques: the detailed information that they provide may well dissolve the traditional distinction between physical and chemical adsorption.

10.1 Summary of Sections 9 and 10

1 The stimulation of vibrations when a surface is bombarded with low energy electrons gives rise to electron energy loss peaks.

2 On Fe(111), the adsorbed molecular precursor in the dissociative adsorption of nitrogen is bound side-on as a π-complex. The resultant lowering of the N—N bond order encourages the subsequent dissociation. N(ad) is probably bound on high-coordination sites.

3 Pre-adsorbed potassium atoms strengthen the surface—N_2 binding, and potential energy diagrams show how this lowers the activation energy for dissociation of N_2(ad). It has been suggested that the electropositive potassium encourages electron donation from iron to the $1\pi_g$ orbital in N_2.

SAQ 23 Tungsten, like iron, has the b.c.c. structure. When N_2 is adsorbed on W(100) at 125 K, the EELS spectrum contains a strong band at 2 140 cm^{-1}, and two weaker bands at 1 450 cm^{-1} and 970 cm^{-1}. When the surface is warmed to room temperature, all three peaks disappear, a single new peak appears at 480 cm^{-1}, and the LEED pattern corresponds to a $c(2 \times 2)$ structure. Suggest possible assignments for the four bands.

SAQ 24 The new experiments on potassium promotion described in Sections 7 and 10 used unadulterated atoms adsorbed on iron from potassium metal vapour. But in a real industrial catalyst, the surface potassium is oxygenated. Would you expect this to enhance the promoting effect?

SAQ 25 One important, measurable property of a metal surface is the *work function*, which is effectively an ionisation energy of the surface. In the light of our explanation of potassium promotion, how would you expect the work function of an iron surface to be affected by adsorbed potassium atoms?

11 CONCLUSION

In this Block, we have introduced you to three branches of electron spectroscopy, and to low energy electron diffraction. These techniques were used to obtain information about the mechanism of ammonia synthesis. Summaries of this information are given in Sections 4.5, 5.6, 8.4.5 and 10.1. Here we simply give brief answers to the four questions listed in the Introduction.

Question 1 The nature of the catalyst surface
The surface of the active, promoted catalyst for ammonia synthesis consists mainly of oxygenated potassium, calcium and aluminium, and of metallic iron. The surface concentrations of potassium and aluminium are much higher than their bulk concentrations. The metallic iron is covered by a layer of oxygenated potassium, perhaps only a single atom thick, but the oxygenated aluminium and calcium avoid the iron, and segregate into regions of their own.

Question 2 The mechanism of the reaction
The mechanism of ammonia synthesis is dissociative in both nitrogen and hydrogen, NH_3(ad) being formed by the reaction of N(ad) with successive adsorbed hydrogen atoms. In the case of the dissociative adsorption of nitrogen, there is evidence of an adsorbed molecular precursor, the rate-limiting step being the breakdown of N_2(ad) into N(ad).

Question 3 The active sites
The active sites on the catalyst are to be found on the metallic iron, but at present it is hard to be more precise than this. Current speculation about the detailed molecular changes during the rate-limiting step suggests that the sites should be places where both ends of an N_2 molecule can readily become bound to iron. This 'side-on' position allows a marked lowering of the N—N bond order. On pure iron catalysts, the rather open Fe(111) plane is especially active and, in this case, it has been suggested that the active sites are the recesses containing seven-coordinate iron atoms. However, it is hard to connect this suggestion with the complicated reconstruction of the Fe(111) surface that occurs during nitrogen adsorption.

Question 4 The role of the promoters
Oxygenated aluminium and calcium are structural promoters, which prevent sintering of iron crystallites and thus enlarge the iron surface area. Potassium is an electronic promoter, which is thought to enhance electron density on the iron surface in its vicinity. This encourages iron to bind N_2 'side-on' by donating electrons to the vacant $1\pi_g$ antibonding orbital of the nitrogen molecule. It can be argued, from the Lennard-Jones potential energy diagram, that a strengthening of the Fe—N_2 binding leads to a lowering of the activation energy for the dissociation of N_2(ad).

OBJECTIVES FOR BLOCK 6

Now that you have completed Block 6, you should be able to do the following things:

1 Recognise valid definitions of and use in a correct context, the terms, concepts and principles in the following Table.

Term	Page No.	Term	Page No.
Auger spectroscopy (AES)	12	low energy electron diffraction (LEED)	29
chemical shift	9	Miller indices	26
depth-profiling	16	scanning Auger electron spectroscopy (SAES)	15
Einstein equation	6	spin–orbit coupling	8
elastic scattering	12	sputter-ion etching	15
electron energy loss spectroscopy (EELS)	41	ultra-high vacuum (UHV)	4
electron states	13	UV photoelectron spectroscopy (UPS)	6
frozen-orbital approximation	6	X-ray photoelectron spectroscopy (XPS)	5
inelastic scattering	31		
j quantum number	9		
Koopman's theorem	6		

2 Use XPS spectra to identify the existence of non-equivalent atoms in a molecule, or on a surface. (SAQs 2, 3, 9 and 10)

3 Use electron spectroscopy to perform qualitative analyses of surfaces, and use Auger spectra of a surface to follow approximate changes in relative elemental composition on that surface. (SAQs 4, 5 and 20)

4 Draw conclusions about the variation in elemental composition over a surface area from scanning Auger maps of the area for the elements concerned. (SAQs 6 and 7)

5 Distinguish associative and dissociative adsorption by isotopic distribution experiments. (SAQ 8)

6 Assign Miller indices to sets of planes through simple structures. (SAQs 11–15 and 18)

7 Express changes in unit cell parameters and unit cell orientation on a surface by means of shorthand notation. (SAQs 16, 19–22)

8 Given a low-index plane in a simple metallic structure, determine its LEED pattern. (SAQs 17–19)

9 Determine relative surface compositions from surface structures. (SAQ 20)

10 Combine structural data and vibrational spectra for appropriate molecular compounds with EELS spectra of surfaces to draw conclusions about the bonding of adsorbed species. (SAQ 23)

11 Predict measurable consequences of theories of promoter action in catalysts. (SAQs 24 and 25)

SAQ ANSWERS AND COMMENTS

SAQ 1 Values of E_k are given, and $h\nu = 1\,487$ eV, so values of I can be computed from Einstein's equation, $E_k = h\nu - I$, and compared with the values in Table 1. Thus the peak at 415 eV corresponds to a binding energy of $(1\,487 - 415)$eV $= 1\,072$ eV (sodium). The other ten peaks listed correspond to binding energies of 1 008 (nickel), 872 (nickel), 532 (oxygen), 438 (calcium), 350 (calcium), 284 (carbon), 229 (sulphur), 165 (sulphur), 112 (nickel), and 63 eV (sodium).

SAQ 2 Figure 8c clearly shows the presence of two non-equivalent nitrogen atoms, and this therefore rules out the symmetrical structure **1**, but does not distinguish between **2** and **3**. (The correct structure is thought to be **2**.)

SAQ 3 In the molecule $CF_3COOCH_2CH_3$, the carbon atom with the three very electronegative fluorine atoms has the greatest chemical shift, followed by the adjacent carbon linked to two oxygen atoms. The next carbon atom is linked to one oxygen atom and has an even lower chemical shift. The final carbon atom, with an electronegativity of 2.5, is bound to three hydrogen atoms less electronegative than itself, so it has the lowest chemical shift of all.

SLC 19

SAQ 4 The only impurities are carbon (271 eV) and oxygen (503 eV).

SAQ 5 If the sputter-ion rate is 20 nm per minute, then the required depths are reached at 0.5, 5 and 10 minutes, respectively. The corresponding atomic concentrations can then be read off Figure 20b. The approximate values are:

10 nm: Cr 35%; O 55%; Ni 8%; Si 1%; C 1%
100 nm: C 7%; Si 12%; O 12%; Ni 24%; Cr 45%
200 nm: Si 72%; Cr 12%; C 10%; O 3%; Ni 3%

SAQ 6 Examination of Figure 21 suggests that point 1 will be high in iron and potassium, that point 2 will be low in these elements, and that both these points will be relatively low in aluminium. Point 3, on the other hand, will have a rather high aluminium concentration. Thus spectrum (b) is from point 3, (c) is from point 1 and (d) is from point 2.

SAQ 7 Between them, the elements aluminium, calcium, potassium and iron cover the entire area of Figure 21. With the exception of iron, they are all oxygenated. But as we have seen, there is evidence that even iron is covered with a thin layer of oxygenated potassium. Thus the oxygen map should be uniformly white. This is the case.

SAQ 8 The nitrogen desorbed at about 160 K has the same isotopic composition as the gas adsorbed: no $^{29}N_2$ is produced, so no N≡N bonds were broken, and all the gas desorbed at 160 K was present on the surface as N_2(ad). However, the species adsorbed at 300 K, and desorbed at 800 K must be much more tightly held, and the large proportion of $^{29}N_2$ in the desorbed gas is proof of the rupture of N≡N bonds and the formation of N(ad).

The 1:2:1 ratio is proof that there is complete mobility of adsorbed nitrogen atoms on the surface prior to the attainment of the desorption temperature. Thus, after adsorption of the $^{28}N_2$ and $^{30}N_2$ mixture, there are equal large numbers, Z say, of ^{14}N(ad) and ^{15}N(ad). When a ^{14}N atom is desorbed, then if there is complete surface mobility, all the other $(Z - 1)$ ^{14}N and Z ^{15}N atoms are equally accessible to it for partnership in an N_2 molecule. But as Z is very large, Z and $Z - 1$ are effectively equal, so the chance of desorption as $^{28}N_2$ equals that of desorption as $^{29}N_2$. Likewise, for any ^{15}N atom, the chance of desorption as $^{29}N_2$ equals that of desorption as $^{30}N_2$. You can see that as *both* types of atom can be desorbed as $^{29}N_2$, the ratio $^{28}N_2$:$^{29}N_2$:$^{30}N_2$ at complete mobility is 1:2:1. Likewise, in Section 5.2, complete mobility of H(ad) on Fe(110) is established by this ratio for desorbed H_2, HD and D_2.

SAQ 9 As SAQ 8 and Section 5.1 showed, N_2(ad) is desorbed below 200 K, and could not be retained on the iron surface after evacuation at 300 K.

SAQ 10 The low temperature peak at 401 eV is due to NH_3(ad), and the high temperature peak at 397.0 eV is due to N(ad). It seems that, following exposure to ammonia at 350 K, the main surface species gives a signal at 397.3 eV. But mass spectrometry suggests that this species is NH(ad) (Section 5.3). The final step is to recall the discussion in Section 5.4, where we concluded that the 399 eV peak (the one mentioned in SAQ 9) was due to *either* NH(ad) *or* NH_2(ad): our additional evidence favours the choice of NH_2(ad).

SAQ 11 A body-centred cubic unit cell is illustrated in Figure 59a. The atom at the centre is surrounded by eight *identical* atoms at the corners of the cube: the coordination number is 8. Figure 59b shows two close-packed layers, A and B. When a third layer is added, it can be directly over layer A, in which case the stacking sequence is ABABAB . . . etc., or it can be over the dots in which case the sequence is ABCABC . . . etc. The first arrangement leads to hexagonal close-packing, and the second to cubic close-packing. In both arrangements any atom in layer B is surrounded by six atoms at the corners of a hexagon in its own layer, by three atoms at the corners of a triangle in the layer above, and by three atoms at the corners of a triangle in the layer below: in both h.c.p. and c.c.p., the coordination number is 12. *Remember that for c.c.p., the unit cell is face-centred cubic (Figure 59c), and that the close-packed planes are perpendicular to the cube diagonals.* The coordination number of an atom on the surface of both unit cells is 4.

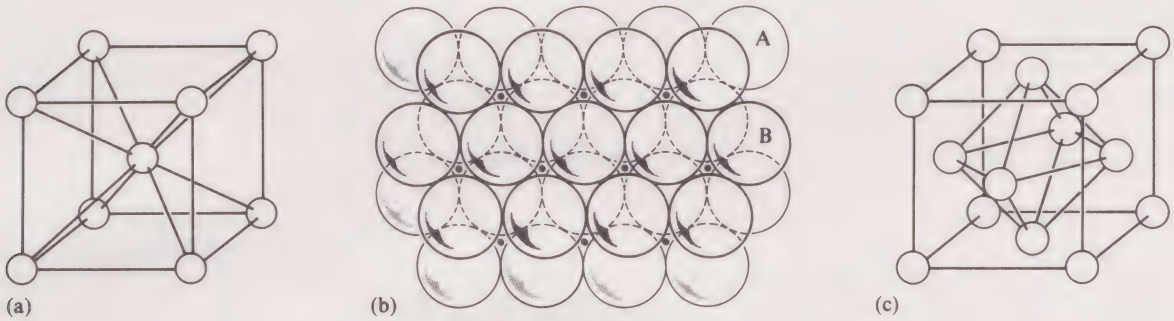

Figure 59 (a) Body-centred cubic unit cell; (b) two close-packed layers (top view); (c) face-centred unit cell for cubic close-packing.

SAQ 12 Figure 60 shows the four sets of lines with a unit cell and the indices marked. (By choosing a different line, you may have come up with the answers: $(\bar{1}1)$, $(0\bar{1})$, $(\bar{2}1)$ and $(2\bar{1})$. These are equally valid answers.)

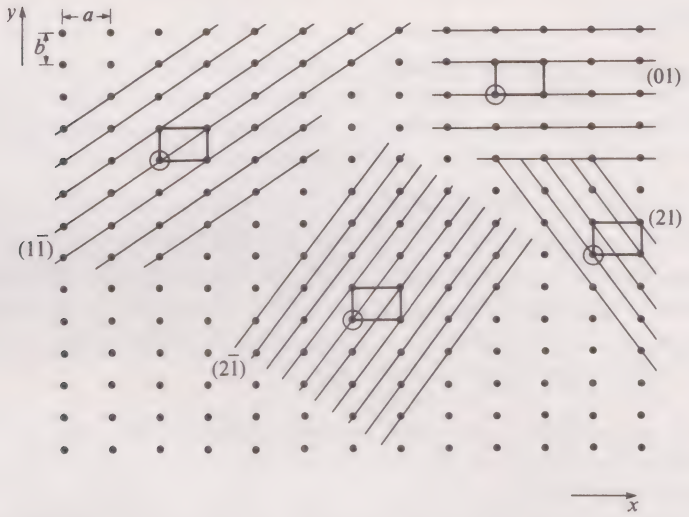

Figure 60 A rectangular net showing four sets of lines with unit cells and Miller indices marked.

SAQ 13 Figure 32b shows the (200) planes: the planes are parallel to y and z and divide a into two. Figure 32c shows the (220) planes: the planes are parallel to z and divide both a and b into two. Figure 32d shows the $(11\bar{1})$ planes: they leave a, b and c undivided.

SAQ 14 Figure 34a shows the (200) planes: the planes lie parallel to y and z but divide a into two. Figure 34b shows the (110) planes: the planes lie parallel to z and leave a and b undivided. Figure 34c shows the $(22\bar{2})$ planes: the planes divide a, b and c into two.

SAQ 15 Figure 61 shows the pattern of atomic positions for each plane—*it is printed on the loose-leaf sheet.* For each net a two-dimensional unit cell has been drawn in : the unit cell dimensions are also given in terms of a, the unit cell dimension of the three-dimensional cubic unit cell of the crystal. For metallic iron, $a = 286$ pm. Notice that the pattern on f.c.c. (111) must be hexagonal, reflecting the arrangement in the close-packed layers.

SAQ 16 Figure 62 shows the nets with the two-dimensional unit cells drawn in for the adsorbates; a is the unit cell dimension for the three-dimensional unit cell of the bulk crystal. The notation for each of the adsorbate unit cells is: (a) f.c.c. (111)- (1 × 1); (b) f.c.c. (111)- (2 × 2); (c) f.c.c. (100)- (2 × 2); (d) f.c.c. (110)- (1 × 2); (e) b.c.c. (110)- (3 × 1); (f) f.c.c. (100)- $(\sqrt{2} \times 2\sqrt{2})$R45°. Figure 62g shows the geometry of this rotation: if the two-dimensional unit cell length of the substrate is q (where $q = a/\sqrt{2}$) then simple trigonometry shows that the unit cell lengths (x, y) of the new cell are: $x = \sqrt{2}q$; $y = 2\sqrt{2}q$, and that the angle of rotation is 45°.

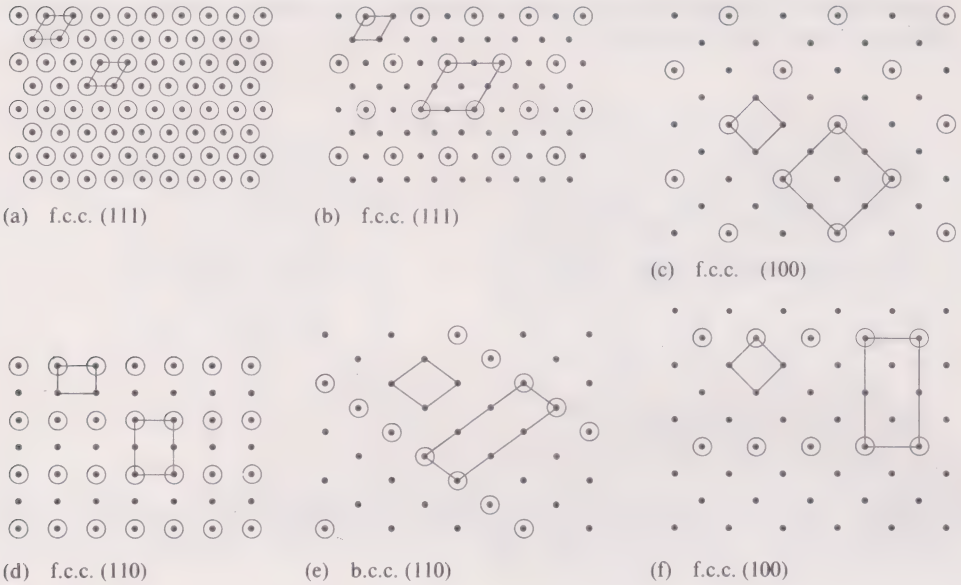

(a) f.c.c. (111) (b) f.c.c. (111) (c) f.c.c. (100)

(d) f.c.c. (110) (e) b.c.c. (110) (f) f.c.c. (100) (g)

Figure 62 Unit cells of the adsorbed layers.

SAQ 17 See Figure 63.

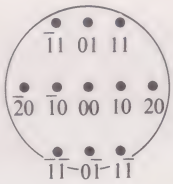

Figure 63 Hypothetical LEED pattern showing indexing of spots.

SAQ 18 Platinum has a c.c.p. (f.c.c.) structure thus: (a) the (100) face has a square unit cell; (b) the (110) face has a rectangular unit cell; (c) the (111) face has a hexagonal unit cell. (d) The (200) face of Fe(b.c.c.) has a square unit cell. The diffraction patterns from these thus correspond to those in Figure 46a, 46b, 46c and 46a, respectively.

The cell sizes and the spacings in the diffraction patterns are: (a) the unit cell for the (100) face has side length $a/\sqrt{2}$, and the diffraction pattern is also square with side length $\sqrt{2}\lambda r/a$; (b) the (110) face has cell dimensions a and $a/\sqrt{2}$, so the diffraction pattern has spacings $\lambda r/a$ and $\sqrt{2}\lambda r/a$, respectively; (c) the (111) hexagonal unit cell has unit cell length $a/\sqrt{2}$ and the diffraction spacing is $\sqrt{2}\lambda r/a$; (d) Fe(200) has a square unit cell of side length a, and the diffraction pattern is thus square with a spacing of $\lambda r/a$.

SAQ 19 Figure 64 shows the faces with both the substrate and the adsorbate unit cells drawn. The new unit cells are (a) (2 × 2), (b) c(2 × 2), and (c) (2 × 2), respectively. If all sites are filled on the (100) face, the unit cell of the adsorbate becomes (1 × 1). The unit cell is still square, which is reflected in the LEED pattern, but the cell dimension is halved so the LEED spacing is doubled.

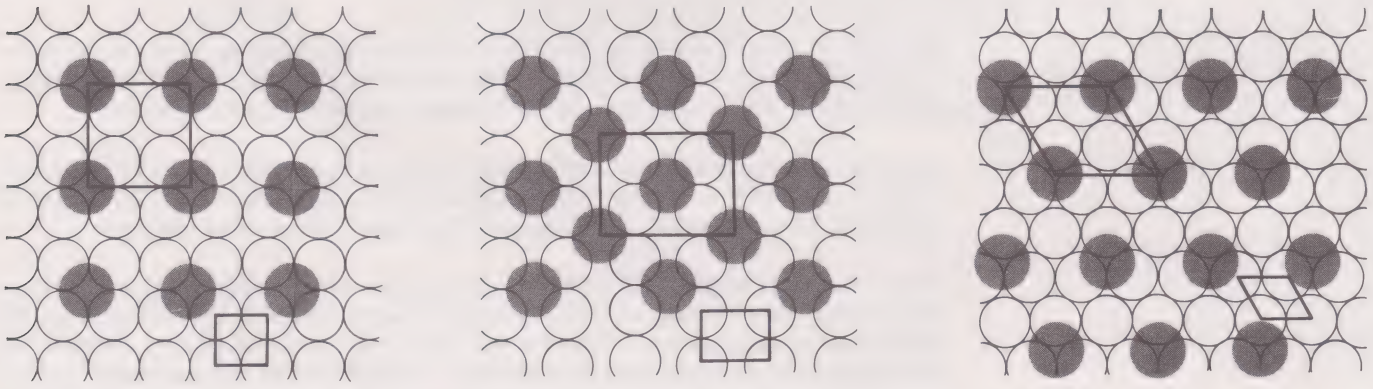

(a) face (100) (b) face (110) (c) face (111)

Figure 64 Low-index faces of an f.c.c. metal showing substrate and adsorbate unit cells

SAQ 20 When ρ no longer increases, we can assume that Fe(100) is then covered with the $c(2 \times 2)$ structure shown in Figure 49. Each unit cell contains four iron and two nitrogen atoms, so $\rho = 0.9$ corresponds to a surface N:Fe ratio of 1:2. Consequently, after the reaction on the iron, when $\rho = 0.12$, N:Fe = $(0.5 \times 0.12/0.9) = 1{:}15$. Because N(ad) is the only species retained during evacuation at 580 K, this is the N:Fe ratio during the reaction. As noted in Section 5.4, the value is small and far from saturation.

SAQ 21 With $a = 3x$ and $b = 2x$, equation 20 tells us that c, the side of the unit cell, is $\sqrt{19}x$. Using equation 21, $\cos\beta = 4/\sqrt{19}$ which means that β, the angle of rotation in Figure 53b, is 23.4°. The unit cell is therefore that of a $(\sqrt{19} \times \sqrt{19})$R23.4° structure.

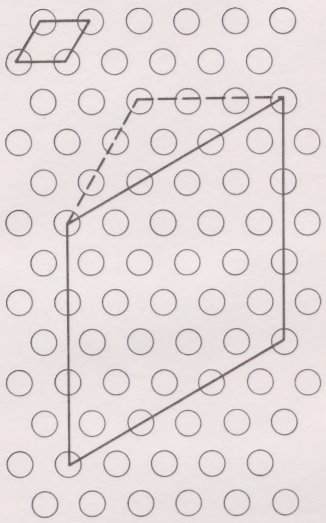

Figure 65 The unit cell for the $(\sqrt{27} \times \sqrt{27})$R30° structure formed by nitrogen adsorption on Fe(111).

SAQ 22 See Figure 65. Since the angle of rotation is 30°, one pair of unit cell sides must be parallel to the long diagonal of the simple cell at the top left in Figures 53b and 53c. This means that the sides a and b of the dotted 120° triangle equivalent to those in Figures 53b and 53c must be equal. Since, in this triangle, $c = \sqrt{27}x$, from equation 20, $a = b = 3x$, a requirement fulfilled in Figure 65.

SAQ 23 The room temperature peak at 480 cm^{-1} can be assigned to monatomic nitrogen bound at a high coordinate site, because it matches the value of 450 cm^{-1} found for N(ad) at such sites on Fe(111). This is in perfect agreement with the observed $c(2 \times 2)$ structure, corresponding to Figure 49, where the coordination number is 4.

The low temperature peaks can be tentatively assigned to nitrogen bound in three different ways. Those at 2 140 cm^{-1} and 1 450 cm^{-1} match the values for end-on and side-on N_2(ad), as discussed in Section 9.1. On the basis of the 1 020 cm^{-1} vibration observed in $[O_3Os{\equiv}N]^-$, the 970 cm^{-1} peak has been assigned to N(ad) bound to just one tungsten atom.

SAQ 24 The presence of electronegative oxygen among the potassium atoms should reduce the ability of potassium to enhance electron density on adjacent iron atoms, so the promoting effect should be diminished. This is observed experimentally. Under industrial conditions, the reduced effectiveness must be accepted, because oxygenation binds the potassium fairly strongly to the surface. Unadulterated potassium atoms are rather volatile and would be lost at industrial working temperatures.

SAQ 25 By enhancing the electron density on the iron surface, adsorbed potassium atoms should ease surface ionisation and lower the work function. This is observed.

ACKNOWLEDGEMENTS

Grateful acknowledgement is made to the following sources for material used in this Block:

Figures 4(a) and 13 M. Roberts and C. McKee, *Chemistry of the Metal–Gas Interface*, Oxford University Press, 1978; *Figure 5* R. Holm, 'Imaging and analysis of surfaces with a scanning electron microscope and electron spectrometer', in *Angewandte Chemie International Edition*, vol. 10, 1971, Verlag Chemie; *Figures 7, 8 and 17* A. Baker, C. Brundle and M. Thompson, 'Electron Spectroscopy', in *Chemical Society Reviews*, vol. 1, 1972, The Royal Society of Chemistry; *Figure 9* C. Nording, 'Electron spectroscopy for chemical analysis', in *Angewandte Chemie International Edition*, vol. 11, 1972, Verlag Chemie; *Figures 11 and 29* G. Ertl and N. Thiele, 'XPS studies with ammonia synthesis catalysts', in *Applications of Surface Science*, vol. 3, 1979, North-Holland Physics Publishing; *Figure 18* G. Ertl, 'Elementary processes at gas/metal interfaces', in *Angewandte Chemie International Edition*, vol. 15, 1976, Verlag Chemie; *Figures 19 and 20* PHI Data Sheet 1052 6-78 15M, courtesy of Perkin-Elmer; *Figures 21 and 23* G. Ertl *et al.*, 'Surface characterisation of ammonia synthesis catalysts', in *Catalysis Reviews*, vol. 21, pt. 2, 1980, Marcel Dekker; *Figure 36* F. Bozco *et al.*, 'Interaction of nitrogen with iron surfaces', in *Journal of Catalysis*, vol. 50, 1977, Academic Press; *Figure 46* G. Harburn *et al.*, *Atlas of Optical Transforms*, 1975, Bell and Hyman; *Figure 57* M. Grunze *et al.*, 'π-bonded N_2 on Fe(111): the precursor for dissociation', in *Physical Review Letters*, vol. 53, no. 8, 1984, The American Physical Society.

The Course Team would like to thank Professor Gerhard Ertl of the University of Munich for his generosity in answering queries about his research on the mechanism of ammonia synthesis.

Units and their definitions

Physical quantity (and symbol)	Unit	Symbol and definition of unit
length (l)	metre	m
volume (V)	litre	l (= $dm^3 = 10^{-3}\ m^3$)
mass (m)	kilogram	kg
amount of substance (n)	mole	mol
time (t)	second	s
frequency (f, ν)	hertz	Hz (= s^{-1})
energy (U), enthalpy (H)	joule	J (= $kg\,m^2\,s^{-2}$)
	calorie	cal (= 4.184 J)
force	newton	N (= $kg\,m\,s^{-2} = J\,m^{-1}$)
power	watt	W (= $kg\,m^2\,s^{-3} = J\,s^{-1}$)
pressure (p)	pascal	Pa (= $kg\,m^{-1}\,s^{-2} = N\,m^{-2} = J\,m^{-3}$)
	atmosphere	atm (= 101 325 Pa)
electric current (I)	ampere	A (= $C\,s^{-1}$)
electric charge (Q)	coulomb	C (= A s)
electric potential difference (V), emf (E)	volt	V (= $kg\,m^2\,s^{-3}\,A^{-1} = J\,A^{-1}\,s^{-1} = J\,C^{-1}$)
resistance (R)	ohm	Ω (= $V\,A^{-1}$)
temperature (T)	kelvin	K
	degree Celsius	°C (0 °C = 273.15 K)
extent of reaction (ξ)	mole	mol
molar concentration of substance Y ([Y], c_Y)		mol dm^{-3}
rate of reaction per unit volume (J)		mol $dm^{-3}\,s^{-1}$ (with concentrations in mol dm^{-3})

Fundamental constants

speed of light	c	$2.997\,925 \times 10^8\ m\,s^{-1}$
charge of proton	e	$1.602\,189 \times 10^{-19}$ C
charge of electron	$-e$	
Avogadro constant	$N_A(L)$	$6.022\,045 \times 10^{23}\ mol^{-1}$
Boltzmann constant	k	$1.380\,662 \times 10^{-23}\ J\,K^{-1}$
gas constant	$R = N_A k$	$8.314\,41\ J\,K^{-1}\,mol^{-1}$
Faraday constant	$F = N_A e$	$9.648\,456 \times 10^4\ C\,mol^{-1}$
Planck constant	h	$6.626\,176 \times 10^{-34}$ J s

SI prefixes

10^{-12}	10^{-9}	10^{-6}	10^{-3}	10^{-2}	10^{-1}	10^3	10^6	10^9
pico	nano	micro	milli	centi	deci	kilo	mega	giga
p	n	μ	m	c	d	k	M	G

Mathematical information

$\log \equiv \log_{10}$ $\quad \ln \equiv \log e$ $\quad \ln x = (\ln 10) \log x = 2.303 \log x$

$\pi = 3.141\,593$ $\quad e = 2.718\,282$

Physical Chemistry: Principles of chemical change

0 335 16188 X